

SOME OPTIMAL CONTROL PROBLEMS IN ELECTRIC VEHICLES

A THESIS SUBMITTED TO  
THE GRADUATE SCHOOL OF NATURAL AND APPLIED SCIENCES  
OF  
MIDDLE EAST TECHNICAL UNIVERSITY

KENAN AHISKA

IN PARTIAL FULFILLMENT OF THE REQUIREMENTS  
FOR  
THE DEGREE OF DOCTOR OF PHILOSOPHY  
IN  
ELECTRICAL AND ELECTRONICS ENGINEERING

DECEMBER 2016



Approval of the thesis:

**SOME OPTIMAL CONTROL PROBLEMS IN ELECTRIC VEHICLES**

submitted by **KENAN AHISKA** in partial fulfillment of the requirements for the degree of **Doctor of Philosophy in Electrical and Electronics Engineering Department, Middle East Technical University** by,

Prof. Dr. Gülbin Dural Ünver  
Dean, Graduate School of **Natural and Applied Sciences** \_\_\_\_\_

Prof. Dr. Tolga Çiloğlu  
Head of Department, **Electrical and Electronics Engineering** \_\_\_\_\_

Prof. Dr. Mehmet Kemal Leblebicioğlu  
Supervisor, **Electrical and Electronics Eng. Dept., METU** \_\_\_\_\_

Prof. Dr. Mustafa Kemal Özgören  
Co-supervisor, **Mechanical Eng. Dept., METU** \_\_\_\_\_

**Examining Committee Members:**

Prof. Dr. Mehmet Önder Efe  
Computer Engineering Department, Hacettepe University \_\_\_\_\_

Prof. Dr. Mehmet Kemal Leblebicioğlu  
Electrical and Electronics Engineering Department, METU \_\_\_\_\_

Assoc. Prof. Dr. Afşar Saranlı  
Electrical and Electronics Engineering Department, METU \_\_\_\_\_

Assoc. Prof. Dr. Umut Orguner  
Electrical and Electronics Engineering Department, METU \_\_\_\_\_

Assoc. Prof. Dr. Klaus W. Schmidt  
Mechatronics Engineering Department, Çankaya University \_\_\_\_\_

**Date:** 29/12/2016

**I hereby declare that all information in this document has been obtained and presented in accordance with academic rules and ethical conduct. I also declare that, as required by these rules and conduct, I have fully cited and referenced all material and results that are not original to this work.**

Name, Last Name: KENAN AHISKA

Signature :

# ABSTRACT

## SOME OPTIMAL CONTROL PROBLEMS IN ELECTRIC VEHICLES

Ahıska, Kenan

Ph.D., Department of Electrical and Electronics Engineering

Supervisor : Prof. Dr. Mehmet Kemal Leblebiciođlu

Co-Supervisor : Prof. Dr. Mustafa Kemal Özgören

December 2016, 125 pages

Conventional internal combustion engine-powered vehicles are the mainstream mean in nowadays private transportation. However, their fuel consumption results in environmental problems. Electric vehicles, on the other hand, have zero pollutant emission and benefit from high highly-efficient electric motor technology. These make the electric vehicles as the most promising alternative in private transportation. However, limitations in current battery technology aggravate the widespread usage of electric cars. The question of optimal solutions even for the small travel distances in urban traffic are very intriguing.

In this thesis, several optimal control problems concerning electric vehicles are studied: (1) energy optimality of electric vehicles moving along roads with uphill and downhill sections, (2) energy and time optimality of electric vehicles cornering arcs with various radii along asphalt road and the Pareto-front between these two objectives, and (3) vehicle handling of electric cars cornering around arcs with various radii along icy roads.

A mathematical model for electric vehicles including longitudinal, lateral and rotational dynamics is constructed. Wheel skidding kinematics and battery dynamics are incorporated into the mathematical model. This model is derived through necessary simplification of a previously derived more comprehensive mathematical model that

includes the suspension characteristics as well. The simplified model is named gross motion model and it is verified with in several tests.

Energy and time optimality problems are solved with methods based on classical optimal control theory. A solution method for these two-point boundary value problems with defined state boundaries and free final time has been developed and the obtained solutions are compared with constant velocity cruise controllers. For roads including icy uphill and downhill sections a skidding compensation logic is proposed to reduce the wheel slippage. It has been observed that the optimal control solution has superiority in energy management against the cruise controllers and it reaches a solution near the global optimum without being influenced by the skidding compensation logic. The sensitivity of the energy optimal controller on passenger seating configurations and initial state-of-charge of the battery turns out to be smaller in magnitude compared to the changes in the parameters. The superiority of the energy optimal controller against the cruise controllers becomes more evident in the scenarios where the battery is far from being fully charged.

The vehicle cornering problems for electric vehicles are evaluated in terms of both energy and time optimality. Significant improvements compared to the cruise control solutions for both objectives are obtained with the solutions based on classical optimal control approach. A Pareto-front analysis is carried out with multi-objective energy and time minimization. The analysis provides a multi-objective solution to the vehicle cornering problem with a compromise between travel time and energy consumption that enables the vehicle to travel over the corner with minimum energy consumption within the given speed limits. The optimality of the Pareto-front results is discussed. Furthermore, a sensitivity analysis is performed and it is confirmed that the optimal control solution is insensitive to the different passenger seating arrangements.

The vehicle handling problem for electric cars cornering around roads with low friction coefficients is studied and an autopilot design is proposed to satisfy desired handling performance. A novel hierarchical optimization approach is presented to generate off-line solutions for cornering along roads with different friction coefficients and radii of curvature. Vehicle motion as the output of this optimization process, together with vehicle states and control commands at each sampling time are generated and stored for different selected scenario parameters with various rotation radii and friction coefficients. A vehicle status definition is presented as a function of vehicle states that contains the most informative data to evaluate the vehicle handling performance. The vehicle statuses at each decision instant among these off-line optimized data are clustered with the k-means clustering technique. These are associated with the control commands applied. A cluster centre-control command corresponds to a rule that produces the unique control command to be applied as a function of vehicle status. The autopilot is constructed by a convex combination of these rules. This basic idea of autopilot design has been extended for motions along a specific rotation radii and friction coefficients; the control commands corresponding to arbitrary sce-

nario parameters are obtained by a runtime scheduling of the weighted-interpolation among the control commands corresponding to different scenario parameters.

Keywords: electric vehicles, optimal control, sensitivity analysis, Pareto-front analysis, vehicle handling, cornering autopilot, skidding autopilot

# ÖZ

## ELEKTRİKLİ ARAÇLARDA BAZI OPTİMAL KONTROL PROBLEMLERİ

Ahıska, Kenan

Doktora, Elektrik ve Elektronik Mühendisliği Bölümü

Tez Yöneticisi : Prof. Dr. Mehmet Kemal Lelebicioğlu

Ortak Tez Yöneticisi : Prof. Dr. Mustafa Kemal Özgören

Aralık 2016 , 125 sayfa

Geleneksel içten yanmalı motorlu taşıtlar, günümüz kişisel ulaşımında en çok tercih edilen araçlardır. Ancak, yakıt tüketimleri çevresel sorunlar ortaya çıkarmaktadır. Elektrikli araçlar ise sıfır kirlilik salınımına sahiptir ve yüksek verimli elektrik motoru teknolojilerinden yararlanırlar. Bunlar elektrikli araçları kişisel ulaşım için en ümit veren alternatif haline getirmektedir. Ancak, mevcut batarya teknolojilerindeki kısıtlar elektrikli arabaların yaygın kullanımını zorlaştırmaktadır. En iyilenmiş çözümlerin aranması, kent hayatındaki kısa seyahat mesafeleri için bile ilgi çekicidir.

Bu tezde, elektrikli araçların optimal kontrolü çeşitli problemlerde değerlendirilmiştir: (1) yokuş ve iniş kısımları içeren yollarda giden elektrikli araçlar için enerji eniyilemesi, (2) asfalt yollarda dönüş yapan elektrik araçlar için enerji ve zaman eniyilemesi, ve bu iki hedef arasındaki Pareto-yüzey, ve (3) buzlu yolda dönüş yapan elektrikli araçlar için araç hakimiyeti problemleri çalışılmıştır.

Elektrikli araçlar için boylamsal, yanal ve dönüş dinamiklerini içeren bir matematiksel model oluşturulmuştur. Tekerleklerin kayma kinematikleri ve batarya dinamikleri bu model içerisine gömülmüştür. Bu model, süspansiyon karakteristiklerini de içeren daha ayrıntılı bir matemaiksel modelde gerekli sadeleştirilmelerin yapılması ile elde edilmiştir. Büyük hareket modeli olarak isimlendirilen bu sadeleştirilmiş model, çeşitli test senaryolarında doğulanmıştır.

Enerji ve zaman eniyileme problemleri klasik optimal kontrol yöntemleri ile çalışılmıştır. Durum sınırları tanımlı, serbest son zamanlı bu iki-nokta sınır değer problemleri için bir çözüm tekniği geliştirmiş ve elde edilen çözümler sabit hızlı seyir kontrolcülerine karşılaştırılmıştır. Buzlu yokuş ve iniş kısımları içeren yollar için bir kayma giderme mantığı önerilmiştir. Optimal kontrol çözümünün seyir kontrolcülerine kıyasla enerji tüketimi açısından üstünlüğü gözlemlenmiş ve bu çözümün global optimum çözümüne yakın olduğu ve kayma giderme mantığından etkilenmediği tespit edilmiştir. Enerji optimal çözümün değişik yolcu oturma konfigürasyonları ve bataryanın ilk şarj durumuna olan duyarlılığının, bu değerlerdeki değişimlerine kıyasla düşük olduğu ortaya çıkmıştır. Enerji optimal kontrolcünün seyir kontrolcülerine olan üstünlüğü, batarya tam doluluktan uzaklaştıkça daha belirgin olmuştur.

Elektrikli araçlar için dönüş problemi hem enerji hem de zaman eniyilemesi açısından değerlendirilmiştir. Seyir kontrolcülerine kıyasla, klasik optimal kontrol tekniği ile elde edilen çözümler, amaçları cinsinden önemli iyileştirmeler sağlamışlardır. Enerji ve zaman çok amaçlı eniyileştirme ile bir Pareto-yüzey analizi yapılmıştır. Bu analiz, yolculuk zamanı ve enerji harcaması arasında bir ödünleşme ile dönüş problemi için çok amaçlı bir çözüm sağlayarak aracın verilen hız limitleri içinde minimum enerji harcaması yaparak dönüşü tamamlamasını sağlamaktadır. Pareto-yüzey çözümlerinin optimalitesi tartışılmıştır. Ayrıca, bir duyarlılık analizi ile optimal kontrol çözümlerinin değişik yolcu yerleşimlerine duyarsız olduğu doğrulanmıştır.

Düşük sürtünme katsayılı yollarda dönüş hareketi yapan elektrikli araçlar için araç hakimiyeti problemi çalışılmış ve istenilen performansı sağlayan bir otopilot tasarım önerilmiştir. Hiyerarşik bir optimization methodu önerilmiş ve çevrimdışı optimization sonuçları durum ve komut vektör çiftleri olarak her bir karar anında değişik dönüş çapları ve sürtünme kuvvetleri için kaydedilmiştir. Araç hakimiyetini değerlendirmek için en bilgilendirici verileri içeren, araç durumlarının bir fonksiyonu olarak araç statüsü tanımlanmıştır. Çevrimdışı eniyilenmiş çözümler içinde her bir karar anı için araç statüleri k-means kümelemesi tekniği ile kümelenebilir ve her bir küme merkezine kontrol komutları atanmıştır. Her bir küme merkezi-kontrol komutu, araç durumunun bir fonksiyonu olarak bir kural tanımlar. Otopilot bu kuralların konvesk birleşiminden oluşmaktadır. Otopilot tasarımındaki temel fikir herhangi bir dönüş çapı ve sürtünme katsayısı için genişletilebilir: herhangi bir senaryo değişkenine karşılık gelen kontrol komutları, değişik senaryolardaki kontrol komutlarının ağırlıklı ortalamasının koşan-zamanda ayarlanması ile elde edilebilir.

Anahtar Kelimeler: elektrikli araçlar, optimal denetleç, duyarlılık analizi, Pareto yüzey analizi, araç hakimiyeti, dönüş otopilotu, kayma otopilotu

*To my family,*

## ACKNOWLEDGMENTS

I would like to express my sincerest thanks to my supervisor Prof. Dr. Kemal Leblebiciođlu and my co-supervisor Prof. Dr. Kemal Özgoren for their guidance, support and valuable contributions throughout the preparation of this thesis.

Furthermore, I owe my gratitude to Assoc. Prof. Dr. Umut Orguner and Assoc. Prof. Dr. Klaus Werner Schmidt for their contributions on this study by their technical critics and enlightening ideas during our committee meetings.

I would also like to thank Turkish Scientific and Technological Research Council (TÜBİTAK) for their financial support during my Ph.D. studies.

I am really grateful to my colleagues from ASELSAN Inc. for their support and encouragement throughout my Ph.D. studies.

I also wish to express my warm thanks to Murat Kumru who have contributed to the process of review of this dissertation and to Emre Salmanođlu who helped me in organization of the visualizations in this thesis.

I express my sincerest thanks to my family and friends who have given me endless support all along the years of my educational life.

# TABLE OF CONTENTS

ABSTRACT . . . . .	v
ÖZ . . . . .	viii
ACKNOWLEDGMENTS . . . . .	xi
TABLE OF CONTENTS . . . . .	xii
LIST OF TABLES . . . . .	xvi
LIST OF FIGURES . . . . .	xviii
LIST OF ABBREVIATIONS . . . . .	xxv
CHAPTERS	
1 INTRODUCTION . . . . .	1
1.1 Motivation . . . . .	1
1.2 Thesis Organization and Contributions . . . . .	3
2 MATHEMATICAL MODELLING . . . . .	9
2.1 Reference Frames . . . . .	10
2.1.1 Earth-Fixed Reference Frame . . . . .	10
2.1.2 Local Ground Reference Frame . . . . .	10
2.1.3 Chassis Fixed Reference Frame . . . . .	10

2.1.4	Body Fixed Reference Frame . . . . .	11
2.1.5	Transformations between Reference Frames . . . . .	11
2.2	Vector Form of Dynamic Relationships . . . . .	13
2.2.1	Vector Newton-Euler Equations for the Chassis . . .	13
2.2.2	Vector Newton-Euler Equations for the Suspended Body . . . . .	13
2.3	Matrix Form of Dynamic Relationships . . . . .	14
2.3.1	Matrix Newton-Euler Equations for the Chassis . . .	14
2.3.2	Matrix Newton-Euler Equations for the Suspended Body . . . . .	14
2.4	Aerodynamic Forces and Moments . . . . .	14
2.5	Suspension System Related Forces and Moments . . . . .	15
2.6	Wheel Dynamics and Interaction Forces and Moments . . . . .	15
2.6.1	Orientation Matrices for the Wheels . . . . .	16
2.6.2	Vector Newton-Euler Equations for the Wheels . . .	16
2.6.3	Matrix Newton-Euler Equations for the Wheels . . .	16
2.6.4	Interaction Forces and Moments . . . . .	17
2.7	Angular Velocities . . . . .	18
2.8	Angular Accelerations . . . . .	19
2.9	Overall Dynamic Motion Model of the Vehicle . . . . .	20
2.10	Simplified Motion Model for Gross Motion of the Vehicle . . .	22
2.11	Cornering Motion . . . . .	27

2.12	Power Consumption Dynamics . . . . .	29
2.13	Open Loop Simulations of the Vehicle Model . . . . .	30
2.13.1	Scenario-1: Uphill/Downhill Motion along Asphalt Road . . . . .	30
2.13.2	Scenario-2: Braking along Asphalt and Icy Roads . . . . .	34
2.13.3	Scenario-3: Cornering along Asphalt Road . . . . .	34
3	ENERGY OPTIMALITY . . . . .	37
3.1	Introduction . . . . .	37
3.2	Optimal Controller Design . . . . .	41
3.3	Results . . . . .	46
3.4	Skidding Compensation . . . . .	54
3.5	Sensitivity Analysis . . . . .	58
3.6	Conclusions and Discussions . . . . .	59
4	VEHICLE CORNERING . . . . .	63
4.1	Introduction . . . . .	63
4.2	Optimal Controller Design . . . . .	66
4.3	Results . . . . .	70
4.4	Pareto Front Analysis . . . . .	77
4.5	Sensitivity Analysis . . . . .	83
4.6	Conclusions and Discussions . . . . .	83
5	VEHICLE HANDLING . . . . .	87
5.1	Introduction . . . . .	87

5.2	Solution Approach . . . . .	90
5.3	Optimization Algorithms . . . . .	91
5.3.1	Outer Layer Optimization: from easy problem to difficult problem, from simple solution to complex solution . . . . .	92
5.3.2	Inner Layer Optimization: non-gradient based op- timization algorithm . . . . .	93
5.4	Status Clustering and Rule Generation . . . . .	98
5.4.1	Autopilot Design: Runtime Decision Making . . .	100
5.5	Results . . . . .	101
5.5.1	Tuning Cluster Parameters . . . . .	101
5.5.2	Autopilot Performance Compared against Off-line Optimization Results . . . . .	103
5.5.3	Autopilot Performances in Test Scenarios . . . . .	104
5.6	Conclusion . . . . .	107
6	CONCLUSIONS . . . . .	111
	REFERENCES . . . . .	115
	CURRICULUM VITAE . . . . .	123

## LIST OF TABLES

### TABLES

Table 2.1	Parameters of the model . . . . .	32
Table 3.1	Optimal control solution algorithm . . . . .	45
Table 3.2	Test scenarios . . . . .	47
Table 3.3	Average speeds of the vehicles under energy optimal controllers (km/h) . . . . .	51
Table 3.4	$EC$ s of the vehicle under different controllers ( $kJ$ ) and $EE$ s of the energy optimal controller with respect to cruise controllers (%) . . . . .	53
Table 3.5	Number of iterations to find the energy optimal solution . . . . .	54
Table 3.6	Efficiency of the energy optimal controller compared to the cruise controllers in (%) and changes in power consumption of the vehicle un- der optimal control with and without skidding compensation logic, and the reduction in slippage on the wheels with skidding compensation logic enabled(%) . . . . .	57
Table 3.7	Corresponding change in total $EC$ of the vehicle under different controllers (%) for different configurations (%), average of all scenarios . .	59
Table 3.8	For different initial $SOC$ values changes in total energy consump- tions of the vehicle under different controllers, average of all scenarios . .	59
Table 3.9	Comparison against methods in the literature . . . . .	61

Table 4.1	Test scenarios . . . . .	71
Table 4.2	Energy consumptions $EC$ and time consumptions $TC$ of the vehicles under energy optimal controller $EOC$ and time optimal controller $TOC$ for different initial vehicle speeds for SC-01 ( $NS$ indicates no solution) . . . . .	72
Table 4.3	Energy performances of the optimal controllers, $EOC$ : Energy Optimal Controller, $TOC$ : Time Optimal Controller, $EC$ : Energy consumption in $J$ , $EE$ : Energy efficiency . . . . .	72
Table 4.4	Time consumption performances of the optimal controllers, $EOC$ : Energy Optimal Controller, $TOC$ : Time Optimal Controller, $TC$ : Time consumption in $s$ , $TE$ : Time efficiency . . . . .	73
Table 4.5	Average speeds of the vehicles under energy and time optimal controllers (km/h) . . . . .	76
Table 4.6	Number of iterations to find the energy and time optimal solutions .	78
Table 4.7	Number of iterations to find the Pareto-front . . . . .	82
Table 5.1	Outer layer optimization algorithm . . . . .	95
Table 5.2	Non-gradient based optimization algorithm: search cone optimization	97

## LIST OF FIGURES

### FIGURES

Figure 2.1	Reference frames defined in vehicle dynamics . . . . .	11
Figure 2.2	Vehicle model (top view) . . . . .	24
Figure 2.3	Vehicle model (longitudinal view) . . . . .	25
Figure 2.4	Vehicle model (Lateral view) . . . . .	26
Figure 2.5	Ackerman steering . . . . .	28
Figure 2.6	Charging characteristics of the battery package . . . . .	29
Figure 2.7	Discharging characteristics of the battery package . . . . .	30
Figure 2.8	Simulink model developed to test the gross motion model . . . . .	31
Figure 2.9	The difference in vehicle positions of Simulink model and the model developed in this study throughout the test scenario between . . . . .	33
Figure 2.10	The difference in vehicle speeds of Simulink model and the model developed in this study throughout the test scenario between . . . . .	33
Figure 2.11	Change in the positions of the braking vehicles along asphalt and icy roads (solid line: asphalt road and dashed line: icy road) . . . . .	34
Figure 2.12	Change in the speeds of the braking vehicles along asphalt and icy roads (solid line: asphalt road and dashed line: icy road) . . . . .	35
Figure 2.13	Change in the position of a vehicle cornering a quarter circle along asphalt road obeying constant Ackerman's steering law . . . . .	35

Figure 2.14 Change in the tangential velocities of a vehicle and its four wheels during cornering a quarter circle along asphalt road obeying constant Ackerman's steering law (blue: vehicle, red: front left wheel, yellow: front right wheel, violet: rear left wheel and green: rear right wheel) . . . . .	36
Figure 3.1 Uphill downhill motion representation . . . . .	41
Figure 3.2 Iterative solution approach proposed for free-final time optimal control problems . . . . .	44
Figure 3.3 Normalized difference between modified and discontinuous Hamiltonian functions for different values of $\eta$ . . . . .	48
Figure 3.4 An example of slope smoothing at edges . . . . .	49
Figure 3.5 Marks for the start and stop points of the sloped sections . . . . .	49
Figure 3.6 Histogram of the speed profiles of vehicle under energy optimal controller for various scenarios (top left: Scenario-01, top middle: Scenario-05, top right: Scenario-09, bottom left: Scenario-13, bottom middle: Scenario-17, and bottom right: Scenario-21) . . . . .	50
Figure 3.7 Torque commands applied to the wheels for Scenario 20 (red: cruise controller with 110 km/h speed reference, green: cruise controller with 90 km/h speed reference, blue: cruise controller with 70 km/h speed reference and black: energy optimal controller; top left: front left wheel, top right: front right wheel, bottom left: rear left wheel and bottom right: rear right wheel) . . . . .	52
Figure 3.8 Longitudinal friction forces applied to the wheels for Scenario 19 (red: cruise controller with 110 km/h speed reference, green: cruise controller with 90 km/h speed reference, blue: cruise controller with 70 km/h speed reference and black: energy optimal controller; top left: front left wheel, top right: front right wheel, bottom left: rear left wheel and bottom right: rear right wheel) . . . . .	52

Figure 3.9	Change in state of charge of vehicle battery package (black: cruise controller with 110 km/h speed reference, red: cruise controller with 90 km/h speed reference, green: cruise controller with 70 km/h speed reference and blue: energy optimal controller; top right: Scenario-09, top left: Scenario-10, bottom right: Scenario-11 and bottom left: Scenario-12) . . .	54
Figure 3.10	Skidding conditions of the wheels under different controllers in icy sloped version of Scenario-01 (red: cruise controller with 110 km/h speed reference, green: cruise controller with 90 km/h speed reference, blue: cruise controller with 70 km/h speed reference and black: energy optimal controller; top left: front left wheel, top right: front right wheel, bottom left: rear left wheel and bottom right: rear right wheel) . . . . .	55
Figure 3.11	Skidding compensation logic transfers the command to be applied during wheel slippage to the instants prior to the skidding section . . . . .	56
Figure 4.1	Motion representation for vehicle cornering . . . . .	66
Figure 4.2	Optimal controller design algorithm . . . . .	67
Figure 4.3	Normalized difference between modified and discontinuous Hamiltonian functions for different values of $\eta$ . . . . .	70
Figure 4.4	Time consumptions of the controllers: $t_{min}$ : minimum time to complete the road (with the maximum speed in the range), $t_{max}$ : maximum time to complete the road (with the minimum speed in the range), $t_{cc}$ : time to complete the road under cruise controller, $t_{eo}$ : time to complete the road under energy optimal controller, $t_{to}$ : time to complete the road under time optimal controller . . . . .	73
Figure 4.5	Positions and accelerations of the vehicle under different controllers (top: cruise controller, middle: energy optimal controller and bottom: time optimal controller) . . . . .	75

Figure 4.6 Speed of the vehicle under different controllers (solid line: cruise controller, dashed line: energy optimal controller and dash-dotted line: time optimal controller) . . . . .	76
Figure 4.7 Torque commands applied to the vehicle under different controllers (solid line: cruise controller, dashed line: energy optimal controller and dash-dotted line: time optimal controller; top left: front left wheel, top right: front right wheel, bottom left: rear left wheel and bottom right: rear right wheel) . . . . .	77
Figure 4.8 Friction forces on the wheels of the vehicle under different controllers (solid line: cruise controller, dashed line: energy optimal controller and dash-dotted line: time optimal controller; top left: front left wheel, top right: front right wheel, bottom left: rear left wheel and bottom right: rear right wheel) . . . . .	78
Figure 4.9 Pareto-front analysis of multi-objective energy and time optimization with NSGA-II algorithm . . . . .	80
Figure 4.10 Speed profiles for the steps along Pareto-front of time and energy multi-objective controller (colour codes matches with Fig. 4.9) . . . . .	80
Figure 4.11 Torque commands applied to the wheels along Pareto-front of time and energy multi-objective controller (colour codes matches with Fig. 4.9; top left: front left wheel, top right: front right wheel, bottom left: rear left wheel and bottom right: rear right wheel) . . . . .	81
Figure 4.12 Pareto-Front for Time and Energy Multi-Objective Optimization and Weighted Optimal Control Results . . . . .	82

Figure 4.13 Speed profiles of the vehicle under optimal control strategies for different passenger configurations (red: *Configuration-1* and time optimal, orange: *Configuration-2* and time optimal, light green: *Configuration-3* and time optimal, green: *Configuration-4* and time optimal, turquoise: *Configuration-1* and energy optimal, blue: *Configuration-2* and energy optimal, violet: *Configuration-3* and energy optimal, and purple: *Configuration-4* and energy optimal) . . . . . 84

Figure 4.14 Torque commands applied to the wheels of the vehicle under optimal control strategies for different passenger configurations; (red: *Configuration-1* and time optimal, orange: *Configuration-2* and time optimal, light green: *Configuration-3* and time optimal, green: *Configuration-4* and time optimal, turquoise: *Configuration-1* and energy optimal, blue: *Configuration-2* and energy optimal, violet: *Configuration-3* and energy optimal, and purple: *Configuration-4* and energy optimal; top left: front left wheel, top right: front right wheel, bottom left: rear left wheel and bottom right: rear right wheel) . . . . . 85

Figure 5.1 Motion representation for vehicle handling problem . . . . . 90

Figure 5.2 Solution approach for vehicle handling problem . . . . . 92

Figure 5.3 The outer layer optimization logic . . . . . 94

Figure 5.4 The inner layer optimization logic . . . . . 97

Figure 5.5 Definitions of vehicle statuses,  $\Theta = [p_d, v, \theta]^T$ ;  $p_d$ : radial position deviation normalized with rotation radius ( $r$ ),  $v$ : velocity of the vehicle,  $\theta$ : angle of velocity of the vehicle with respect to tangent of the desired route 99

Figure 5.6 Vehicle cornering under control of autopilots with different number of clusters for scenario  $r = 115m, \mu = 0.19$  (green:  $k=20$ , blue:  $k=10$  and red:  $k=5$ ) . . . . . 101

Figure 5.7 Vehicle cornering under control of autopilots with different number of clusters for scenario $r = 110m, \mu = 0.19$ (green: $k=20$ , blue: $k=10$ and red: $k=5$ ) . . . . .	102
Figure 5.8 Autopilot results compared with off-line optimization results, for $r = 115m, \mu = 0.19$ , normalized differences on various features (blue: position error, red: rotation radius commands, yellow: velocity of the vehicle and violet: power consumption of the vehicle) . . . . .	103
Figure 5.9 Autopilot results compared with off-line optimization results, for $r = 110m, \mu = 0.19$ , normalized differences on various features (blue: position error, red: rotation radius commands, yellow: velocity of the vehicle and violet: power consumption of the vehicle) . . . . .	104
Figure 5.10 Autopilot performance for $r = 112m, \mu = 0.19$ with runtime scheduling of the weighted-interpolation the rule bases from different rotation radii (black: ground truth, blue: rule bases of $r = 115m, \mu = 0.19$ only, red: rule bases of $r = 110m, \mu = 0.19$ only and green: runtime scheduling of the weighted-interpolation of the rule bases) . . . . .	105
Figure 5.11 Autopilot performance measures for $r = 112m, \mu = 0.19$ with runtime scheduling of the weighted-interpolation of the rules from different rotation radii, normalized differences on various features (blue: rule bases of $r = 115m, \mu = 0.19$ only, red: rule bases of $r = 110m, \mu = 0.19$ only and green: runtime scheduling of the weighted-interpolation of the rule bases) . . . . .	106
Figure 5.12 Test road with gradually decreasing friction coefficient . . . . .	107
Figure 5.13 Autopilot performance for $r = 110m, \mu = 0.72 - 0.19$ with runtime scheduling of the weighted-interpolation of the rules from different friction coefficients (black: ground truth, red: rule bases of $r = 110m, \mu = 0.19$ only, blue: rule bases of $r = 110m, \mu = 0.24$ only, cyan: rule bases of $r = 110m, \mu = 0.72$ only, and green: runtime scheduling of the weighted-interpolation of the rule bases) . . . . .	108

Figure 5.14 Autopilot performance measures for  $r = 110m, \mu = 0.72 - 0.19$  with runtime scheduling of the weighted-interpolation of the rules from different friction coefficients, normalized differences on various features (red: rule bases of  $r = 110m, \mu = 0.19$  only, blue: rule bases of  $r = 110m, \mu = 0.24$  only, cyan: rule bases of  $r = 110m, \mu = 0.72$  only, and green: runtime scheduling of the weighted-interpolation of the rule bases) 109

## LIST OF ABBREVIATIONS

$F$	Force ( $N$ )
$M$	Moment ( $Nm$ )
$m$	Mass ( $kg$ )
$I$	Moment of inertia ( $kg\ m^2$ )
$a$	Linear acceleration ( $m/s^2$ )
$\alpha$	Angular acceleration ( $rad/s^2$ )
$v$	Linear velocity ( $m/s$ )
$\omega$	Angular velocity ( $rad/s$ )
$x$	Longitudinal position ( $m$ )
$\phi$	Roll position ( $rad$ )
$\theta$	Pitch position ( $rad$ )
$\psi$	Yaw position ( $rad$ )
$CoG$	Centre of gravity of the vehicle
$l$	Distance to $CoG$ ( $m$ )
$R$	Radius of the wheels ( $m$ )
$G$	Gravitational force ( $N$ )
$D$	Drag coefficient]
$A$	Nominal cross sectional area of the vehicle ( $m^2$ )
$\rho$	Density ( $kg/m^3$ )
$\mu$	Friction coefficient
$SoC$	State of charge of the battery package
$J$	Cost function
$u$	Unit vector entry
$\eta$	Smoothing factor
$\mathcal{H}$	Hamiltonian function
$\gamma$	One dimensional search step
$\beta$	One dimensional search step rate
$\mathcal{F}$	Reference frame

$\hat{C}^{(x,y)}$	The transformation matrix from $\mathcal{F}_y$ to $\mathcal{F}_x$
$\mathbb{C}$	Cluster
$\Theta$	Vehicle status vector
$\mathbf{x}$	State vector
$\mathbf{p}$	Augmented state
$\mathbf{f}$	An abstract representation of the function in the vehicle model: $\dot{\mathbf{x}} = \mathbf{f} \left( \mathbf{x}, SoC, M_{wc,y}^{(c)} \right)$
$\mathbf{u}$	Control input vector at a time instant
$\mathbf{U}$	Time-discretized augmented control vector
$\hat{\mathbf{U}}$	Position-discretized augmented control vector

#### Subscripts (before comma)

$c$	Chassis
$fl$	Front left wheel
$fr$	Front right wheel
$rl$	Rear left wheel
$rr$	Rear right wheel
$a$	Surrounding air
$g$	Ground
$w$	Any of the wheel
$v$	Vehicle including chassis and the wheels
$s$	Static
$d$	Dynamic
$l$	Lagrange multiplier
$ab$	To destination $a$ from source $b$

#### Subscripts (after comma)

$x$	Component in $x$ -axes
$y$	Component in $y$ -axes
$z$	Component in $z$ -axes
$k$	Time instant stamp
$i$	Iteration stamp

#### Superscripts (indicating the reference frame)

$(c)$	In chassis-fixed reference frame
$(w)$	In the wheel-fixed reference frame (valid for each wheel)
$(o)$	In pseudo-inertial Earth-fixed reference frame

# CHAPTER 1

## INTRODUCTION

### 1.1 Motivation

Mankind of our age produce new technologies very fast and bound their life to these technologies even faster. Within less than one and a half century, auto-mobiles has become part of many people's life, and it is estimated that today there are more than one billion auto-mobiles around the world [50]. Conventional internal combustion engine-powered vehicles, matured over the last 100 years, have the majority share in private transportation means; yet they still require significant improvements to reduce their fuel consumption and pollution emissions [14].

Electric vehicles (EVs) are proposed as a highly-efficient environmentally friendly alternative in private transportation. They have one or sometimes more electric motors which have high efficiency in electric to mechanical power transformation and fast response in control loops. The electric motors are powered with rechargeable battery packages. With their propulsion systems, EVs can be considered to have zero pollutant emission [24, 54]. That's why the increasing public concerns of the environmental issues and energy efficiency praise electric vehicles [27, 26, 60].

Electric vehicles are known to be cutting-edge of technology; however, we were introduced to them as long time ago as the vehicles with conventional internal combustion engines were first deployed. Following the invention of the first DC-powered motor by Joseph Henry in 1830, the first practical EV is created by Thomas Davenport in 1834. In 1851, Charles Page built a 20 mph electric car. The rechargeable battery was introduced in 1859, and in 1899 Camille Jenatzy achieved a speed record of 66 mph with an electric vehicle powered by two 12 V motors. It has been recorded that by 1912, there were 34000 electric vehicles registered in the U.S. and 50 companies were producing them between 1895 and 1920 [6]. In 1912, the invention of electric starters by Charles Kettering eliminated problems in gasoline-powered cars and the conventional internal combustion engines gained the dominion over the transportation sector. However, the environmental pollution and rapid depletion of the natural resources start to shake the throne of the conventional engines and electric vehicles are considered as an alternative again at the dawn of the new century.

On the other hand, the electric vehicles have their own limitations. There are some challenges related with current battery technology, resulting in shorter driving range, longer charging time and higher battery cost [57]. These drawbacks of EVs boost

researches on both improving the battery technology and optimizing the energy usage of the vehicle [55].

This thesis has a chapter devoted to efficient energy management policies for electric vehicles. The major advantage of the electric vehicles over the conventional vehicles are their capability to generate and save energy during regenerative braking. The effective means to benefit from regenerative braking maximally can be developed, especially for roads with uphill and downhill sections. In the thesis, following a detailed literature review, these problems are tried to be solved by methods based on classical optimal control theory.

The design of controllers with various objectives requires a complete and correct modelling of the vehicle. Mike Blundell, et al. notes the following comment in the introduction section of their book entitled as *Multi Body Systems Approaches to Vehicle Dynamics* [9].

*"In 1969, man travelled to the moon and back, using maths invented by Kepler, Newton and Einstein to calculate trajectories hundreds of thousands of miles long and spacecraft with less on-board computing power than today's pocket calculator. With today's computing power and the mathematical frameworks handed down to us by Newton and Lagrange, it is scarcely credible that the motor car, itself over 100 years old, can exercise so many minds and still show scope for improvement. Yet we are still repeating errors in the dynamic design of our vehicles that were made in the 1960s."*

It has been observed that, the literature of vehicle control studies, uses simplified motion models for vehicles. The coupling between motions along different axes are sometimes ignored, or the fidelity of the power consumption dynamics are selected inadequate. The methods proposed in the literature lack being valid in all the cases whether the wheels are in slippage or not. Hence, in this thesis, before the optimal control problems being handled, a detailed mathematical model incorporated with wheel skidding kinematics and the power consumption dynamics of the vehicle is presented. The high fidelity model is used in all the considered problems.

As the amount of time we spent in auto-mobiles increases, the accidents caused by or with cars become a major problem. The first driving accident was recorded in 1770, just a year after the development of the first motor driven vehicle, and since then researches to understand the nature of accidents and to find the ways to avoid them have been conducted [33]. It has been observed that the incidence of the car accidents occur when the vehicle is under not under drivers control is over 50% [74]. Vehicle handling defines a measure of control of vehicle according to the drivers command. Other than mechanical problems, the wheel slippage is the main cause of low vehicle handling [38].

A detailed literature review on the systems developed by the engineers throughout the years to prevent wheel skidding and to increase handling capabilities are introduced in this thesis. A method to find control commands that optimizes the vehicle handling along roads with different friction coefficients is proposed, and data collected through motions with optimized handling performances are used to generate rules to be used in the runtime decision making process of the autopilot proposal.

## 1.2 Thesis Organization and Contributions

This thesis is composed of six chapters: Chapter 1: Introduction, Chapter 2: Mathematical Modelling, Chapter 3: Energy Optimality, Chapter 4: Vehicle Cornering, Chapter 5: Vehicle Handling and Chapter 6: Conclusions.

In Chapter 2: Mathematical Modelling, a mathematical model of an electrically driven, four-wheel vehicle will be explained. The vehicle is considered to be front-drive, front-steering, and all wheels able to brake. In the literature, depending on the application, mathematical models with different fidelity has been proposed for electric vehicles. The mathematical models used in optimal vehicle cornering problem, as well as other yaw motion characteristics, such as yaw stability, of the vehicle are quite simplified models [62, 32]. Similar to the one employed in this study; however, a vehicle model can be constructed as a combination of subsystems such as the chassis, the suspended body and the wheels [9, 78, 4].

The chapter starts with definition of reference frames and the transformations between the reference frames. Vector and matrix representations of dynamic relationships, i.e., Newton-Euler equations are stated. Aerodynamic forces and moments, and interaction forces and moments due to suspension system are explained. Then, wheel dynamics are studied. The chapter continues with calculations of angular velocities and angular accelerations. Thereafter, an overall dynamic motion model of the vehicle is presented. The cornering behaviour is introduced. The power consumption dynamics are presented to complete the model the electric vehicle.

One of the main aims of this thesis is to develop an overall detailed mathematical model of an electric vehicle. This model is then can be simplified to study different problems such as energy, time and handling optimality. Necessary assumptions related to gross motion of the vehicle are made to simplify the model for handling the optimal control problems addressed in this thesis.

The gross motion model developed is tested in three scenarios: uphill/downhill motion along asphalt road, braking along asphalt and icy roads, and cornering around asphalt roads. The aim is to give an insight about the validity of the developed method compared against the daily-life experiences. It has been observed that in Matlab/Simulink 2016b, there is a vehicle model for longitudinal motion only. The first scenario is tested against the model in Matlab/Simulink to verify the modelling approach with the commercial vehicle models.

In Chapter 3: Energy Optimality, for the gross motion model of the vehicle moving on a variable-slope road, an energy optimal controller is designed with torque, speed and battery constraints. The energy consumption of the vehicle under the optimal controller is compared against the standard cruise controllers of various speed references in several scenarios including uphill and downhill motions with various slopes and lengths. According to the simulation results, the optimal controller is shown to be more energy efficient than the cruise controllers in all the considered scenarios.

The tests are repeated along icy road sections, and the superiority of the energy optimal controller is verified for roads with low friction coefficients as well. A skidding compensation logic is proposed and tested to minimize the wheel slippage and it is

observed that energy optimality of the solution is not affected by this compensation. A sensitivity analysis has been performed and it has been shown that, as a representative of different combinations of passengers, the sensitivity of the energy optimal controller on the mass change and distribution is small in magnitude. Furthermore, the tests with different initial values of the state-of-charge of the battery demonstrates that the superiority of the energy optimal controller against cruise controllers becomes significant especially when the battery is not fully charged and battery characteristics limit the charging capability during regenerative braking. The assumptions and the coverage of the presented optimal control approach is compared qualitatively with some recent studies addressing the similar problems.

This chapter introduces the following outcomes:

1. Energy optimal control problem is defined for the vehicle. The problem is a free-final time problem. On the other hand, the distance to be travelled is fixed. A numerical method based on mapping the control inputs from the time domain to position domain has been developed and utilized to satisfy the fixed distance constraint (see Section 3.2).
2. The energy optimal controller is compared against cruise controller with different reference speeds in extensive simulations. The results depicts the superiority of the energy optimal controller. The energy optimal solutions obey the speed constraints, avoids wheel slippage, and completes the roads in a travel time still comparable with the cruise controllers (see Section 3.3).
3. The energy optimal controller is shown to preserve its superiority in terms of the energy consumption of the electric vehicle for all the considered scenarios where the uphill and downhill sections of the road is icy. A skidding compensation logic is proposed to reduce the wheel slippage. The results show that, with no compromise in energy consumption of the vehicle, the occurrence of the wheel slippage is reduced with this compensation (see Section 3.4).
4. It has been shown that as a representative of different combinations of passengers, the sensitivity of the energy optimal controller on the mass change and distribution is smaller in magnitude. Furthermore, the tests with different initial values of the state-of-charge of the battery demonstrates that the superiority of the energy optimal controller against cruise controllers becomes significant especially when the battery is not fully charged and battery characteristics limit the charging capability during regenerative braking (see Section 3.5).

A qualitative comparison with the literature is performed and the following points are presented as the main contributions of this study (see Section 3.6):

1. A numerical method based on mapping the control inputs from the time domain to position domain has been proposed to deal with the free-final time two point boundary value problems.
2. A skidding compensation approach is proposed to reduce the percentages of the time instants when the wheels are in slippage. The skidding compensation

logic is shown to be effective in reducing slippage and it has been observed that the energy optimality of the solution is preserved.

3. The superiority of the optimal control theory based solution for the energy management problem of electric vehicles is shown with comparisons against standard cruise controllers in asphalt and icy roads, which depicts that autopilot designs for electric vehicles based on optimal control solutions will be far more energy efficient.
4. The low sensitivity of the energy optimal controller with respect to passenger arrangements and initial state-of-charge of the battery in electric vehicles are demonstrated.

The results of the studies introduced in Chapter 3: Energy Optimality are submitted to publication in *"International Journal of Control"* with an article entitled as *"Energy Optimal Controller for an Electric Vehicle on a Variable-Slope Road"*. Furthermore, some sections of the chapter are presented in a conference article in *"15th International Conference on Control, Automation and Systems (ICCAS 2015)"* entitled as *"Energy Optimal Controller for Electric Vehicles on Partially Icy Roads with Heuristic Skidding Compensation"*, see [4].

In Chapter 4: Vehicle Cornering, vehicle cornering under constant Ackerman's steering law is investigated. The average power consumption of the vehicle, and the amount of time vehicle corners the circular arc are calculated as merits of energy and time optimal control problems. Applying wheel torque, vehicle speed and battery power constraints to the problem, the performances of the optimal controllers are evaluated in simulations. In terms of battery charge and time consumption measures, the behaviour of the vehicle under optimal controllers are compared with those under cruise controllers. The simulation results confirm the effectiveness of the optimal controllers against standard cruise controllers.

A Pareto-front analysis is carried out with multi-objective energy and time minimization using NSGA-II algorithm. The analysis provides a multi-objective solution of the vehicle cornering problem with a compromise between travel time and energy consumption of the vehicle that enables vehicle to complete cornering with minimum energy consumption within the given speed limits. The optimality of the Pareto-front results are discussed. Furthermore, a sensitivity analysis is performed and it is confirmed that the optimal control solution is insensitive to the different passenger seating arrangements.

The studies in this chapter aim to generate the following contributions to the literature available on the optimality problem in vehicle cornering motion:

1. The optimal control problem is discussed on vehicle mathematical model which is sufficiently detailed to be applicable for any gross motion. In addition to the motion model, battery model and regenerative braking capability of the electric drive are included.
2. The classical optimal control is shown to be a valid and applicable technique for time and energy optimization for vehicle motion. Time and energy optimality problems are both handled in a single solution structure.

3. Both time and energy optimal control problems are free-final time problems. On the other hand, the distance to be covered is chosen to be fixed. A numerical method based on mapping the control inputs from the time domain to the position domain has been developed and utilized to satisfy the fixed distance constraint.
4. It has been shown with NSGA-II genetic algorithm that there is a Pareto-front between time and energy optimization problems. The optimality of this Pareto-front is validated with classical optimal control approach.
5. A sensitivity analysis is performed and it is confirmed that the optimal control solution is insensitive to the different passenger seating arrangements.

The results of the studies introduced in Chapter 4: Vehicle Cornering are submitted to publication in *"Optimal Control Applications and Methods"* with an article entitled as *"Multi Objective Optimal Vehicle Cornering Behaviour under Constant Ackermann Steering"*.

In Chapter 5: Vehicle Handling, vehicle cornering around roads with low friction coefficients is studied and an autopilot design is proposed to satisfy desired handling performance. A novel hierarchical optimization approach is presented to generate off-line solutions for cornering along roads with different friction coefficients and radii of curvature. Vehicle motion as the output of this optimization process, together with vehicle states and control commands at each sampling time are generated and stored for different selected scenario parameters with various rotation radii and friction coefficients. A vehicle status definition is presented as a function of vehicle states that contains the most informative data to evaluate the vehicle handling performance. The vehicle statuses at each decision instant among these off-line optimized data are clustered with the k-means clustering technique. These are associated with the control commands applied. A cluster centre-control command corresponds to a rule that produces the unique control command to be applied as a function of vehicle status. The autopilot is constructed by a convex combination of these rules. This basic idea of autopilot design has been extended for motion along a specific rotation radii and friction coefficients; the control commands corresponding to arbitrary scenario parameters are obtained by a runtime scheduling of the weighted-interpolation among the control commands corresponding to different scenario parameters.

Vehicles under autopilots with different number of clusters are tested in cornering motions along the icy roads, and according to the vehicle handling performances, the number of clusters is tuned. The autopilot design is compared with the off-line optimized control command sequences along the same test scenarios. It has been observed that performance of a vehicle under autopilot control does not differentiate from those under off-line optimized control commands in terms of vehicle states, vehicle handling performances and energy consumptions more than 5%. The performance of the autopilot proposal is also tested with different scenarios, and the approach based on runtime scheduling of the weighted-interpolation between the control commands corresponding to different scenario parameters is verified.

The main contributions of the studies introduced in this chapter can be summarized as follows:

1. The vehicle handling problem is tried to be solved with a high fidelity mathematical model of electric vehicles for all road conditions.
2. An optimization technique, as proposed in the outer layer of the hierarchical optimization procedure, to find the probably complex solution of the relatively difficult problem, cornering around icy roads, is presented. The method attacks the problem by proposing simpler solutions to the relatively easier problems, cornering around higher friction roads, and gradually decreasing the friction coefficients.
3. An optimization technique, as proposed in the inner layer of the hierarchical optimization procedure, to minimize deviation of the position of the vehicle from the desired route, is presented. The method makes search around a neighbourhood of a solution proposal in a search cone. The centreline of the search cone is generated as the difference between two consecutive optimization steps, and the volume of the cone is adjusted according to the changes in the cost throughout these steps.
4. An autopilot for vehicle cornering around icy roads is proposed based on runtime decision making process. The rule sets to be used in the process are generated by clustering the vehicle statuses and calculating control command vectors at centroids of each clusters. The control commands corresponding to arbitrary scenario parameters are obtained by a runtime scheduling of the weighted-interpolation among the control commands corresponding to different scenario parameters

The results of the studies introduced in Chapter 5: Vehicle Handling are submitted to publication in "*IEEE Transactions on Vehicular Technology*" with an article entitled as "*Autopilot Design for Vehicle Cornering Through Icy Roads*".



## CHAPTER 2

### MATHEMATICAL MODELLING

In this chapter, mathematical modelling of an electrically driven, four-wheel vehicle will be explained. The vehicle is considered to be front-drive, front-steering, and all wheels are able to brake. In the literature, depending on the application, mathematical models with different fidelities have been proposed for electric vehicles. The mathematical models used in the optimal vehicle cornering problem, as well as other yaw motion characteristics, such as yaw stability, of the vehicle are quite simplified models [62, 32]. Similar to the one employed in this study; however, a vehicle model can be constructed as a combination of subsystems such as the chassis, the suspended body and the wheels [9, 78, 4].

The chapter starts with definition of reference frames and the transformations between the reference frames. Vector and matrix representations of dynamic relationships, i.e., Newton-Euler equations are stated. Aerodynamic forces and moments, and interaction forces and moments due to the suspension system are explained. Then, wheel dynamics are studied. The chapter continues with calculations of angular velocities and angular accelerations. Thereafter, an overall dynamic motion model of the vehicle is presented. The cornering behaviour is introduced. The power consumption dynamics are presented to complete of the model of the electric vehicle.

One of the main aims of this thesis is to develop a comprehensive mathematical model of an electric vehicle. This model includes the suspension characteristics as well. Depending on the motion scenarios, the model is then simplified to study different problems such as energy, time and handling optimality. The simplified model is such that the wheels and the suspension system are assumed to be rigid. The motion of the simplified model is designated as the "gross motion of the vehicle".

The simplified gross motion model mentioned above is tested in three scenarios: up-hill/downhill motion along asphalt road, braking along asphalt and icy roads, and cornering around asphalt roads. The aim of these tests is to verify the validity of the developed method as compared to the daily-life experiences. It has been observed that in Matlab/Simulink 2016b, there is a vehicle model for longitudinal motion only. Therefore, in the first scenario, the model used in this thesis is tested additionally against the model used in Matlab/Simulink. Both models gave similar results.

## 2.1 Reference Frames

In this section, reference frames are defined. There are four reference frames: Earth-fixed reference frame ( $\mathcal{F}_o$ ), local ground reference frame ( $\mathcal{F}_e$ ), chassis-fixed reference frame ( $\mathcal{F}_c$ ) and body-fixed reference frame ( $\mathcal{F}_b$ ).

### 2.1.1 Earth-Fixed Reference Frame

Earth-fixed reference frame is denoted by  $\mathcal{F}_o$ . This is an inertial reference frame with its  $z$ -axis towards the centre of Earth. The other two axes can be chosen to satisfy the right hand rule. The reference frame can have origin as the projection of the centre of gravity of the chassis ( $G_c$ ) at initial position.

It is assumed that, throughout the movement of the vehicle, the Earth surface is flat. In other words, the elliptic shape of the globe is ignored; however, the contact surface between wheels and the ground can be changing. Earth-fixed reference frame  $\mathcal{F}_o$  is depicted in Fig. 2.1.

### 2.1.2 Local Ground Reference Frame

The local ground reference frame is denoted by  $\mathcal{F}_e$ . The frame is also called wheel-base frame. It moves with the vehicle so that the contact points of the wheels are on it. It is assumed that all four wheel contacts with the ground are confined in a common plane. The reference frame has  $x$ -axis towards the movement of the vehicle,  $y$ -axis in the direction towards lateral surface of vehicle, and  $z$ -axis according to right hand rule. The frame has origin as the projection of  $G_c$  on the frame.

The frame has roll and pitch orientations with respect to  $\mathcal{F}_o$ . The rates of change of these orientations are assumed to be small compared to the respective orientation changes of the chassis. Hence, it is assumed that the reference frame is parallel to the chassis fixed reference frame with a translation in common  $z$ -axis. Therefore, the contact points between ground and wheels are fixed on this reference frame.

It is also assumed that the ground surface is flat for any instant throughout the movement of the vehicle. Hence contact points of wheel all have 0 position in  $z$ -axis, corresponding to different  $z$ -positions in  $\mathcal{F}_o$  due to roll and pitch orientations of  $\mathcal{F}_e$  with respect to  $\mathcal{F}_o$ . The local ground reference frame  $\mathcal{F}_e$  is depicted in Fig. 2.1.

### 2.1.3 Chassis Fixed Reference Frame

Chassis fixed reference frame is denoted by  $\mathcal{F}_c$ . The reference frame has origin as  $G_c$ . It has  $x$ -direction in longitudinal axis of the chassis,  $y$ -direction in the lateral axis of the chassis and  $z$ -direction according to the right hand rule.  $\mathcal{F}_c$  is parallel in common  $z$ -axis with  $\mathcal{F}_e$ . The chassis fixed reference frame  $\mathcal{F}_c$  is depicted in Fig. 2.1.

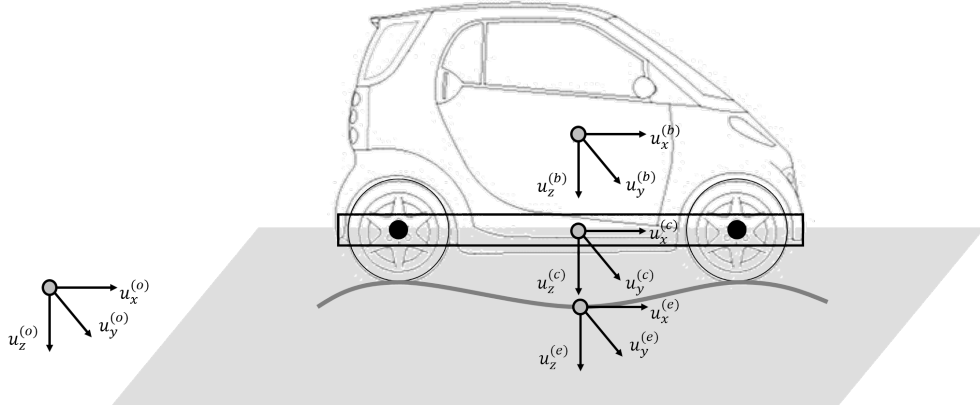


Figure 2.1: Reference frames defined in vehicle dynamics

### 2.1.4 Body Fixed Reference Frame

Body fixed reference frame is denoted by  $\mathcal{F}_b$ . The reference frame has origin as  $G_b$  of the suspended body of the vehicle which is connected to chassis with four suspension systems. It has  $x$ -direction in longitudinal axis of the body,  $y$ -direction in the lateral axis of the body and  $z$ -direction according to the right hand rule.  $\mathcal{F}_b$  has an orientation with respect to  $\mathcal{F}_c$ . It is assumed that due to mechanical limitations  $\mathcal{F}_b$  has no yaw orientation with respect to  $\mathcal{F}_c$ . The body fixed reference frame  $\mathcal{F}_b$  is depicted in Fig. 2.1.

### 2.1.5 Transformations between Reference Frames

Let  $\mathcal{F}_x$  and  $\mathcal{F}_y$  be two reference frames.  $\hat{C}^{(x,y)}$  is the transformation matrix from  $\mathcal{F}_y$  to  $\mathcal{F}_x$  so that the matrix representation of vector  $\vec{r}$  in  $\mathcal{F}_x$  and  $\vec{r}^{(x)}$ , i.e.,  $\vec{r}^{(x)} = \{\vec{r}\}_{\mathcal{F}_x}$  and  $\vec{r}^{(y)} = \{\vec{r}\}_{\mathcal{F}_y}$  are related as follows:

$$\vec{r}^{(x)} = \hat{C}^{(x,y)} \vec{r}^{(y)} \quad (2.1)$$

At the same time,  $\hat{C}^{(x,y)}$  represents orientation of  $\mathcal{F}_y$  with respect to  $\mathcal{F}_x$ . Multiple transformations between orientations of reference frames is also possible.

$$\hat{C}^{(x,z)} = \hat{C}^{(x,y)} \hat{C}^{(y,z)} \quad (2.2)$$

Inverse transformation is defined as:

$$\hat{C}^{(x,y)} = \hat{C}^{(y,x)^{-1}} = \hat{C}^{(y,x)^T} \quad (2.3)$$

A skew symmetric matrix is defined corresponding to its column matrix is defined as:

$$\bar{c} = \begin{bmatrix} c_x \\ c_y \\ c_z \end{bmatrix} \Rightarrow \tilde{c} = \begin{bmatrix} 0 & -c_z & c_y \\ c_z & 0 & -c_x \\ -c_y & c_x & 0 \end{bmatrix} \quad (2.4)$$

A general orientation matrix can be written as:

$$\begin{aligned} \hat{C}^{(x,y)} &= e^{\tilde{u}_z \psi_{xy}} e^{\tilde{u}_y \theta_{xy}} e^{\tilde{u}_x \phi_{xy}} \\ &= \begin{bmatrix} \cos(\psi_{xy}) & -\sin(\psi_{xy}) & 0 \\ \sin(\psi_{xy}) & \cos(\psi_{xy}) & 0 \\ 0 & 0 & 1 \end{bmatrix} \begin{bmatrix} \cos(\theta_{xy}) & 0 & \sin(\theta_{xy}) \\ 0 & 1 & 0 \\ -\sin(\theta_{xy}) & 0 & \cos(\theta_{xy}) \end{bmatrix} \begin{bmatrix} 1 & 0 & 0 \\ 0 & \cos(\phi_{xy}) & -\sin(\phi_{xy}) \\ 0 & \sin(\phi_{xy}) & \cos(\phi_{xy}) \end{bmatrix} \end{aligned} \quad (2.5)$$

Using (2.5), orientation matrices between the defined reference frames can be defined. Between local ground reference frame ( $\mathcal{F}_e$ ) and Earth-fixed reference frame ( $\mathcal{F}_o$ ) all three orientations are different than zero.

$$\hat{C}^{(o,e)} = e^{\tilde{u}_z \psi_{oe}} e^{\tilde{u}_y \theta_{oe}} e^{\tilde{u}_x \phi_{oe}} \quad (2.6)$$

Between chassis-fixed reference frame ( $\mathcal{F}_c$ ) and local ground reference frame ( $\mathcal{F}_e$ ), roll and pitch orientations are very small, and yaw orientation of ( $\mathcal{F}_e$ ) is chosen to be coincided with that of ( $\mathcal{F}_c$ ).

$$\phi_{ec} \approx 0, \theta_{ec} \approx 0, \psi_{ec} = 0 \quad (2.7)$$

$$\begin{aligned} \hat{C}^{(e,c)} &= e^{\tilde{u}_z \psi_{ec}} e^{\tilde{u}_y \theta_{ec}} e^{\tilde{u}_x \phi_{ec}} = (\hat{I}) e^{\tilde{u}_y \theta_{ec}} e^{\tilde{u}_x \phi_{ec}} \\ &= (\hat{I})(\hat{I} + \tilde{u}_y \theta_{ec})(\hat{I} + \tilde{u}_x \phi_{ec}) = \hat{I} + \tilde{u}_y \theta_{ec} + \tilde{u}_x \phi_{ec} \approx \hat{I} \end{aligned} \quad (2.8)$$

$$\hat{C}^{(o,c)} = \hat{C}^{(o,e)} \hat{C}^{(e,c)} \approx \hat{C}^{(o,e)} \quad (2.9)$$

Between body-fixed reference frame ( $\mathcal{F}_b$ ) and chassis-fixed reference frame ( $\mathcal{F}_c$ ), there is no yaw orientation due to mechanical limitations, but roll and pitch orientations exist, yet they are very small as well.

$$\phi_{cb} \approx 0, \theta_{cb} \approx 0, \psi_{cb} = 0 \quad (2.10)$$

$$\hat{C}^{(c,b)} = e^{\tilde{u}_z \psi_{cb}} e^{\tilde{u}_y \theta_{cb}} e^{\tilde{u}_x \phi_{cb}} = (\hat{I}) e^{\tilde{u}_y \theta_{cb}} e^{\tilde{u}_x \phi_{cb}} = \hat{I} + \tilde{u}_y \theta_{cb} + \tilde{u}_x \phi_{cb} \approx \hat{I} \quad (2.11)$$

$$\hat{C}^{(e,b)} = \hat{C}^{(e,c)} \hat{C}^{(c,b)} \approx \hat{I} \quad (2.12)$$

$$\hat{C}^{(o,b)} = \hat{C}^{(o,e)} \hat{C}^{(e,c)} \hat{C}^{(c,b)} \approx \hat{C}^{(o,e)} \quad (2.13)$$

Inverse transformations are transpose of the forward transformations. The reference frame is depicted in Fig. 2.1.

## 2.2 Vector Form of Dynamic Relationships

In this section, vector form of Newton-Euler equations for chassis and suspended body [68] are presented.

### 2.2.1 Vector Newton-Euler Equations for the Chassis

$$m_c \vec{a}_{oc} = \sum_{k=1}^4 \left( \vec{F}_{w_k c} + \vec{F}_{s_k c} \right) + m_c \vec{g} \quad (2.14)$$

$$\hat{J}_c \cdot \vec{\alpha}_{oc} + \vec{\omega}_{oc} \times \hat{J}_c \cdot \vec{\omega}_{oc} = \sum_{k=1}^4 \left[ \left( \vec{M}_{w_k c} + \vec{M}_{s_k c} \right) + \vec{r}_{cp_k} \times \left( \vec{F}_{w_k c} + \vec{F}_{s_k c} \right) \right] \quad (2.15)$$

In 2.14 and 2.15,

$\vec{g}$  is the acceleration of gravity.

$m_c$  is the mass of the chassis.

$\hat{J}_c$  is the inertia tensor of the chassis about its centre of mass  $G_c$ .

$\vec{a}_{oc} = (d^2 \vec{r}_{oc} / dt^2) |_{\mathcal{F}_o}$  is the acceleration of  $G_c$  with respect to  $\mathcal{F}_o(O_o)$ .

$\vec{r}_{oc} = \vec{r}_{O_o G_c}$  is the position vector of  $G_c$ . with respect to  $\mathcal{F}_o(O_o)$ .

$\vec{\omega}_{oc}$  is the angular velocity of the chassis with respect to  $\mathcal{F}_o(O_o)$ .

$\vec{\alpha}_{oc} = (d\vec{\omega}_{oc}/dt) |_{\mathcal{F}_o}$  is the angular acceleration of the chassis with respect to  $\mathcal{F}_o(O_o)$ .

$\vec{F}_{w_k c}$  is the interaction force applied by the  $k$ -th wheel to the chassis.

$\vec{F}_{s_k c}$  is the interaction force applied by the  $k$ -th suspension unit to the chassis.

$\vec{M}_{w_k c}$  is the interaction moment applied by the  $k$ -th wheel to the chassis about the wheel centre  $C_k$ .

$\vec{M}_{s_k c}$  is the interaction moment applied by the  $k$ -th suspension unit to the chassis about the connection point  $P_k \approx C_k$ .

$\vec{r}_{cp_k}$  is the position vector of  $P_k \approx C_k$  with respect to  $\mathcal{F}_c(G_c) = \mathcal{F}_c(O_c)$ .

### 2.2.2 Vector Newton-Euler Equations for the Suspended Body

$$m_b \vec{a}_{ob} = \sum_{k=1}^4 \vec{F}_{s_k b} + \vec{F}_{ab} + m_b \vec{g} \quad (2.16)$$

$$\hat{J}_b \cdot \vec{\alpha}_{ob} + \vec{\omega}_{ob} \times \hat{J}_b \cdot \vec{\omega}_{ob} = \sum_{k=1}^4 \left[ \vec{M}_{s_k b} + \vec{r}_{bp_k} \times \vec{F}_{s_k b} \right] + \vec{M}_{ab} \quad (2.17)$$

In 2.16 and 2.17,

$m_b$  is the mass of the suspended body.

$\hat{J}_b$  is the inertia tensor of the suspended body about its centre of mass  $G_b$ .

$\vec{a}_{ob} = (d^2 \vec{r}_{ob} / dt^2) |_{\mathcal{F}_o}$  is the acceleration of  $G_b$  with respect to  $\mathcal{F}_o(O_o)$ .

$\vec{r}_{ob} = \vec{r}_{O_o G_b}$  is the position vector of  $G_b$ . with respect to  $\mathcal{F}_o(O_o)$ .

$\vec{\omega}_{ob}$  is the angular velocity of the suspended body with respect to  $\mathcal{F}_o(O_o)$ .

$\vec{\alpha}_{ob} = (d\vec{\omega}_{ob}/dt)|_{\mathcal{F}_o}$  is the angular acceleration of the suspended body with respect to  $\mathcal{F}_o(O_o)$ .

$\vec{F}_{s_k b}$  is the interaction force applied by the  $k$ -th suspension unit to the suspended body.

$\vec{M}_{s_k b}$  is the interaction moment applied by the  $k$ -th suspension unit to the suspended body about the wheel centre  $P_{bk} \approx C_k$ .

$\vec{r}_{bp_k}$  is the position vector of  $P_{bk} \approx C_k$  with respect to  $\mathcal{F}_b(G_b) = \mathcal{F}_b(O_b)$ .

$\vec{F}_{ab}$  is the aerodynamic force applied to the suspended body.

$\vec{M}_{ab}$  is the aerodynamic moment applied to the suspended body about  $G_b$ .

## 2.3 Matrix Form of Dynamic Relationships

In this section, matrix form of Newton-Euler equations for chassis and suspended body are presented.

### 2.3.1 Matrix Newton-Euler Equations for the Chassis

$$m_c \hat{C}^{(c,o)} \bar{a}_{oc}^{(o)} = \sum_{k=1}^4 (\bar{F}_{w_k c}^{(c)} + \bar{F}_{s_k c}^{(c)}) + m_c g \hat{C}^{(c,o)} \bar{u}_z \quad (2.18)$$

$$\hat{J}_c^{(c)} \bar{\alpha}_{oc}^{(c)} + \tilde{\omega}_{oc}^{(c)} \hat{J}_c^{(c)} \bar{\omega}_{oc}^{(c)} = \sum_{k=1}^4 [\bar{M}_{w_k c}^{(c)} + \bar{M}_{s_k c}^{(c)} + \tilde{r}_{cp_k}^{(c)} (\bar{F}_{w_k c}^{(c)} + \bar{F}_{s_k c}^{(c)})] \quad (2.19)$$

### 2.3.2 Matrix Newton-Euler Equations for the Suspended Body

$$m_b \hat{C}^{(b,o)} \bar{a}_{ob}^{(o)} = \sum_{k=1}^4 \bar{F}_{s_k b}^{(b)} + m_b g \hat{C}^{(b,o)} \bar{u}_z + \bar{F}_{ab}^{(b)} \quad (2.20)$$

$$\hat{J}_b^{(b)} \bar{\alpha}_{ob}^{(b)} + \tilde{\omega}_{ob}^{(b)} \hat{J}_b^{(b)} \bar{\omega}_{ob}^{(b)} = \sum_{k=1}^4 \left( \bar{M}_{s_k b}^{(b)} + \tilde{r}_{bp_k}^{(b)} \bar{F}_{s_k b}^{(b)} \right) + \bar{M}_{ab}^{(b)} \quad (2.21)$$

## 2.4 Aerodynamic Forces and Moments

Aerodynamic forces and moments are acting on the suspended body. The forces are related to linear velocity of the suspended body. The disturbances due to wind gusts are neglected. The air drag force can be as follows:

$$\vec{F}_{ab} = -\frac{1}{2} \rho_a \|\vec{v}_{ob}\|^2 DA \frac{\vec{v}_{ob}}{\|\vec{v}_{ob}\|} \quad (2.22)$$

In (2.22),

$\rho_a$  is the density of air.

$D$  is the air drag coefficient as a function of angle of drag with respect to  $\vec{u}_x^{(b)}$ .

$A$  is the nominal surface area of the vehicle.

This force is in the opposite direction of  $\vec{v}_{ob}$  and it is assumed that  $\vec{F}_{ab,z}^{(b)} \approx 0$ .

If there is a difference between geometric centre of the vehicle and midpoint of  $A$ , then aerodynamic forces will result in moments as well. It is assumed that the vehicle is symmetric and its geometric centre coincides with its aerodynamic centre; hence, the air drag does not create a moment on the vehicle.

## 2.5 Suspension System Related Forces and Moments

It is assumed that suspension system between chassis and suspended mass can be modelled a spring and damper system [68]. The suspension system is assumed to induce forces only in  $\vec{u}_z^{(e)} \approx \vec{u}_z^{(c)} \approx \vec{u}_z^{(b)}$ .

$$\vec{F}_{s_k,z} = k_k(s_k - s_{0_k}) + b_k\dot{s}_k + u_k \quad (2.23)$$

In (2.23),

$k_k$  is the stiffness coefficient of  $k$ -th suspension unit.

$b_k$  is the damper coefficient of  $k$ -th suspension unit.

$s_k$  is the length of the  $k$ -th suspension unit.

$s_{0_k}$  is the free length of the  $k$ -th suspension unit.

$u_k$  is the active suspension force input to the  $k$ -th suspension unit.

$s_k$  is the length of the suspension unit at the corner connection points. Note that  $\vec{r}_{oc}^{(o)}$  and  $\vec{r}_{ob}^{(o)}$  can change; in other words, centre of gravities of chassis and suspended body are not supposed to be the same. However, the corner points are fixed and may have motion in  $\vec{u}_z^{(e)} \approx \vec{u}_z^{(c)} \approx \vec{u}_z^{(b)}$ . Small angle assumption can be made for  $\phi_{cb}$  and  $\theta_{cb}$ . Therefore,

$$s_k = \vec{u}_z^T \vec{r}_{ob}^{(o)} - \vec{u}_z^T \vec{r}_{oc}^{(o)} + \vec{u}_z^T \tilde{r}_{bp_k} \times [\phi_{cb} \theta_{cb} 0]^T \quad (2.24)$$

## 2.6 Wheel Dynamics and Interaction Forces and Moments

In this section, orientation matrices, and Newton-Euler equations in vector and matrix forms for the wheels are defined. Then the interaction forces and moments are explained. The vehicle has fixed axes for rear wheels and orientable axes for front wheels.

### 2.6.1 Orientation Matrices for the Wheels

Ignoring the slight deformations, the wheels can be considered to be spinning symmetric bodies. Thus, Newton-Euler equations can be defined in their associated non-spinning frames. Since rear wheels have fixed axes,  $\mathcal{F}_c$  can be used instead of  $\mathcal{F}_{w_{rl}}$  and  $\mathcal{F}_{w_{rr}}$ , and the orientation matrices are as follows.

$$\hat{C}^{(o,w_{rl})} = \hat{C}^{(o,w_{rr})} = \hat{C}^{(o,c)} \approx \hat{C}^{(o,e)} = e^{\tilde{u}_z \psi_{oe}} e^{\tilde{u}_y \theta_{oe}} e^{\tilde{u}_x \phi_{oe}} \quad (2.25)$$

Front wheels are steered by angles  $\psi_{fl}$  and  $\psi_{fr}$  about  $\tilde{u}_z^{(c)}$ ; hence, the orientation matrices for  $\mathcal{F}_{w_{fl}}$  and  $\mathcal{F}_{w_{fr}}$  can be written as follows.

$$\begin{aligned} \hat{C}^{(o,w_{fl})} &= \hat{C}^{(o,c)} \hat{C}^{(o,w_{fl})} \approx \hat{C}^{(o,e)} e^{\tilde{u}_z \psi_{fl}} = e^{\tilde{u}_x \phi_{oe}} e^{\tilde{u}_y \theta_{oe}} e^{\tilde{u}_z (\psi_{oe} + \psi_{fl})} \\ \hat{C}^{(o,w_{fr})} &= \hat{C}^{(o,c)} \hat{C}^{(o,w_{fr})} \approx \hat{C}^{(o,e)} e^{\tilde{u}_z \psi_{fr}} = e^{\tilde{u}_x \phi_{oe}} e^{\tilde{u}_y \theta_{oe}} e^{\tilde{u}_z (\psi_{oe} + \psi_{fr})} \end{aligned} \quad (2.26)$$

### 2.6.2 Vector Newton-Euler Equations for the Wheels

For each wheel,  $k = 1, 2, 3,$  and  $4$ :

$$m_{w_k} \vec{a}_{ow_k} = \vec{F}_{cw_k} + \vec{F}_{gw_k} + m_{w_k} \vec{g} \quad (2.27)$$

$$\hat{J}_{w_k} \cdot \vec{\alpha}_{ow_k} + \vec{\omega}_{ow_k} \times \hat{J}_{w_k} \cdot \vec{\omega}_{ow_k} = \vec{M}_{cw_k} + \vec{M}_{gw_k} + \vec{r}_{w_k q_k} \times \vec{F}_{gw_k} \quad (2.28)$$

In 2.27 and 2.28,

$m_{w_k}$  is the mass of the  $k$ -th wheel.

$\hat{J}_{w_k}$  is the inertia tensor of the  $k$ -th wheel about its centre of mass  $C_k$ .

$\vec{a}_{ow_k} = (d^2 \vec{r}_{ow_k} / dt^2) |_{\mathcal{F}_o}$  is the acceleration of  $C_k$  with respect to  $\mathcal{F}_o(O_o)$ .

$\vec{r}_{ow_k}$  is the position vector of  $C_k$  with respect to  $\mathcal{F}_o(O_o)$ .

$\vec{\omega}_{ow_k}$  is the angular velocity of the  $k$ -th wheel with respect to  $\mathcal{F}_o(O_o)$ .

$\vec{\alpha}_{ow_k} = (d\vec{\omega}_{ow_k} / dt) |_{\mathcal{F}_o}$  is the angular acceleration of the  $k$ -th wheel with respect to  $\mathcal{F}_o(O_o)$ .

$\vec{F}_{cw_k}$  is the interaction force applied by the chassis to the  $k$ -th wheel.  $\vec{F}_{cw_k} = -\vec{F}_{w_k c}$ .

$\vec{F}_{gw_k}$  is the interaction force applied by the ground to the  $k$ -th wheel.

$\vec{M}_{cw_k}$  is the interaction moment applied by the chassis to the  $k$ -th wheel about  $C_k$ .  $\vec{M}_{cw_k} = -\vec{M}_{w_k c}$ .

$\vec{M}_{gw_k}$  is the interaction moment applied by the ground to the  $k$ -th wheel by the contact point  $Q_k$ .

$\vec{r}_{w_k q_k}$  is the position vector of  $Q_k$  with respect to  $\mathcal{F}_{w_k}(C_k) = \mathcal{F}_{w_k}(O_{w_k})$ .

### 2.6.3 Matrix Newton-Euler Equations for the Wheels

For each wheel,  $k = 1, 2, 3,$  and  $4$ :

$$m_{w_k} \hat{C}^{(w_k, o)} \bar{u}_{ow_k}^{(o)} = \bar{F}_{cw_k}^{(w_k)} + \bar{F}_{gw_k}^{(w_k)} + m_{w_k} g \hat{C}^{(w_k, o)} \bar{u}_z \quad (2.29)$$

$$\hat{J}_{w_k}^{(w_k)} \bar{\alpha}_{ow_k}^{(w_k)} + \tilde{\omega}_{ow_k}^{(w_k)} \hat{J}_{w_k}^{(w_k)} \bar{\omega}_{ow_k}^{(w_k)} = \bar{M}_{cw_k}^{(w_k)} + \bar{M}_{gw_k}^{(w_k)} + \tilde{r}_{w_k q_k}^{(w_k)} \bar{F}_{gw_k}^{(w_k)} \quad (2.30)$$

#### 2.6.4 Interaction Forces and Moments

In this section interaction forces and moments applied by the ground on the wheels and the chassis are studied. The wheel has suspension system model as simple stiffness generating the force in  $\bar{u}_z^{(e)}$  from ground to the chassis through the wheels.

$$\vec{F}_{gw_k, z} = k_{w_k} (s_{w_k} - s_{0w_k}) \quad (2.31)$$

In (2.31),

$k_{w_k}$  is the stiffness coefficient between the wheel and the ground of the  $k$ -th wheel.

$s_{w_k}$  is the length of the stiffness of the  $k$ -th wheel from chassis to ground.

$s_{0w_k}$  is the free length of the stiffness of the  $k$ -th wheel from chassis to ground.

Note that  $\hat{C}^{(o, w_{rl})} = \hat{C}^{(o, c)}$ ,  $\hat{C}^{(o, w_{rrl})} = \hat{C}^{(o, c)}$ ,  $\hat{C}^{(o, w_{fl})} = \hat{C}^{(o, c)} e^{\tilde{u}_z \psi_{fl}}$  and  $\hat{C}^{(o, w_{fr})} = \hat{C}^{(o, c)} e^{\tilde{u}_z \psi_{fr}}$ . Small angle assumption can be made for  $\psi_{oc}$  and  $\theta_{oc}$ . Therefore,

$$s_{w_k} = \bar{u}_z^T \bar{r}_{oc}^{(o)} + d_{w_k} + \tilde{r}_{w_k q_k} \times [\phi_{oc} \theta_{oc} 0]^T \quad (2.32)$$

In (2.32),  $d_{w_k}$  is the disturbance from the road.

There are many tire-road friction models available in the literature [12, 82]. Coulomb's friction law, Lu-Gre friction model [11], finite element method based friction models [36] and Magic formula [65] are among the most famous models explaining the nature of tire contact friction effects. Some cruising algorithms exclude tire-road friction effects or assume a road-tire static friction proportional to weight of wheel [19].

In this study, wheels are assumed to be rigid and are subject to the friction forces according to the Coulombs law. In other words, Magic Formula [65], which is an empiric equation commonly used to model tire friction forces, is simplified to Coulomb's friction law owing to the rigid wheel assumption [69]. Even if this assumption does not reduce the computational complexity, the nature of wheel skidding becomes easier to handle in the rigid wheel model.

The Coulomb's friction law is formulated as in 2.33 for each wheel. In the equation,  $\bar{u}_{vw_k}$  is the unit vector indicating the direction the linear velocity of the  $k$ -th wheel,  $\mu_{s, w_k}$  and  $\mu_{d, w_k}$  are static and dynamic friction coefficients of the road at the contact point with  $k$ -th wheel.

$$\begin{aligned}
\bar{u}_{v_{w_k}}^T \bar{v}_{w_k}^{(o)} &= R\bar{\omega}_{ow_k}^{(w_k)} & \text{if } |\bar{u}_{v_{w_k}}^T \bar{F}_{gw_k}^{(w_k)}| < \mu_{s,w_k} \bar{u}_z^T \bar{F}_{gw_k}^{(w_k)} \\
\bar{u}_{v_{w_k}}^T \bar{F}_{gw_k}^{(w_k)} &= \mu_{d,w_k} \bar{u}_z^T \bar{F}_{gw_k}^{(w_k)} & \text{if } \bar{u}_{v_{w_k}}^T \bar{v}_{w_k}^{(o)} \neq R\bar{\omega}_{ow_k}^{(w_k)}
\end{aligned} \tag{2.33}$$

During wheel slippage, the friction force is known; however, the speed of the wheel cannot be deduced from the speed of the vehicle. During no-slippage condition; on the other hand, the relation between speeds of the wheel and the chassis velocities are in action, but the exact value of the static friction force is unknown. The unknown friction force, as well as the accelerations of the wheels and the chassis, are calculated by solving the Newton-Euler equations. All structural forces can also be extracted through this computation.

## 2.7 Angular Velocities

In this section, angular velocities of the vehicle subsystems in their inertial frames are defined.

$$\begin{aligned}
\tilde{\omega}_{oc}^{(c)} &= \hat{C}^{(e,o)} \dot{\hat{C}}^{(o,c)} \approx \hat{C}^{(e,o)} \dot{\hat{C}}^{(o,c)} \\
&= (e^{-\tilde{u}_z \psi_{oe}} e^{-\tilde{u}_y \theta_{oe}} e^{-\tilde{u}_x \phi_{oe}}) (e^{\tilde{u}_x \phi_{oc}} e^{\tilde{u}_y \theta_{oc}} e^{\tilde{u}_z \psi_{oc}}) \\
&\left[ \tilde{u}_z \dot{\psi}_{oc} \left( \hat{I} + \tilde{u}_y \theta_{oc} + \tilde{u}_x \phi_{oc} \right) + \tilde{u}_y \dot{\theta}_{oc} \left( \hat{I} + \tilde{u}_z \psi_{oc} + \tilde{u}_x \phi_{oc} \right) \right. \\
&\left. + \tilde{u}_x \dot{\phi}_{oc} \left( \hat{I} + \tilde{u}_y \theta_{oc} + \tilde{u}_z \psi_{oc} \right) \right]
\end{aligned} \tag{2.34}$$

Here, it is assumed that inclination of the ground changes slowly, and as stated above,  $\mathcal{F}_c$  has no orientation difference compared to  $\mathcal{F}_e$  are small in magnitude. Hence, the equation above becomes:

$$\begin{aligned}
\tilde{\omega}_{oc}^{(c)} &\approx (e^{-\tilde{u}_z \psi_{oe}} e^{-\tilde{u}_y \theta_{oe}} e^{-\tilde{u}_x \phi_{oe}}) (e^{\tilde{u}_x \phi_{oc}} e^{\tilde{u}_y \theta_{oc}} e^{\tilde{u}_z \psi_{oc}}) \\
&\left[ \tilde{u}_z \dot{\psi}_{oc} \left( \hat{I} + \tilde{u}_y \theta_{oc} + \tilde{u}_x \phi_{oc} \right) + \left( \tilde{u}_z \dot{\psi}_{ec} + \tilde{u}_y \dot{\theta}_{ec} + \tilde{u}_x \dot{\phi}_{ec} \right) \right]
\end{aligned} \tag{2.35}$$

$$\tilde{\omega}_{oc}^{(c)} \approx \tilde{u}_z \dot{\psi}_{oc} \left( \hat{I} + \tilde{u}_y \theta_{oc} + \tilde{u}_x \phi_{oc} \right) + \left( \tilde{u}_y \dot{\theta}_{ec} + \tilde{u}_x \dot{\phi}_{ec} \right) \tag{2.36}$$

$$\tilde{\omega}_{oc}^{(c)} \approx \tilde{u}_x \dot{\phi}_{ec} + \tilde{u}_y \dot{\theta}_{ec} + \tilde{u}_z \dot{\psi}_{oc} \tag{2.37}$$

$$\bar{\omega}_{oc}^{(c)} \approx \bar{u}_x \dot{\phi}_{ec} + \bar{u}_y \dot{\theta}_{ec} + \bar{u}_z \dot{\psi}_{oc} \tag{2.38}$$

Similarly,

$$\bar{\omega}_{ob}^{(b)} \approx \bar{u}_x (\dot{\phi}_{ec} + \dot{\phi}_{cb}) + \bar{u}_y (\dot{\theta}_{ec} + \dot{\theta}_{cb}) + \bar{u}_z \dot{\psi}_{oc} \tag{2.39}$$

$$\bar{\omega}_{cb}^{(b)} \approx \bar{u}_x \dot{\phi}_{cb} + \bar{u}_y \dot{\theta}_{cb} \tag{2.40}$$

For the angular velocities of the wheels, remember that rear wheels have non-spinning inertial frames  $\mathcal{F}_{w_{rl}} = \mathcal{F}_c$  and  $\mathcal{F}_{w_{rr}} = \mathcal{F}_c$ .

$$\bar{\omega}_{ow_{rl}}^{(w_{rl})} = \bar{\omega}_{ow_{rl}}^{(c)} \approx \bar{u}_x \dot{\phi}_{ec} + \bar{u}_y (\dot{\theta}_{ec} + \dot{\theta}_{cw_{rl}}) + \bar{u}_z \dot{\psi}_{oe} \quad (2.41)$$

$$\bar{\omega}_{ow_{rr}}^{(w_{rr})} = \bar{\omega}_{ow_{rr}}^{(c)} \approx \bar{u}_x \dot{\phi}_{ec} + \bar{u}_y (\dot{\theta}_{ec} + \dot{\theta}_{cw_{rr}}) + \bar{u}_z \dot{\psi}_{oe} \quad (2.42)$$

For the front wheels, angular velocities are defined in their own non-spinning frames  $\mathcal{F}_{w_{fl}}$  and  $\mathcal{F}_{w_{fr}}$ .

$$\bar{\omega}_{ow_{fl}}^{(w_{fl})} \approx \bar{u}_x \dot{\phi}_{ec} + \bar{u}_y (\dot{\theta}_{ec} + \dot{\theta}_{cw_{fl}}) + \bar{u}_z (\dot{\psi}_{oe} + \dot{\psi}_{fl}) \quad (2.43)$$

$$\bar{\omega}_{ow_{fr}}^{(w_{fr})} \approx \bar{u}_x \dot{\phi}_{ec} + \bar{u}_y (\dot{\theta}_{ec} + \dot{\theta}_{cw_{fr}}) + \bar{u}_z (\dot{\psi}_{oe} + \dot{\psi}_{fr}) \quad (2.44)$$

## 2.8 Angular Accelerations

In this section, angular accelerations are calculated for chassis, body and the wheels. According to the Coriolis theorem, for reference frames  $\mathcal{F}_x$ ,  $\mathcal{F}_y$  and  $\mathcal{F}_z$ , the following relation can be defined:

$$\begin{aligned} \vec{\alpha}_{xz} &= (d\vec{\omega}_{xz}/dt)|_{\mathcal{F}_x} = (d\vec{\omega}_{xz}/dt)|_{\mathcal{F}_z} (d\vec{\omega}_{xz}/dt)|_{\mathcal{F}_y} + \vec{\omega}_{xy} \times \vec{\omega}_{xz} \\ &= (d\vec{\omega}_{xz}/dt)|_{\mathcal{F}_y} + \vec{\omega}_{xy} \times \vec{\omega}_{yz} \end{aligned} \quad (2.45)$$

The corresponding matrix equation is written in  $\mathcal{F}_y$  as

$$\bar{\alpha}_{xz}^{(y)} = \dot{\bar{\omega}}_{xz}^{(y)} + \tilde{\omega}_{xy}^{(y)} \bar{\omega}_{xz}^{(y)} = \dot{\bar{\omega}}_{xz}^{(y)} + \tilde{\omega}_{xy}^{(y)} \bar{\omega}_{yz}^{(y)} \quad (2.46)$$

Hence, the accelerations can be stated as

$$\bar{\alpha}_{oc}^{(c)} = \dot{\bar{\omega}}_{oc}^{(c)} = \bar{u}_x \ddot{\phi}_{ec} + \bar{u}_y \ddot{\theta}_{ec} + \bar{u}_z \ddot{\psi}_{ec} \quad (2.47)$$

$$\bar{\alpha}_{ob}^{(b)} = \dot{\bar{\omega}}_{ob}^{(b)} = \bar{u}_x (\ddot{\phi}_{ec} + \ddot{\phi}_{cb}) + \bar{u}_y (\ddot{\theta}_{ec} + \ddot{\theta}_{cb}) + \bar{u}_z \ddot{\psi}_{ec} \quad (2.48)$$

$$\bar{\alpha}_{cb}^{(b)} = \dot{\bar{\omega}}_{cb}^{(b)} = \bar{u}_x \ddot{\phi}_{cb} + \bar{u}_y \ddot{\theta}_{cb} + \bar{u}_z \ddot{\psi}_{ec} \quad (2.49)$$

$$\begin{aligned} \bar{\alpha}_{cw_{rl}}^{(c)} &= \dot{\bar{\omega}}_{cw_{rl}}^{(c)} + \tilde{\omega}_{oc}^{(c)} \bar{\omega}_{cw_{rl}}^{(c)} \\ &= \bar{u}_x (\ddot{\phi}_{ec} - \dot{\theta}_{cw_{rl}} \dot{\psi}_{oe}) + \bar{u}_y (\ddot{\theta}_{ec} + \ddot{\theta}_{cw_{rl}}) + \bar{u}_z (\ddot{\psi}_{ec} + \dot{\theta}_{cw_{rl}} \dot{\phi}_{ec}) \end{aligned} \quad (2.50)$$

$$\begin{aligned} \bar{\alpha}_{cw_{rr}}^{(c)} &= \dot{\bar{\omega}}_{cw_{rr}}^{(c)} + \tilde{\omega}_{oc}^{(c)} \bar{\omega}_{cw_{rr}}^{(c)} \\ &= \bar{u}_x (\ddot{\phi}_{ec} - \dot{\theta}_{cw_{rr}} \dot{\psi}_{oe}) \\ &\quad + \bar{u}_y (\ddot{\theta}_{ec} + \ddot{\theta}_{cw_{rr}}) + \bar{u}_z (\ddot{\psi}_{ec} + \dot{\theta}_{cw_{rr}} \dot{\phi}_{ec}) \end{aligned} \quad (2.51)$$

$$\begin{aligned}
\bar{\alpha}_{cw_{fl}}^{(w_{fl})} &= \dot{\tilde{\omega}}_{cw_{fl}}^{(w_{fl})} + \tilde{\omega}_{oc}^{(w_{fl})} \bar{\omega}_{cw_{fl}}^{(w_{fl})} \\
&= \bar{u}_x \left[ \ddot{\phi}_{ec} - \dot{\theta}_{cw_{fl}} (\dot{\psi}_{oe} + \dot{\psi}_{fl}) \right] \\
&\quad + \bar{u}_y (\ddot{\theta}_{ec} + \ddot{\theta}_{cw_{fl}}) + \bar{u}_z (\ddot{\psi}_{ec} + \ddot{\psi}_{fl} + \dot{\theta}_{cw_{fl}} \dot{\phi}_{ec})
\end{aligned} \tag{2.52}$$

$$\begin{aligned}
\bar{\alpha}_{cw_{fr}}^{(w_{fr})} &= \dot{\tilde{\omega}}_{cw_{fr}}^{(w_{fr})} + \tilde{\omega}_{oc}^{(w_{fr})} \bar{\omega}_{cw_{fr}}^{(w_{fr})} \\
&= \bar{u}_x \left[ \ddot{\phi}_{ec} - \dot{\theta}_{cw_{fr}} (\dot{\psi}_{oe} + \dot{\psi}_{fr}) \right] \\
&\quad + \bar{u}_y (\ddot{\theta}_{ec} + \ddot{\theta}_{cw_{fr}}) + \bar{u}_z (\ddot{\psi}_{ec} + \ddot{\psi}_{fr} + \dot{\theta}_{cw_{fr}} \dot{\phi}_{ec})
\end{aligned} \tag{2.53}$$

## 2.9 Overall Dynamic Motion Model of the Vehicle

In the previous sections, Newton-Euler equations for chassis, suspended body, and four wheels are derived. There are six equations for each set and with total 36 equations. However, many of the forces and torques are due to structural effects and they can be eliminated. In this section, these eliminations will be performed and an overall dynamic model for the vehicle is obtained.

Note that, in  $x$  and  $y$  axes and yaw orientation of motion, suspended body and chassis cannot move independently, and  $\bar{u}_x^T \bar{F}_{s_k c}^{(c)} = -\bar{u}_x^T \bar{F}_{s_k b}^{(b)}$ ,  $\bar{u}_y^T \bar{F}_{s_k c}^{(c)} = -\bar{u}_y^T \bar{F}_{s_k b}^{(b)}$ , and  $\bar{M}_{s_k c}^{(c)} + \tilde{r}_{cp_k}^{(c)} \bar{F}_{s_k c}^{(c)} = -\left( \bar{M}_{s_k b}^{(b)} + \tilde{r}_{bp_k}^{(b)} \bar{F}_{s_k b}^{(b)} \right)$ . Assuming  $\bar{u}_z^T \bar{F}_{ab}^{(b)} \approx 0$ , and substituting angular velocities and accelerations into the Newton-Euler equations, the following motion model for chassis and the body can be attained. Note that in addition to these equations, in order to calculate  $\bar{F}_{s_k c}^{(c)}$ , for each suspension unit  $s_k$  should be considered as a state as well.

$$\begin{aligned}
\bar{u}_x^T (m_c + m_b) \hat{C}^{(c,o)} \bar{a}_{oc}^{(o)} &= \bar{u}_x^T \left( \sum_{k=1}^4 \bar{F}_{w_k c}^{(c)} + \bar{F}_{ab}^{(c)} \right) \\
\bar{u}_y^T (m_c + m_b) \hat{C}^{(c,o)} \bar{a}_{oc}^{(o)} &= \bar{u}_y^T \left( \sum_{k=1}^4 \bar{F}_{w_k c}^{(c)} + \bar{F}_{ab}^{(c)} \right) \\
\bar{u}_z^T m_c \hat{C}^{(c,o)} \bar{a}_{oc}^{(o)} &= \bar{u}_z^T \left( \sum_{k=1}^4 \bar{F}_{w_k c}^{(c)} + m_c g \hat{C}^{(c,o)} \bar{u}_z \right) \\
\bar{u}_z^T m_b \hat{C}^{(b,c)} \bar{a}_{cb}^{(c)} &= \bar{u}_z^T \left( \tilde{\omega}_{oc}^{(c)} \bar{F}_{s_k b}^{(b)} + m_b g \hat{C}^{(b,o)} \bar{u}_z \right) \\
\left( (\hat{J}_c^{(c)} + \hat{J}_b^{(b)}) \bar{\alpha}_{oc}^{(c)} + \tilde{\omega}_{oc}^{(c)} (\hat{J}_c^{(c)} + \hat{J}_b^{(b)}) \bar{\omega}_{oc}^{(c)} \right) &= \sum_{k=1}^4 \bar{M}_{w_k c}^{(c)} + \tilde{r}_{cp_k}^{(c)} \bar{F}_{w_k c}^{(c)} \\
\bar{u}_x^T \left( \hat{J}_b^{(b)} \bar{\alpha}_{cb}^{(b)} + \tilde{\omega}_{cb}^{(b)} \hat{J}_b^{(b)} \bar{\omega}_{cb}^{(b)} \right) &= \bar{u}_x^T \left( \sum_{k=1}^4 \tilde{r}_{bp_k}^{(b)} \bar{F}_{s_k b}^{(b)} - (\hat{J}_b^{(b)} \bar{\alpha}_{oc}^{(c)} + \tilde{\omega}_{oc}^{(c)} \hat{J}_b^{(b)} \bar{\omega}_{oc}^{(c)}) \right) \\
\bar{u}_y^T \left( \hat{J}_b^{(b)} \bar{\alpha}_{cb}^{(b)} + \tilde{\omega}_{cb}^{(b)} \hat{J}_b^{(b)} \bar{\omega}_{cb}^{(b)} \right) &= \bar{u}_y^T \left( \sum_{k=1}^4 \tilde{r}_{bp_k}^{(b)} \bar{F}_{s_k b}^{(b)} - (\hat{J}_b^{(b)} \bar{\alpha}_{oc}^{(c)} + \tilde{\omega}_{oc}^{(c)} \hat{J}_b^{(b)} \bar{\omega}_{oc}^{(c)}) \right)
\end{aligned} \tag{2.54}$$

Note that, wheels are locked to move with chassis and body in  $x$ - and  $y$ - directions. These are satisfied with structural forces in between the wheels and the chassis. Positions of the wheels in  $z$ - direction is not inside the scope of interest, yet note that in addition to these equations, in order to calculate  $\bar{F}_{gq_k}^{(c)}$ , for each wheel  $s_{w_k}$  should be considered as a state as well. Since the structural force between the wheels and the chassis is derived, and the gravitational force has effects on the wheels themselves, in  $z$ - axis no separate equations for wheels are written.

Now note among structural forces  $\vec{M}_{cw_k}$  and  $\vec{M}_{gw_k}$ , all will cancel out except the torque commands to the wheels  $\tau_k$ . In this combination, it is assumed that

$$\sum_{k=1}^4 \left\| \hat{J}_{w_k}^{(w_k)} \bar{\alpha}_{oc}^{(c)} + \tilde{\omega}_{oc}^{(c)} \hat{J}_{w_k}^{(w_k)} \bar{\omega}_{oc}^{(c)} \right\| \ll \left\| (\hat{J}_c^{(c)} + \hat{J}_b^{(b)}) \bar{\alpha}_{oc}^{(c)} + \tilde{\omega}_{oc}^{(c)} (\hat{J}_c^{(c)} + \hat{J}_b^{(b)}) \bar{\omega}_{oc}^{(c)} \right\| \tag{2.55}$$

Following cancellation of structural forces, the overall model can be attained as follows including wheels and torque commands  $\tau_k$

$$\begin{aligned}
\bar{u}_x^T \left( m_c + m_b + \sum_{k=1}^4 m_{w_k} \right) \hat{C}^{(c,o)} \bar{a}_{oc}^{(o)} &= \bar{u}_x^T \left( \sum_{k=1}^4 \bar{F}_{gw_k}^{(c)} + \bar{F}_{ab}^{(c)} \right) \\
\bar{u}_y^T \left( m_c + m_b + \sum_{k=1}^4 m_{w_k} \right) \hat{C}^{(c,o)} \bar{a}_{oc}^{(o)} &= \bar{u}_y^T \left( \sum_{k=1}^4 \bar{F}_{gw_k}^{(c)} + \bar{F}_{ab}^{(c)} \right) \\
\bar{u}_z^T \left( m_c + \sum_{k=1}^4 m_{w_k} \right) \hat{C}^{(c,o)} \bar{a}_{oc}^{(o)} &= \bar{u}_z^T \left( \sum_{k=1}^4 \bar{F}_{gw_k}^{(c)} \bar{F}_{s_k c}^{(c)} + m_c g \hat{C}^{(c,o)} \bar{u}_z \right) \\
\bar{u}_z^T m_b \hat{C}^{(b,c)} \bar{a}_{cb}^{(c)} &= \bar{u}_z^T \left( \tilde{\omega}_{oc}^{(c)} \bar{F}_{s_k b}^{(b)} + m_b g \hat{C}^{(b,o)} \bar{u}_z \right) \\
\left( (\hat{J}_c^{(c)} + \hat{J}_b^{(b)}) \bar{\alpha}_{oc}^{(c)} + \tilde{\omega}_{oc}^{(c)} (\hat{J}_c^{(c)} + \hat{J}_b^{(b)}) \bar{\omega}_{oc}^{(c)} \right) &= \sum_{k=1}^4 \bar{M}_{gw_k}^{(c)} + \tilde{r}_{w_k q_k}^{(c)} \bar{F}_{w_k q_k}^{(c)} \\
\bar{u}_x^T \left( \hat{J}_b^{(b)} \bar{\alpha}_{cb}^{(b)} + \tilde{\omega}_{cb}^{(b)} \hat{J}_b^{(b)} \bar{\omega}_{cb}^{(b)} \right) &= \bar{u}_x^T \left( \sum_{k=1}^4 \tilde{r}_{bp_k}^{(b)} \bar{F}_{s_k b}^{(b)} - (\hat{J}_b^{(b)} \bar{\alpha}_{oc}^{(c)} + \tilde{\omega}_{oc}^{(c)} \hat{J}_b^{(b)} \bar{\omega}_{oc}^{(c)}) \right) \\
\bar{u}_y^T \left( \hat{J}_b^{(b)} \bar{\alpha}_{cb}^{(b)} + \tilde{\omega}_{cb}^{(b)} \hat{J}_b^{(b)} \bar{\omega}_{cb}^{(b)} \right) &= \bar{u}_y^T \left( \sum_{k=1}^4 \tilde{r}_{bp_k}^{(b)} \bar{F}_{s_k b}^{(b)} - (\hat{J}_b^{(b)} \bar{\alpha}_{oc}^{(c)} + \tilde{\omega}_{oc}^{(c)} \hat{J}_b^{(b)} \bar{\omega}_{oc}^{(c)}) \right) \\
\bar{u}_y^T \left( \hat{J}_{w_{fl}}^{(w_{fl})} \bar{\alpha}_{ow_{fl}}^{(w_{fl})} + \tilde{\omega}_{ow_{fl}}^{(w_{fl})} \hat{J}_{w_{fl}}^{(w_{fl})} \bar{\omega}_{ow_{fl}}^{(w_{fl})} \right) &= \tau_{fl} \\
\bar{u}_y^T \left( \hat{J}_{w_{fr}}^{(w_{fr})} \bar{\alpha}_{ow_{fr}}^{(w_{fr})} + \tilde{\omega}_{ow_{fr}}^{(w_{fr})} \hat{J}_{w_{fr}}^{(w_{fr})} \bar{\omega}_{ow_{fr}}^{(w_{fr})} \right) &= \tau_{fr} \\
\bar{u}_y^T \left( \hat{J}_{w_{rl}}^{(w_{rl})} \bar{\alpha}_{ow_{rl}}^{(w_{rl})} + \tilde{\omega}_{ow_{rl}}^{(w_{rl})} \hat{J}_{w_{rl}}^{(w_{rl})} \bar{\omega}_{ow_{rl}}^{(w_{rl})} \right) &= \tau_{rl} \\
\bar{u}_y^T \left( \hat{J}_{w_{rr}}^{(w_{rr})} \bar{\alpha}_{ow_{rr}}^{(w_{rr})} + \tilde{\omega}_{ow_{rr}}^{(w_{rr})} \hat{J}_{w_{rr}}^{(w_{rr})} \bar{\omega}_{ow_{rr}}^{(w_{rr})} \right) &= \tau_{rr}
\end{aligned} \tag{2.56}$$

In (2.56),

the states are:  $\bar{v}_{oc}^{(c)}$ ,  $\bar{v}_{cb,z}^{(c)}$ ,  $\bar{\omega}_{oc}^{(c)}$ ,  $\bar{\omega}_{cb,x}^{(b)}$ ,  $\bar{\omega}_{cb,y}^{(b)}$ ,  $\bar{\omega}_{ow_{fl},y}^{(w_{fl})}$ ,  $\bar{\omega}_{ow_{fr},y}^{(w_{fr})}$ ,  $\bar{\omega}_{ow_{rl},y}^{(w_{rl})}$  and  $\bar{\omega}_{ow_{rr},y}^{(w_{rr})}$ .  
the gravitational forces considered are on the chassis and the suspended body,  
the disturbance is air drag given in (2.22), and road input affecting through  $\tilde{r}_{qk}^{(c)}$   
in  $\bar{F}_{gw_k,z}^{(c)}$  given in 2.31,

the forces due to suspension system given in (2.23),

the forces due to wheel skidding is checked with or determined by 2.33.

## 2.10 Simplified Motion Model for Gross Motion of the Vehicle

The overall dynamic model of the vehicle considered in this study is obtained as a combination of the dynamic models of the subsystems based on the Newton-Euler equations as stated above. The subsystems consist of the chassis, the suspended body and the wheels [39, 44, 4]. The scope of this study requires a simplified model for the gross motion of the vehicle, in which the vibratory motions are neglected. Hence, the following assumptions are made for the motions of the subsystems:

- The chassis can move in longitudinal and lateral directions with respect to its coordinate frames.
- The chassis can make yaw rotation.
- The wheels can move in longitudinal and lateral directions with respect to their coordinate frames.

Since gross motion of the vehicle is considered, the following simplifications in the motion can be assumed:

- The chassis cannot move in the up/down directions.
- The chassis cannot make roll and pitch rotations with respect to its longitudinal and lateral axes.
- The wheels cannot move in in the up/down directions.
- The wheels cannot make roll rotations around their joints attached to the chassis.

Due to the gross motion consideration, the suspended mass and the chassis are incorporated into a single rigid body, which is referred here simply as the chassis. Consequently, the suspension system is ignored. Furthermore, the wheels are modelled to be rigid obeying the well-known Coulomb's friction law.

The vehicle model is presented in Figs. 2.2-2.4. The arrows in the figures indicate positive directions for the forces. Governing equations for chassis can be written as follows.

$$\begin{aligned}
m_c a_{c,x}^{(c)} &= F_{cw_{fl},x}^{(c)} + F_{cw_{fr},x}^{(c)} + F_{cw_{rl},x}^{(c)} + F_{cw_{rr},x}^{(c)} + G_{c,x}^{(c)} + F_{a,x}^{(c)} \\
m_c a_{c,y}^{(c)} &= F_{cw_{fl},y}^{(c)} + F_{cw_{fr},y}^{(c)} + F_{cw_{rl},y}^{(c)} + F_{cw_{rr},y}^{(c)} + G_{c,y}^{(c)} \\
0 &= F_{cw_{fl},z}^{(c)} + F_{cw_{fr},z}^{(c)} + F_{cw_{rl},z}^{(c)} + F_{cw_{rr},z}^{(c)} - G_{c,z}^{(c)} \\
0 &= F_{cw_{fl},z}^{(c)} l_{fl,y} - F_{cw_{fr},z}^{(c)} l_{fr,y} + F_{cw_{rl},z}^{(c)} l_{rl,y} - F_{cw_{rr},z}^{(c)} l_{rr,y} \\
&\quad + M_{cw_{fl},x}^{(c)} + M_{cw_{fr},x}^{(c)} + M_{cw_{rl},x}^{(c)} + M_{cw_{rr},x}^{(c)} \\
0 &= F_{cw_{fl},z}^{(c)} l_{fl,x} + F_{cw_{fr},z}^{(c)} l_{fr,x} - F_{cw_{rl},z}^{(c)} l_{rl,x} - F_{cw_{rr},z}^{(c)} l_{rr,x} \\
&\quad + M_{cw_{fl},y}^{(c)} + M_{cw_{fr},y}^{(c)} + M_{cw_{rl},y}^{(c)} + M_{cw_{rr},y}^{(c)} \\
\left( I_{c,z} + \sum_w I_{w,z} \right) \alpha_{v,z} &= - F_{cw_{fl},x}^{(c)} l_{fl,y} + F_{cw_{fr},x}^{(c)} l_{fr,y} - F_{cw_{rl},x}^{(c)} l_{rl,y} + F_{cw_{rr},x}^{(c)} l_{rr,y} \\
&\quad + F_{cw_{fl},y}^{(c)} l_{fl,x} + F_{cw_{fr},y}^{(c)} l_{fr,x} - F_{cw_{rl},y}^{(c)} l_{rl,x} - F_{cw_{rr},y}^{(c)} l_{rr,x}
\end{aligned} \tag{2.57}$$

In (2.57), it is assumed that there is no air-drag force applied on the chassis along its  $z$  axis. Assuming, the chassis and the wheels share parallel reference frames, in the

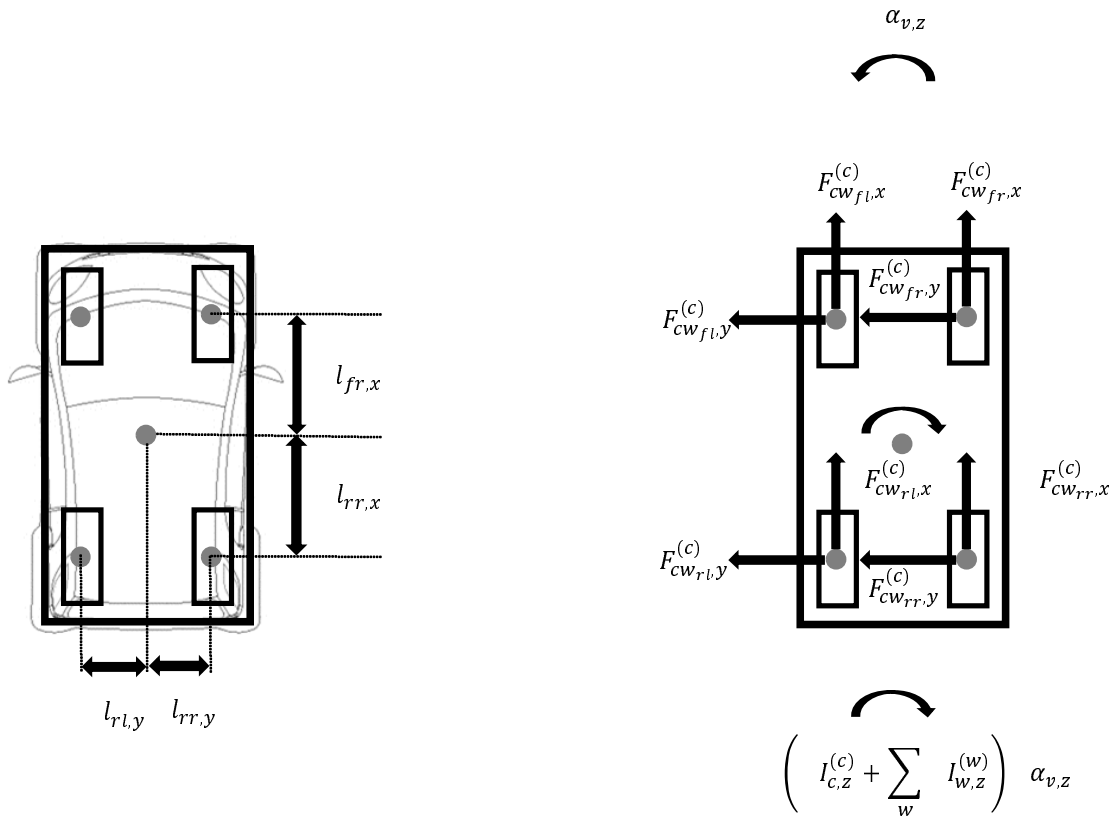


Figure 2.2: Vehicle model (top view)

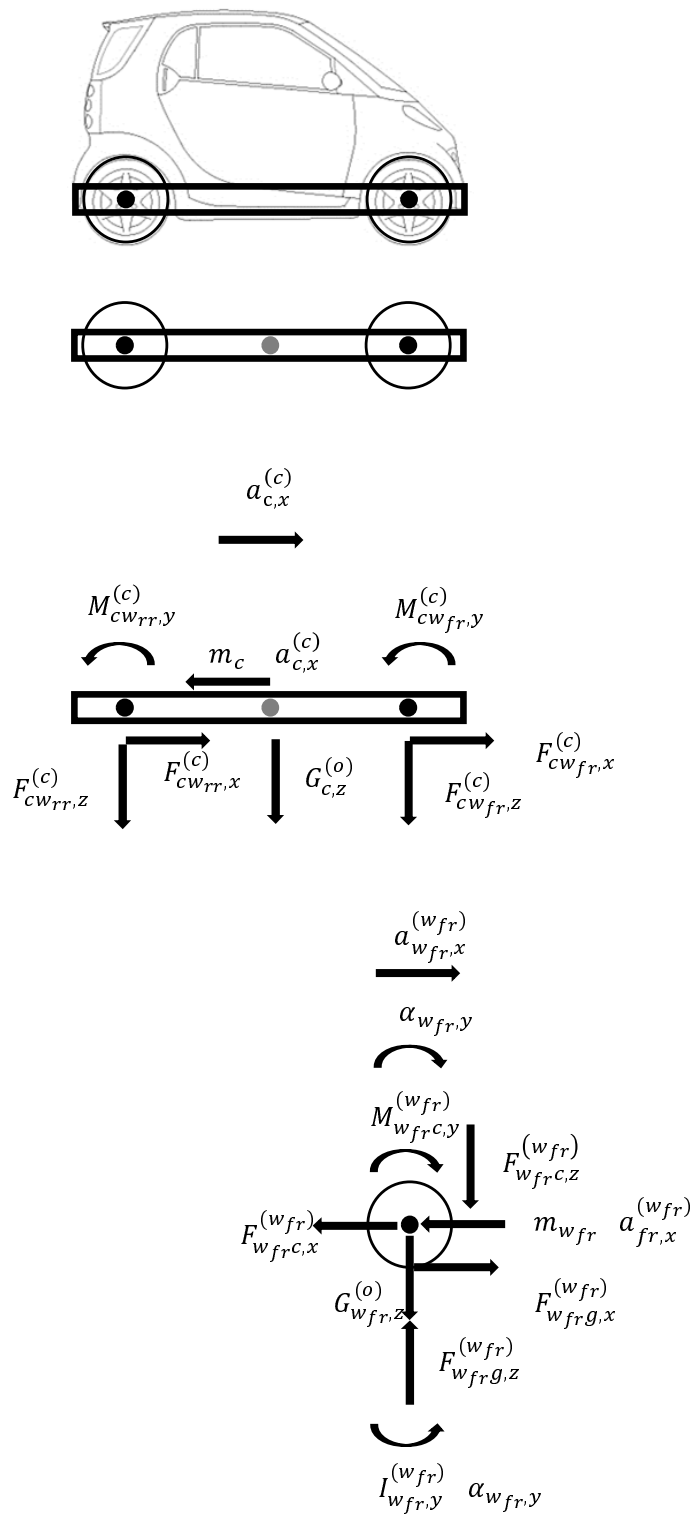


Figure 2.3: Vehicle model (longitudinal view)

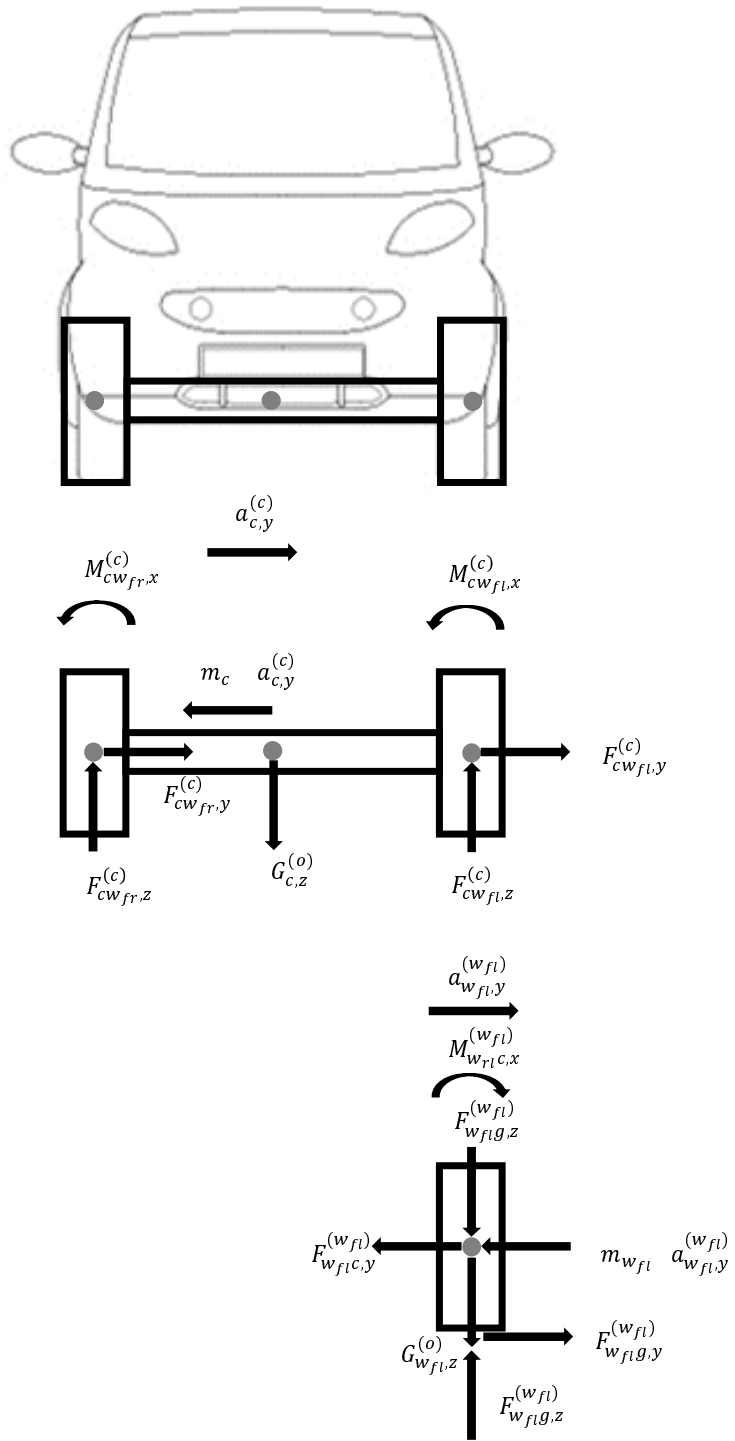


Figure 2.4: Vehicle model (Lateral view)

equation,  $M_{cw,y} = -M_{wc,y}$  stands for the driving/braking torque applied to the wheel  $w$ . The subscript  $v$  denotes the overall vehicle.

$$\begin{aligned}
m_w a_{w,x}^{(w)} &= F_{wg,x}^{(w)} - F_{wc,x}^{(w)} + G_{w,x}^{(w)} \\
m_w a_{w,y}^{(w)} &= F_{wg,y}^{(w)} - F_{wc,y}^{(w)} + G_{w,y}^{(w)} \\
0 &= F_{wg,z}^{(w)} - F_{wc,z}^{(w)} - G_{w,y}^{(w)} \\
0 &= M_{wc,x}^{(w)} - R_w F_{wg,y}^{(w)} \\
I_{w,y} \alpha_{w,y} &= M_{wc,y}^{(w)} - R_w F_{wc,x}^{(w)}
\end{aligned} \tag{2.58}$$

The general vehicle gross motion model is applicable for the motion scenarios considered in this study. The model under consideration is a front-drive front-steered vehicle with all wheels capable of independent braking. The driving commands to the front wheels and the braking commands to all the wheels can be different from each other. The actuation system for wheel driving and gears are assumed to be perfect with a transfer function of unity.

## 2.11 Cornering Motion

The most commonly used steering mechanisms for vehicles are Ackerman steering, differential steering and skid steering [90]. Ackerman steering has good lateral stability and good controllability [70] and low power consumption [75]; however, it creates low manoeuvrability [59]. Differential steering has high manoeuvrability with a zero turning radius [91]; however, it generates low traction and low mobility [90]; hence, it is not preferred in outdoor operations. Skid steering has high manoeuvrability [13], faster response [61], strong traction and high mobility [67]; however, it is difficult to model and control [89], and it is energy inefficient [61].

In this study, during cornering if at least two of the wheels are not in slippage, with its non-skidding wheels, the vehicle obeys the well-known rule of rotational motion of the vehicles: Ackerman's steering law [30] as represented in Fig. 2.5. For the front-drive wheel, the rotation radius  $r$  is taken as the distance of midpoint of the rear axle to the centre of rotation ( $CoR$ ).

For non-skidding wheels and, if at least two of the wheels are not skidding, for the chassis, the radii of rotation, can be calculated according to Ackermann's steering law, and the steering angles for the front wheels can be extracted as a consequence. Since the rotational velocities and accelerations are the same for every point on the vehicle throughout the rotation around a fixed  $CoR$ , they can be calculated as well if the overall non-slippage cornering condition is satisfied. The governing equations for Ackerman's steering law are stated in 2.59.

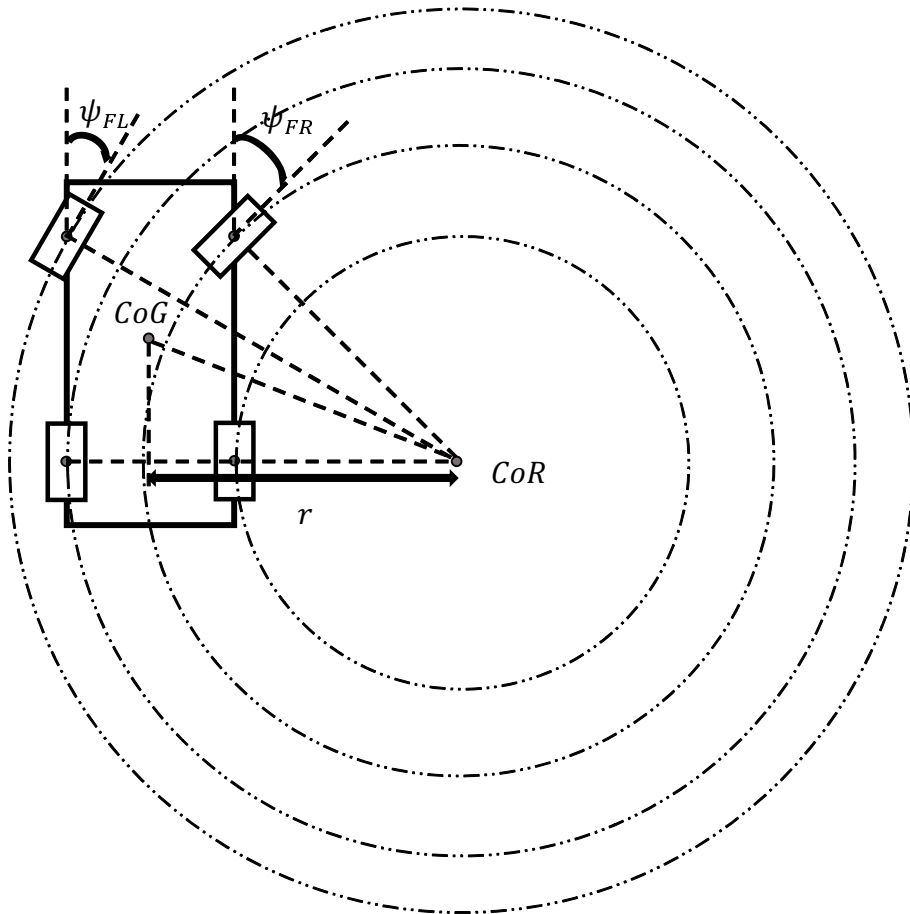


Figure 2.5: Ackerman steering

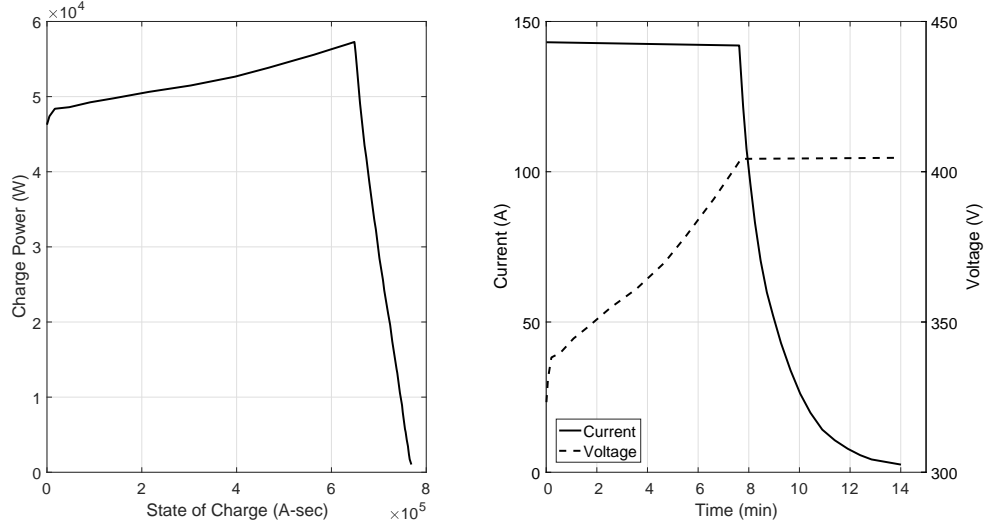


Figure 2.6: Charging characteristics of the battery package

$$\begin{aligned}
 \omega_{v,z} &= \omega_{w,z} \omega_{c,z} \\
 \alpha_{v,z} &= \alpha_{w,z} \alpha_{c,z} \\
 a_{w_x} &= \alpha_{v,z} r_{w,z} \\
 a_{w_y} &= \omega_{w,z}^2 r_{w,z}
 \end{aligned} \tag{2.59}$$

## 2.12 Power Consumption Dynamics

The torque commands to be applied cannot be independent of the power consumption dynamics of the vehicle. The energy requirement of the vehicle motion is fulfilled with 7104 lithium-ion battery packed with 74 in parallel and 96 in series of the cells described in [1]. The charging and discharging characteristics of the battery are presented in Figs. 2.6 and 2.7, respectively. According to the discharging characteristics of the battery package, during driving, the maximum torque that can be applied to the front wheels is determined from discharging power as a function of the state-of-charge (*SoC*) of the package. During regenerative braking, according to the charging characteristics of the battery package, the amount of power below the charging power as a function of the current value of *SoC* can be charged back to the battery. The amount of power exceeding the charging power of the battery is dissipated as heat in the vehicle mechanics. It is assumed that the maximum power points of the electric motors controlling the wheels are always below the charging and discharging powers of the battery for all instants of the scenarios.

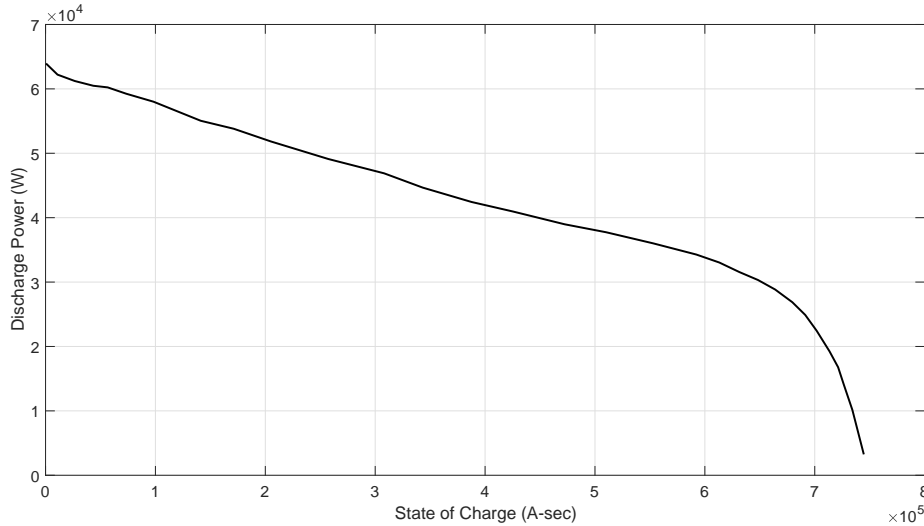


Figure 2.7: Discharging characteristics of the battery package

## 2.13 Open Loop Simulations of the Vehicle Model

In this section, the simplified mathematical model developed in Section 2.10 for the gross motion of the vehicle is tested under different scenarios. Three scenarios are considered: uphill / downhill motion along asphalt road, braking along asphalt and icy roads, and cornering around asphalt roads. The aim is to verify the developed method as compared to the daily-life experiences. It has been observed that in Matlab / Simulink 2016b, there is a vehicle model for longitudinal motion only. . Therefore, in the first scenario, the gross motion model is tested additionally against the model of Matlab/Simulink. It is seen that both models supported each other.

### 2.13.1 Scenario-1: Uphill/Downhill Motion along Asphalt Road

,In this scenario, a 1-km road is considered. The road is composed of five sections: a 200 m of straight section, a 200 m of uphill section with inclination of 3 degs, a 200 m of straight section, a 200 m of downhill section with declination of 3 degs, and finally a 200 m of straight section. The road is asphalt with  $\mu = 0.72$ . Similar scenarios are also considered later in the energy optimality studies in Chapter 3.

Since the motion in the test scenario is longitudinal only, it has been possible to compare the gross motion vehicle model with the model of the Matlab/Simulink 2016b. The Simulink diagram built for this purpose is demonstrated in Fig. 2.8.

In the Simulink diagram, on the right side, a block entitled ScenarioInputs adjusts the commands and road inclination according to the vehicle position. The torque commands are applied according to power consumption dynamics of the vehicle given

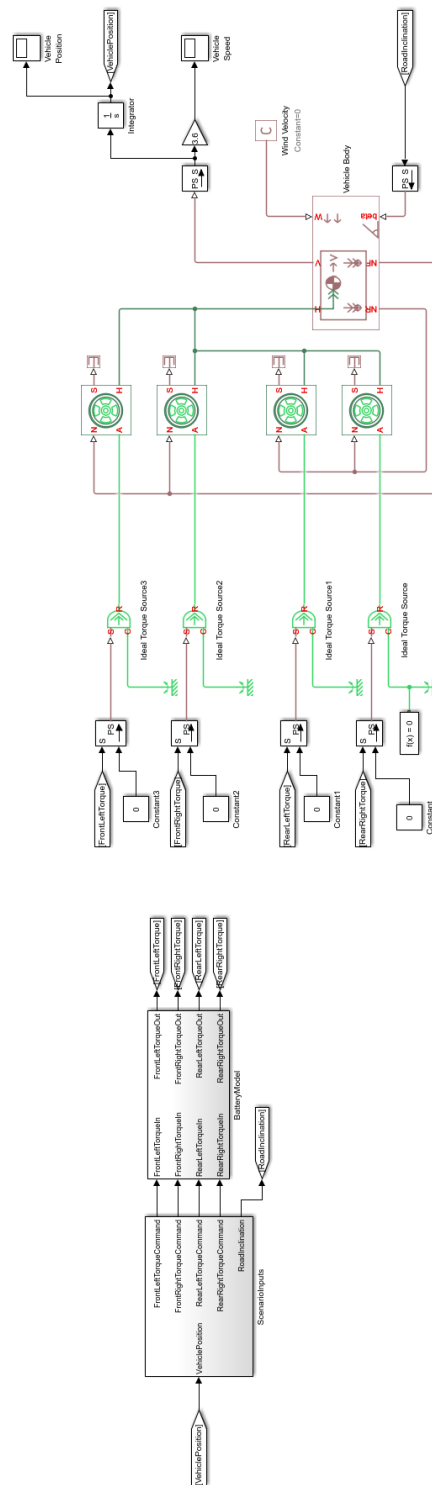


Figure 2.8: Simulink model developed to test the gross motion model

Table 2.1: Parameters of the model

Parameter Name	Value
Chassis mass	1200kg
Passenger/Driver mass	80kg
Wheel mass	12kg
Wheel radius	0.6m
Dimensions of chassis	4m × 2m
Density of air	1.225kg/m <sup>3</sup>
Air drag coefficient	0.682
Average drag area	1m <sup>2</sup>
<i>FPCB</i>	Fig. 2.6
<i>RPCB</i>	Fig. 2.7
Sampling time	1/100s

in 2.12, the torque commands are shaped. The shaped torque commands are applied to the tires. The tire model follows the Coulomb's law of friction. The vehicle model has interactions with tire model through traction and normal forces. The wind velocity is considered to be zero, and the vehicle speed and vehicle position are stored.

The gross motion vehicle model is implemented and compared against the Simulink model. Parameters of the model used in the simulations is given in Table 2.1. These parameters are approximations of the parameters of electric vehicles in the market. All the simulations are carried out for an autonomous vehicle with no passengers. On this occasion, it is to be noted that the same model parameters are used in all the other simulations presented in this thesis.

The vehicle is assumed to have an initial speed of 50 km/h, and the wheels have their initial angular velocities according to the initial velocity of the vehicle. The front wheels are excited with 100 Nm torque commands, and the rear wheels are left unexcited. The motion characteristics of the developed model and the Simulink model are compared and the differences in terms of the vehicle position and vehicle speed between the models are presented in Figs. 2.9 and 2.10, respectively. It has been observed that the difference in vehicle positions is less than 0.25 m throughout the road of 1 km, and the difference in vehicle speeds is less than 0.4 km/h for the reference speed of 50 km/h. Note that these small differences are not only due to the modelling deviations but also due to the fact that, the vehicle model developed in this thesis is run in discrete time with time step of 0.01 s, while the Simulink model is run in continuous time due to continuous time solver requirements of the VehicleBody block in the Simulink model. Nevertheless, the small differences between the two models verify that the modelling work in this thesis is compatible with the commercially available Simulink vehicle model.

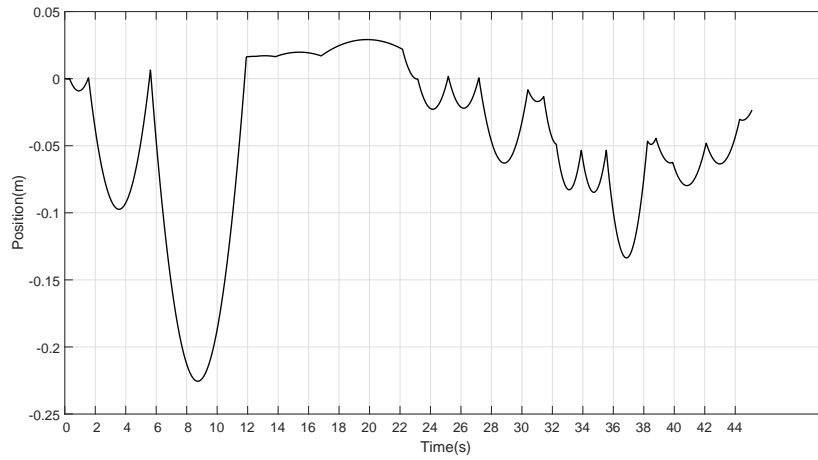


Figure 2.9: The difference in vehicle positions of Simulink model and the model developed in this study throughout the test scenario between

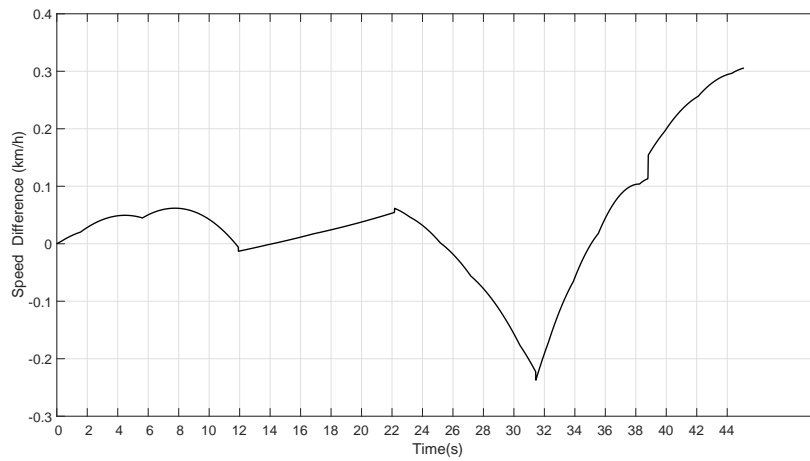


Figure 2.10: The difference in vehicle speeds of Simulink model and the model developed in this study throughout the test scenario between

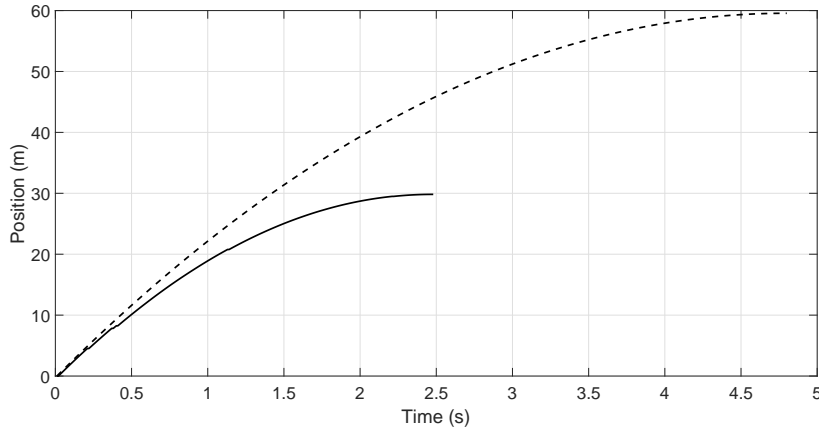


Figure 2.11: Change in the positions of the braking vehicles along asphalt and icy roads (solid line: asphalt road and dashed line: icy road)

### 2.13.2 Scenario-2: Braking along Asphalt and Icy Roads

In this test, vehicle moving at 90 km/h speed will apply braking of 250 Nm in four wheels until the vehicle stops. The test is repeated along asphalt road  $\mu = 0.72$  and icy road  $\mu = 0.19$  to check the effect of friction coefficient on braking characteristics of the vehicle. The changes in position and velocity of the braking vehicle along different road conditions are demonstrated in Figs. 2.11 and 2.12, respectively.

As expected from daily life experience, its it difficult to stop vehicle along icy roads, it takes more time and distance to achieve full stop condition compared to asphalt roads. The results demonstrated in the figures are consistent with the common experience.

### 2.13.3 Scenario-3: Cornering along Asphalt Road

In this scenario, a vehicle with 50 km/h initial speed will start cornering a quarter circle along asphalt road obeying constant Ackerman’s steering law. Front wheels are excited with 50 Nm constant torque throughout the scenario. The position of the vehicle and the tangential velocities of the vehicle and the wheels are presented in Figs. 2.13 and 2.14, respectively.

According to Ackerman’s steering law, the tangential velocities of the vehicle is proportional to their distances to the centre of rotation  $CoR$ . The rotation radius  $r$  is defined as the distance of a hypothetical point in middle of the rear axle to  $CoR$ . The tangential velocity figure depicts the small difference between the speeds of the wheels due to their relative distances to the  $CoR$ .

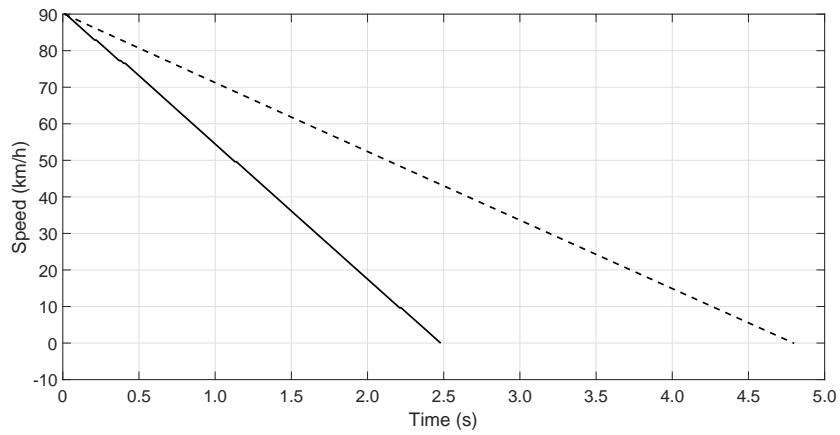


Figure 2.12: Change in the speeds of the braking vehicles along asphalt and icy roads (solid line: asphalt road and dashed line: icy road)

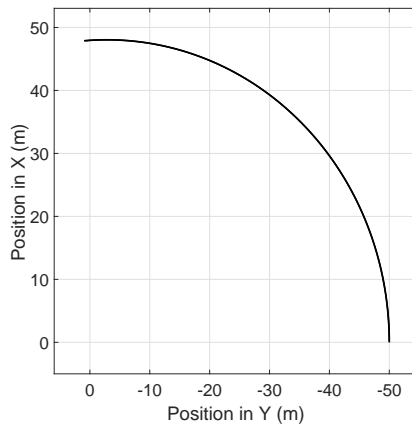


Figure 2.13: Change in the position of a vehicle cornering a quarter circle along asphalt road obeying constant Ackerman's steering law

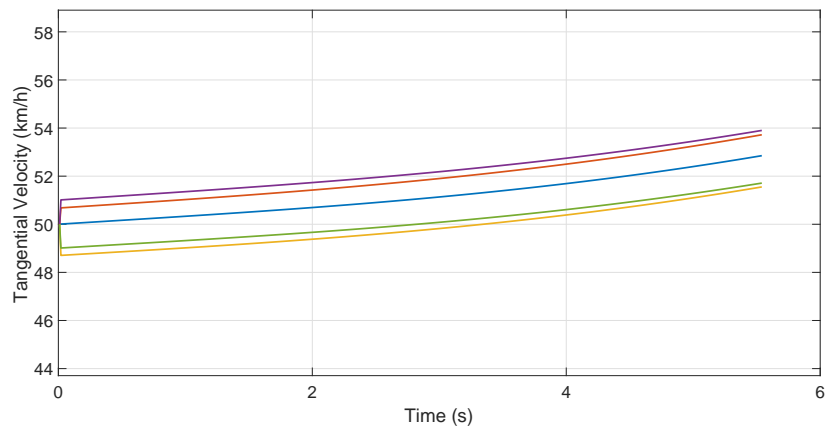


Figure 2.14: Change in the tangential velocities of a vehicle and its four wheels during cornering a quarter circle along asphalt road obeying constant Ackerman's steering law (blue: vehicle, red: front left wheel, yellow: front right wheel, violet: rear left wheel and green: rear right wheel)

## CHAPTER 3

### ENERGY OPTIMALITY

In this chapter, for the gross motion model of the vehicle moving on a variable-slope road, an energy optimal controller is designed with torque, speed and battery constraints. The energy consumption of the vehicle under the optimal controller is compared against the standard cruise controllers of various speed references in several scenarios including uphill and downhill motions with various slopes and lengths. According to the simulation results, the optimal controller is shown to be more energy efficient than the cruise controllers in all the considered scenarios. The tests are repeated along icy road sections, and the superiority of the energy optimal controller is verified for roads with low friction coefficients as well. A skidding compensation logic is proposed and tested to minimize the wheel slippage and it is observed that energy optimality of the solution is not affected by this compensation. A sensitivity analysis has been performed and it has been shown that, as a representative of different combinations of passengers, the sensitivity of the energy optimal controller to the mass change and distribution is small in magnitude. Furthermore, the tests with different initial values of the state-of-charge of the battery demonstrates that the superiority of the energy optimal controller against cruise controllers becomes significant especially when the battery is not fully charged and battery characteristics limit the charging capability during regenerative braking. The assumptions and the coverage of the presented optimal control approach is compared qualitatively with some recent studies addressing the similar problems.

#### 3.1 Introduction

The biggest challenges in the widespread usage of the electric vehicles for private transportation are the limitations due to current battery technology, and as a consequence of it, the requirement of high energy efficiency in vehicle control. Energy optimization in the electric vehicles is of crucial importance since it affects the physical properties of the vehicles through the battery requirements and vehicle capabilities. The uphill and downhill structure of the urban roads is an essential input for the development of energy-efficient driving policies.

There are various studies conducted on controllers to improve energy efficiency or fuel consumption. Corona, *et.al*, review adaptive cruise control systems and make a common benchmark set-up for their comparison. The methods investigated are non-linear model predictive control, on-line piecewise affine model predictive control

with mixed logical dynamical model, control for linear approximation model and for tangent approximation model, and gain scheduling techniques [19].

Khayyam, *et.al*, benefit from neuro-fuzzy inference system to predict road slope with a look-ahead system to improve adaptive cruise control and achieves 3% reduction in energy consumption [48]. Schwickart, *et.al*, propose an energy-efficient model predictive cruise controller for electric vehicles, with a linear prediction model, linear constraints corresponding to piecewise linear system behaviour and a quadratic cost function [72]. Kamal, *et.al*, employ generalized minimum residual method for model predictive control of energy consumption of the vehicles [45].

Hierarchical control schemes for energy efficient drive are available in literature as well. Li *et.al*, propose a low-level controller to compensate the non-linear vehicle dynamics to track the acceleration inputs, and a high-level controller based on model predictive control theory for energy management. To improve computational feasibility, a constraint softening method is applied to optimal control law with quadratic programming algorithm [52]. Chen, *et.al*, constructed a hierarchical control structure consisting of a high-level dynamic sliding mode controller and a low-level adaptive energy-efficient control allocation scheme. For vehicles with four in-wheel motors, they have achieved input-to-state stability of the overall system for planar motion [18]. Wang, *et.al*, present a hierarchical control structure for four-wheel driving and four-wheel steering electric vehicle [85]. The higher-level design is an LQR controller for lateral force and yaw moment controls, and lower-level design checks the tires to work in their stable regions for establishing the tracking control.

In addition to studies proposing improvements on energy management for cruise controllers, various algorithms have been used to minimize energy consumption of the vehicle directly. Kachroudi, *et.al*, proposed a particle swarm optimization algorithm for on-line energy optimisation of an electric vehicle [42]. In the study, battery autonomy, driving comfort indexes and travel time are taken into consideration as optimization measures. Wang, *et.al*, presented a constrained A\* algorithm for energy management for fully electric vehicles taking both the battery capacity and the real-time traffic conditions into account [87]. The context-aware algorithm achieves a route planning under the limited battery conditions. Chen, *et.al*, proposed a Karush-Kuhn-Trucker based optimization to find local optimal solutions, and to select the global optimal among these local solutions for energy-efficient control allocation for over-actuated electric vehicles [17]. The optimization scheme transfers the standard non-linear optimisation problem into a classical eigenvalue problem. Wang, *et.al*, studied optimal control method to maximize the cruising range and to minimize the travelling time for a specified destination under limited battery constraints [86]. The authors adopted an electric vehicle power consumption model for their optimal control application. Furthermore, Li *et.al*, address an approach to overcome the computational complexity of the model predictive control in adaptive cruise controllers. They propose a moving block strategy together with a constraint-set compression technique to reduce the scale of the problem and to relax inequality constraints in the prediction horizon [53]. Similarly, Chen, *et.al*, use terrain preview information to create energy-optimal speed references with the help of dynamic programming and model predictive control [16].

Sciarretta, *et.al*, benefit from optimal control theory and other off-line techniques to find solutions to energy management problem for vehicle families including electric

vehicles [73, 23]. Pennycott, *et.al*, use a look-up table of control allocation outcomes of an off-line optimization study, to increase regenerative braking and energy optimisation in electric drive [66].

In an energy optimal controller design, dependences of the policies on the road topology are investigated as well. Fuel optimal speed profiles based on information from road topology or estimates of the road gradient are studied for various types of vehicles including heavy trucks and trains [15, 39].

Similar to the problem investigated in this paper, Kamal, *et.al*, propose energy optimal control of electric vehicles throughout roads with up-down slopes. The authors utilize non-linear model predictive control with a fast optimization algorithm using road gradient conditions obtained from digital road maps. In simulations, the method reduces the fuel consumption of the vehicle [44, 43].

In controller schemes mentioned above, the vehicle model is simplified to longitudinal motion of vehicle. Lateral affects are discarded. However, even if the desired motion is longitudinal only, for the vehicle with wheels generating uneven traction forces due to road conditions affecting left and right sides differently, lateral dynamics should be included in the model. Slope of road is included in topology-dependent energy optimization methods [19, 44, 43]. State dependent energy consumption model [86], or tabulated databases with road slope, battery's state of charge, motor torque and vehicle speed [63] are used in optimization processes.

In this chapter, an energy optimal control policy is developed considering the gross motion of an electric vehicle. The 3-DoF (degree of freedom) dynamic model presented here for the vehicle includes longitudinal and lateral translational motions as well as planar rotational motions. Since the gross motion of the vehicle is considered, the small oscillatory motions of the suspension system are neglected. Thus, the chassis and the suspended body are treated in unison. The dynamic model employs Coulomb's friction law between the wheels and the road. During the simulations, the wheel contact forces are calculated at each time step by using the dynamic model of the vehicle. The comparison of the tangential contact force acting on a wheel with the static friction threshold determines whether that wheel skids or not. To handle the case of skidding, as the rotational motions of the wheels lose their dependencies on the linear motion of the chassis, the dynamic model of the vehicle is expanded to include the speeds of wheels as separate additional states. Therefore, the proposed dynamic model is general enough and it can be used under all sorts of road conditions with arbitrary friction, slope and curvature. Note that such a detailed model is required when the wheels have independent driving and braking capabilities or where the friction coefficient of the road changes, even if the desired motion is solely longitudinal and the controller designs try to avoid skidding.

In this chapter, the energy management strategy is based on the classical optimal control theory with constraints on vehicle speed, wheel torques and battery limitations. Through extensive simulation studies on different scenarios, the energy optimal controller has been shown to be more effective in energy management compared to the standard cruise controllers with various speed references. The comparisons in simulations are held on roads including variable slopes of various lengths. The scenarios are selected to cover all combinations of the selected possible road slopes seen in

urban traffic network. Main aim in this study is to show through simulations that, preserving the high fidelity of the vehicle and battery models, the optimal control theory based approach is suitable to develop a basis for reference autopilot designs. The energy optimal controller is compared against cruise controllers to fulfil this aim, and verification through simulations are considered to be adequate. Reference sets of outcomes for optimal control based approaches are obtained for future comparison with experimental measurements.

This chapter introduces the following outcomes:

1. Energy optimal control problem is defined for the vehicle. The problem is a free-final time problem. On the other hand, the distance to be travelled is fixed. A numerical method based on mapping the control inputs from the time domain to position domain has been developed and utilized to satisfy the fixed distance constraint (see Section 3.2).
2. The energy optimal controller is compared against cruise controller with different reference speeds in extensive simulations. The results depict the superiority of the energy optimal controller. Energy optimal solutions obey the speed constraints, avoids wheel slippage, and completes the roads in a travel time still comparable with the cruise controllers (see Section 3.3).
3. The energy optimal controller is shown to preserve its superiority in terms of the energy consumption of the electric vehicle for all the considered scenarios where the uphill and downhill sections of the road is icy. A skidding compensation logic is proposed to reduce the wheel slippage. The results show that, with no compromise in energy consumption of the vehicle, the occurrence of the wheel slippage is reduced with this compensation (see Section 3.4).
4. It has been shown that as a representative of different combinations of passengers, the sensitivity of the energy optimal controller on the mass change and distribution is smaller in magnitude. Furthermore, the tests with different initial values of the state-of-charge of the battery demonstrates that the superiority of the energy optimal controller against cruise controllers becomes significant especially when the battery is not fully charged and battery characteristics limit the charging capability during regenerative braking (see Section 3.5).

A qualitative comparison with the literature is performed and the following points are presented as the main contributions of this study (see Section 3.6):

1. A numerical method based on mapping the control inputs from the time domain to position domain has been proposed to deal with the free-final time two point boundary value problems.
2. A skidding compensation approach is proposed to reduce the percentages of the time instants when the wheels are in slippage. The skidding compensation logic is shown to be effective in reducing slippage and it has been observed that the energy optimality of the solution is preserved.

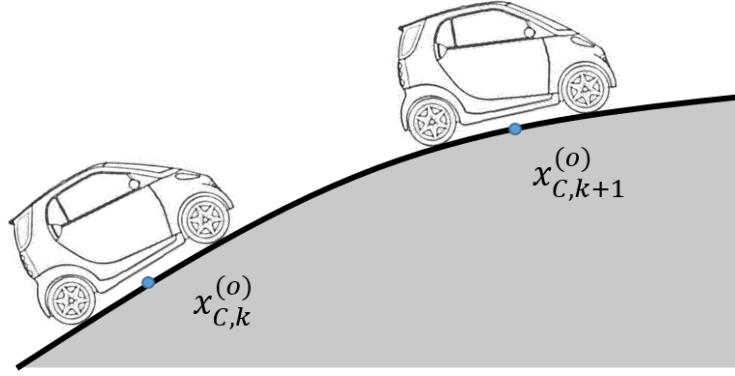


Figure 3.1: Uphill downhill motion representation

3. The superiority of the optimal control theory based solution for the energy management problem of electric vehicles is shown with comparisons against standard cruise controllers in asphalt and icy roads, which depicts that autopilot designs for electric vehicles based on optimal control solutions will be far more energy efficient.
4. The low sensitivity of the energy optimal controller with respect to passenger arrangements and initial state-of-charge of the battery in electric vehicles are demonstrated.

### 3.2 Optimal Controller Design

The optimal control problem addresses the generation of an energy optimal policy for the vehicle, mathematical model of which is described in Chapter 2. The motion of the vehicle along a sloped road can be illustrated as in Fig. 3.1.

The optimal control problem is defined on the state of the vehicle,  $\mathbf{x}$ , in (3.1) which is an abstraction of the positions and velocities of the chassis and the wheels defined in pseudo-inertial ground fixed reference frame. Model in Chapter 2 allows us to determine linear and angular accelerations of the chassis and the wheels, which can be used to update velocities and the positions. This update function is represented in an abstract form as  $\mathbf{f}$  in (3.2). Function  $\mathbf{f}$  is a nonlinear function of the state variables,  $SoC$  of the battery and the driving/braking torque commands,  $M_{wc,y}^{(w)}$ , and it returns the linear and angular accelerations of the chassis and the wheels independently of adherence, curvature or slope of the road.

$$\mathbf{x} = \left[ x_V^{(o)} \quad y_V^{(o)} \quad \psi_V \quad \dot{x}_v^{(o)} \quad \dot{y}_v^{(o)} \quad \omega_{v,z} \quad \omega_{fl,y} \quad \omega_{fr,y} \quad \omega_{rl,y} \quad \omega_{rr,y} \right]^T \quad (3.1)$$

$$\dot{\mathbf{x}} = \mathbf{f} \left( \mathbf{x}, SoC, M_{wc,y}^{(w)} \right) \quad (3.2)$$

The optimal control problem for time-discretized model can be written as in (3.3). Power, as a multiplication of speed and the torque for each wheel, summed throughout time for energy calculation. In (3.3),  $RPCB$  is reverse power capacity of the battery of the vehicle obtained from charging characteristics given in Fig. 2.6. The energy production due to regenerative braking is limited to reverse power capacity of the battery which is a function of  $SoC$ . The amount greater than this limit cannot be charged to the battery, but is dissipated as heat. There can be control input constraints on the optimal control problem. Maximum applied power to the wheels during driving cannot exceed the power supply limits. Furthermore, for preserving safe drive, torque inputs cannot exceed wheel torque capacities. Speed constraints can also be added by the driver/user.  $FPCB$  denotes the Forward Power Capacity of the Battery;  $MTC$  is the Maximum Torque Capacity of each wheel. The latter two constraints in (3.3) are required to prevent skidding of the wheels.

*minimize*

$$J_e \left( \sum_w M_{wc,y}^{(w)} \right) \\ = \sum_{t_0}^{t_f} \left( \begin{array}{ll} M_{w_{fl}c,y}^{(w_{fl})} \omega_{w_{fl},y} + M_{w_{fr}c,y}^{(w_{fr})} \omega_{w_{fr},y} & \text{if } \sum_w M_{wc,y}^{(w)} \geq 0 \\ -\min(M_{w_{fl}c,y}^{(w_{fl})} \omega_{w_{fl},y} + M_{w_{fr}c,y}^{(w_{fr})} \omega_{w_{fr},y} + M_{w_{rl}c,y}^{(w_{rl})} \omega_{w_{rl},y} + M_{w_{rr}c,y}^{(w_{rr})} \omega_{w_{rr},y}, RPCB) & \text{if } \sum_w M_{wc,y}^{(w)} < 0 \end{array} \right)$$

*subject to*

$$\dot{\mathbf{x}} = \mathbf{f}(\mathbf{x}, SoC, M_{wc,y}^{(w)})$$

$$v_{v,x_{min}}^{(o)} \leq v_{v,x}^{(o)} \leq v_{v,x_{max}}^{(o)}$$

$$M_{w_{fl}c,y}^{(w_{fl})} \omega_{w_{fl},y} + M_{w_{fr}c,y}^{(w_{fr})} \omega_{w_{fr},y} \leq FPCB$$

$$M_{wc,y}^{(w)} \leq MTC$$

$$|\bar{u}_{v,w_k}^T \bar{F}_{gw_k}^{(w_k)}| < \mu_{s,w_k} \bar{u}_z^T \bar{F}_{gw_k}^{(w_k)}$$

(3.3)

The energy optimal control problem is defined for a path of a specified length; hence, the initial state is known, and final state can be specified in terms of position. Other than state boundary conditions, optimal control problem has free final time. According to Pontryagin's minimum principle a solution satisfying the control input constraints is found. State constraints follow the artificial state method explained in [49]. Therefore, Hamiltonian at discrete time step,  $k$ , can be written as in (3.4).

$$\mathcal{H}_k = \left( \begin{array}{ll} M_{w_{fl}c,y}^{(w_{fl})} \omega_{w_{fl},y} + M_{w_{fr}c,y}^{(w_{fr})} \omega_{w_{fr},y} & \text{if } \sum_w M_{wc,y}^{(w)} \geq 0 \\ -\min(M_{w_{fl}c,y}^{(w_{fl})} \omega_{w_{fl},y} + M_{w_{fr}c,y}^{(w_{fr})} \omega_{w_{fr},y} + M_{w_{rl}c,y}^{(w_{rl})} \omega_{w_{rl},y} + M_{w_{rr}c,y}^{(w_{rr})} \omega_{w_{rr},y}, RPCB) & \text{if } \sum_w M_{wc,y}^{(w)} < 0 \end{array} \right) \\ + \mathbf{p}^T \mathbf{f}(\mathbf{x}, SoC, M_{wc,y}^{(c)}) + \mathbf{p}_l \left[ \left( v_{v,x_{min}}^{(o)} \leq v_{v,x}^{(o)} \right)^3 \left( v_{v,x_{max}}^{(o)} \leq v_{v,x}^{(o)} \right)^3 \right] \quad (3.4)$$

**state update**

$$\frac{\partial \mathcal{H}}{\partial \mathbf{p}} = \dot{\mathbf{x}}^*(t)$$

$$\dot{\mathbf{x}}_{1:10}(t) = \mathbf{f}(\mathbf{x}, SoC, M_{wc,y}^{(w)})$$

$$\dot{\mathbf{x}}_{11}(t) = \left[ (v_{v,x_{min}}^{(o)} - \|\mathbf{x}_{4:5}(t)\|)^3 (v_{v,x_{max}}^{(o)} - \|\mathbf{x}_{4:5}(t)\|)^3 \right]$$

**co – state update**

$$\frac{\partial \mathcal{H}}{\partial \mathbf{x}} = -\dot{\mathbf{p}}^*(t)$$

**control input**

$$\mathbf{u}^*(t) = \arg \min_{\mathbf{u}} \mathcal{H}$$

**terminal conditions**

$$\mathbf{x}_{initial} = \left[ 0 \ 0 \ 0 \ v_{v,x_{ref}}^{(o)} \ 0 \ 0 \ \omega_{w,y_{ref}} \ \omega_{w,y_{ref}} \ \omega_{w,y_{ref}} \ \omega_{w,y_{ref}} \right]^T \quad (3.5)$$

$$v_{v,x_{ref}}^{(o)} = 90 \text{ km/h}$$

$$\omega_{w,y_{ref}} = \frac{v_{v,x_{ref}}^{(o)}}{R}$$

$$\mathbf{p}_{1:10,initial} = \mathbf{0}$$

**transversality condition**

$$\mathbf{p}_{11,initial} = \left( \|\mathbf{x}_{4:5}(t_f)\| - v_{v,x_{ref}}^{(o)} \right)^2$$

**control input constraints**

$$M_{w_{fl},y}^{(w_{fl})} \omega_{w_{fl},y} + M_{w_{fr},y}^{(w_{fr})} \omega_{w_{fr},y} \leq FPCB$$

$$M_{wc,y}^{(w)} \leq MTC$$

*Characteristics of the battery : Fig. 2.6 and Fig. 2.7.*

In (3.4),  $\mathbf{p}$  denotes the co-state and  $\mathbf{f}(\mathbf{x}, SoC, M_{wc,y}^{(c)})$  denotes the nonlinear state update function. The velocity constraints are taken into consideration in the form given in (3.4) with a Lagrange multiplier  $\mathbf{p}_l$ . This structure comprises a multiplication of upper and lower limit constraints in the form similar to a multiplication of the sign and the modulus for each. This interpretation not only penalize the values exceeding the limits but also drifts the solution towards the midpoint. In other words, the structure preferred to impose velocity constraints tries to keep the velocity at its reference value. In (3.5), equations of optimality, terminal constraints and transversality conditions for this two-point boundary value problem in (3.3) and (3.4) are given.

**Remark:** The optimal control outcome is obtained by an iterative solution of the equations of optimality. Note that state update is in forward direction with the given initial condition while the co-state update is in the backward direction from the given initial condition at final time. In each iteration, the update for the augmented control vector  $\mathbf{U}$  is determined with a one dimensional search algorithm. Note that when time-discretized  $\mathbf{U}$  is updated, the information to be transferred to the next iteration is the control input to be applied at those resultant positions of the vehicle along the path. Time-discretized augmented control vector  $\mathbf{U}$  together with positions of the

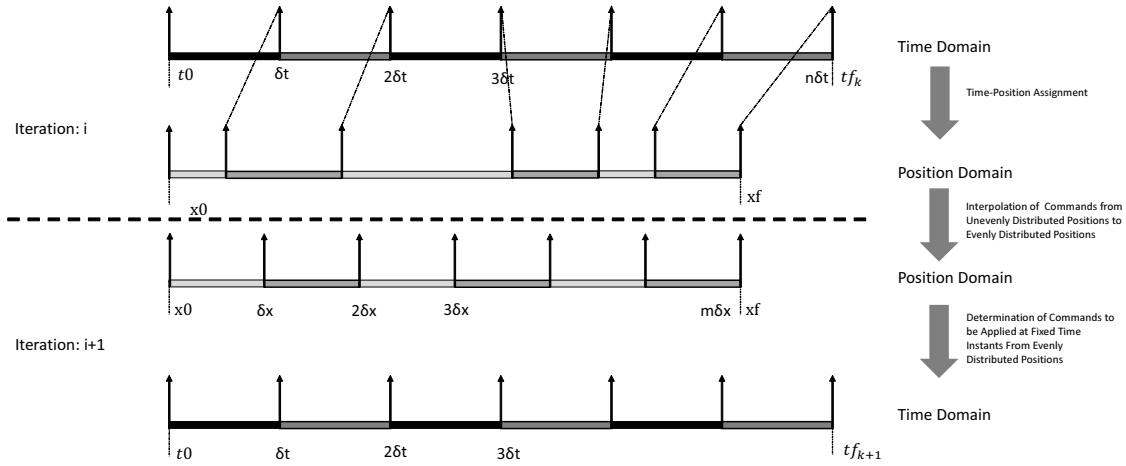


Figure 3.2: Iterative solution approach proposed for free-final time optimal control problems

vehicle at the instants  $u$  being applied are interpolated with fixed position resolution to obtain position-discretized version of  $U$ , denoted as  $\hat{U}$ . At the beginning of each iteration, for current position and velocity, the position of the vehicle at the next time step is predicted, and a new control command is interpolated from  $\hat{U}$ . The solution approach is presented in Fig. 3.2.

The optimal control algorithm is explained as follows. In the algorithm,  $x$  denotes the state vector,  $u$  denotes the control input vector at a given time instant,  $U$  is time discretized control input vector sequence over time instants,  $\hat{U}$  is position discretized the control input vector sequence,  $k$  is the time index,  $i$  is the iteration index,  $\alpha$  is the one dimensional search step vector,  $\beta$  is the one dimensional search step rate and  $\mathcal{H}$  is the Hamiltonian defined as augmented cost function.

State update in (3.5) is performed in step 9, terminal conditions of this two-point boundary value problem is checked in this step of the algorithm as well. The transversality condition is used in step 17 and co-state update is performed in step 18. The numeric derivative of Hamiltonian function with respect to the control input is obtained in step 24 and it is used to update the control input for the next iteration. The constraints on the control input as well as skidding algorithm avoidance logics are taken into consideration in steps 10-14 of the algorithm. The state vector is not augmented with another variable expressing  $SoC$ . Instead, history and update of  $SoC$  is computed separately in step 16 of the algorithm.

Note that in step 24 of the optimal control solution algorithm, derivative of the Hamiltonian function defined in (3.4) with respect to the control input is calculated. When the control input is positive, the vehicle is consuming energy, when it is negative, due to regenerative braking properties of the electric motors, some amount of energy can be stored back to the batteries. Note that Hamiltonian is discontinuous when the control input  $u$  becomes zero. This discontinuity can be solved with an adjustment in

Table3.1: Optimal control solution algorithm

---

01:	<b>Procedure: Optimal Solution</b>
02:	<b>Initialization :</b>
03:	Initialize $\mathbf{U}_{1,1:k_f} = \mathbf{U}_{initial,1:k_f}$ .
04:	Initialize $\mathbf{x}_{1,1} = \mathbf{x}_{initial}$ .
05:	From $\mathbf{x}_{1,1}$ and $\mathbf{U}_{1,1:k_f}$ , generate $\mathbf{x}_{1,1:k_f}$ until $\mathbf{x}_{1,k_f} = \mathbf{x}_{final}$ .
06:	Re-sample time-discretized $\mathbf{U}_{1,1:k_f}$ applied at positions $\mathbf{x}_{1,1:k_f}$ to generate $\hat{\mathbf{U}}_{1,1:k_f}$ sampled at fixed position resolution.
07:	Initialize $i = 1$ , initialize $\gamma$ , set $\beta$ .
08:	<b>Optimal Control Loop :</b>
09:	For each time sample $k$ , with current position and next position predicted with a constant current speed, interpolate position discretized $\hat{\mathbf{U}}_{i,1:k_f}$ , and save as $\mathbf{u}_{i,k}$ .
10:	Apply control input related constraints to $\mathbf{u}_{i,k}$ :
11:	If $\mathbf{u}_{i,k} > MTC$ , then $\mathbf{u}_{i,k} = MTC$ .
12:	If $\mathbf{u}_{i,k} < -MTC$ , then $\mathbf{u}_{i,k} = -MTC$ .
13:	If $ F_{wg,x}^{(w)}  < \mu_{s,x} F_{wh,z}^{(w)}$ or $ F_{wg,y}^{(w)}  < \mu_{s,y} F_{wg,z}^{(w)}$ , skidding begins. If $\sum_w M_{wc,y}^{(w)} \geq 0$ , then decrease $M_{wc,y}^{(w)}$ control commands rationally, until there is no skidding. If $\sum_w M_{wc,y}^{(w)} < 0$ , then increase $M_{wc,y}^{(w)}$ control commands rationally, until there is no skidding.
14:	Limit $\mathbf{u}_{i,k}$ according to current <i>SOC</i> and battery characteristics, according to Fig. 2.6 and Fig.2.7.
15:	Until $\mathbf{x}_{1,k_f} = \mathbf{x}_{final}$ , generate $\mathbf{U}_{i,1:k_f}$ and corresponding $\mathbf{x}_{1,1:k_f}$ .
16:	Update <i>Soc</i> according to $\mathbf{U}_{i,1:k_f}$ and battery characteristics according to Fig. 2.6 and Fig.2.7.
17:	Initialize $\mathbf{p}_{i,k_f} = \mathbf{p}_{initial}$ calculated according to transversality condition in (3.5).
18:	From $\mathbf{x}_{i,1:k_f}$ , $\mathbf{U}_{i,1:k_f}$ and $\mathbf{p}_{i,k_f}$ , generate $\mathbf{p}_{i,1:k_f}$ .
19:	Calculate $\mathcal{H}_{i,1:k_f}$ .
20:	If two consecutive $\sum_1^{k_f} \mathcal{H}_{i,k}$ values are close enough, quit the algorithm.
21:	Update $\alpha$ :
22:	If $\sum_1^{k_f} \mathcal{H}_{i,k} \geq \sum_1^{k_f} \mathcal{H}_{i-1,k}$ , then $\alpha_{i+1} = \alpha_i / \beta$ .
23:	If $\sum_1^{k_f} \mathcal{H}_{i,k} < \sum_1^{k_f} \mathcal{H}_{i-1,k}$ , then $\alpha_{i+1} = \alpha_i * \beta$ .
24:	Calculate $\frac{\partial \mathcal{H}}{\partial \mathbf{U}} _{i,1:k_f}$ .
25:	$\mathbf{U}_{i+1,1:k_f} = \mathbf{U}_{i,1:k_f} - \alpha \frac{1}{\ \frac{\partial \mathcal{H}}{\partial \mathbf{U}} _{i,1:k_f}\ } \frac{\partial \mathcal{H}}{\partial \mathbf{U}} _{i,1:k_f}$ .
26:	Re-sample time-discretized $\mathbf{U}_{i+1,1:k_f}$ to be applied at positions $\mathbf{x}_{i,1:k_f}$
26:	to generate $\hat{\mathbf{U}}_{i+1,1:k_f}$ sampled at fixed position resolution.
27:	Increment $i$ , go back to the step 9.
28:	<b>end procedure</b>

---

the definition of the Hamiltonian. Instead of using two disjoint functions for positive and negative control inputs, their averaged sum weighted with a continuous function, such as  $\tan^{-1}(\cdot)$  can be used. The modified Hamiltonian can be expressed as in (3.6). Together with this modification, in this study an energy optimal control algorithm is proposed. The energy optimal control problem is a free-final time problem. On the other hand, the distance to be covered is fixed. A numerical method based on mapping the control inputs from the time domain to position domain has been developed and utilized to satisfy the fixed distance constraint.

$$\begin{aligned}
\mathcal{H}_k = & \left( 0.5 + \frac{1}{\pi} \tan^{-1} \left( \eta \sum_w M_{wc,y}^{(w)} \right) \right) \left( M_{w_{fl}c,y}^{(w_{fl})} \omega_{w_{fl},y} + M_{w_{fr}c,y}^{(w_{fr})} \omega_{w_{fr},y} \right) \\
& - \left( -0.5 + \frac{1}{\pi} \tan^{-1} \left( \eta \sum_w M_{wc,y}^{(w)} \right) \right) \left[ \min \left( M_{w_{fl}c,y}^{(w_{fl})} \omega_{w_{fl},y} + M_{w_{fr}c,y}^{(w_{fr})} \omega_{w_{fr},y} \right. \right. \\
& \left. \left. M_{w_{rl}c,y}^{(w_{rl})} \omega_{w_{rl},y} + M_{w_{rr}c,y}^{(w_{rr})} \omega_{w_{rr},y}, RPCB \right) \right] \\
& + \mathbf{p}^T \mathbf{f}(\mathbf{x}, SoC, M_{wc,y}^{(c)}) + \mathbf{pl} \left[ \left( v_{v,x_{min}}^{(o)} \leq v_{v,x}^{(o)} \right)^3 \left( v_{v,x_{max}}^{(o)} \leq v_{v,x}^{(o)} \right)^3 \right]
\end{aligned} \tag{3.6}$$

In (3.6),  $\eta$  stands for the smoothing factor, and it has been chosen sufficiently large so that the smoothed Hamiltonian approximates the discontinuous one. In Fig. 3.3, for different values of  $\eta$  and control commands, the normalized differences between the modified Hamiltonian given in (3.6) and the discontinuous Hamiltonian given in (3.4) is presented. The vehicle speed is chosen to be 90 km/h, the wheel speeds are calculated accordingly, and other components in Hamiltonian equations are taken to be the same.

It has been observed in Fig. 3.3 that for  $\eta$  greater than 1, the normalized difference between modified and discontinuous Hamiltonian functions are less than 1E-4, which is negligible. Since the modified Hamiltonian has smoother characteristics compared to the discontinuous one, the convergence of the solution is faster with the modified Hamiltonian function.

### 3.3 Results

The energy optimal controller is compared with cruise controllers of 70 km/h, 90 km/h and 110 km/h speed references with respect to their energy consumptions under the scenarios presented in Table 3.2. The cruise controller speed references are chosen to represent the speed limits defined for the optimal controller adequately. The scenarios are selected to cover all the possible combinations of the uphill/downhill sections with 100 m and 200 m. A road with a total length of 1 km is divided into two equal parts. The comparison scenarios are defined categorically as presented in Table 3.2.

The first categorization is based on which half includes uphill section. For example, in scenarios 1-12, the first 500 m comprises an uphill section, then the second 500

Table3.2: Test scenarios

Scenario ID	1 <sup>st</sup> Slope Angle (°)	1 <sup>st</sup> Slope Location (m)	2 <sup>nd</sup> Slope Angle (°)	2 <sup>nd</sup> Slope Location (m)
Scenario-01	+3	200-300	-3	700-800
Scenario-02	+3	200-300	-6	700-800
Scenario-03	+6	200-300	-3	700-800
Scenario-04	+6	200-300	-6	700-800
Scenario-05	+3	100-300	-3	700-800
Scenario-06	+3	100-300	-6	700-800
Scenario-07	+6	100-300	-3	700-800
Scenario-08	+6	100-300	-6	700-800
Scenario-09	+3	200-300	-3	600-800
Scenario-10	+3	200-300	-6	600-800
Scenario-11	+6	200-300	-3	600-800
Scenario-12	+6	200-300	-6	600-800
Scenario-13	-3	200-300	+3	700-800
Scenario-14	-3	200-300	+6	700-800
Scenario-15	-6	200-300	+3	700-800
Scenario-16	-6	200-300	+6	700-800
Scenario-17	-3	100-300	+3	700-800
Scenario-18	-3	100-300	+6	700-800
Scenario-19	-6	100-300	+3	700-800
Scenario-20	-6	100-300	+6	700-800
Scenario-21	-3	200-300	+3	600-800
Scenario-22	-3	200-300	+6	600-800
Scenario-23	-6	200-300	+3	600-800
Scenario-24	-6	200-300	+6	600-800

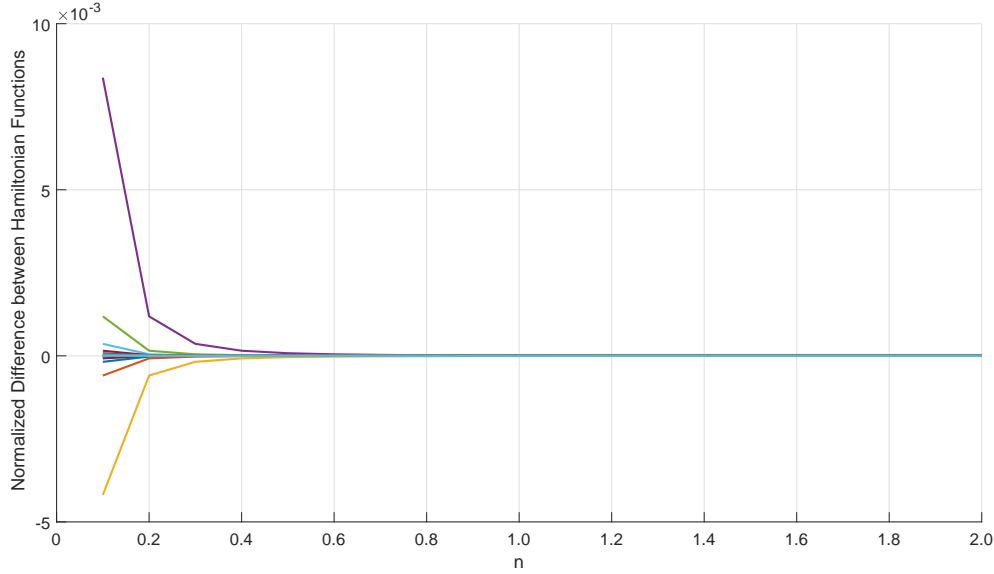


Figure 3.3: Normalized difference between modified and discontinuous Hamiltonian functions for different values of  $\eta$

m comprises a downhill section. In scenarios 13-24, this selection is reversed. The second categorization is based on the lengths of the sloped sections. For example, in scenarios 1-4, the road starts with an uphill section of 100 m, then continues with a downhill section of 100 m. In scenarios 13-16, the lengths of the sloped sections are the same but the slopes are reversed. The other categories include mixed patterns such as, first uphill of 200 m, then downhill of 100 m (e.g., scenarios 5-8), first downhill of 200 m, then uphill of 100 m (e.g., scenarios 17-20), first uphill of 100 m, then downhill of 200 m (e.g., scenarios 9-12), and first downhill of 100, then uphill of 200 m (e.g., scenarios 21-24).

The scenarios are selected such that all possible combinations of  $\pm 3$  deg, and  $\pm 6$  deg slopes are included as given in Table 3.2. Thus, a total of 24 different scenarios are studied. In urban traffic, such instant slope changes are not available; hence, the slope change is smoothed with a hypothetical radius curvature tangent to the sections of the roads at 10 m distance to the slope edges. The smoother slope transition is demonstrated in Fig. 3.4.

In order to create references in the upcoming figures, start and stop points of the first and the second slope are marked with A, B, C and D. For Scenario-1, the marks are shown in Fig. 3.5.

To show typical samples in limited space, the vehicle speed variations under standard cruise controller with different speed references and optimal control policy are presented in Fig. 3.6 for Scenarios 01, 05, 09, 13, 17 and 21. The histogram of the speed profile of the vehicle under optimal controller is observed to obey the defined speed limits. Since the cruise controllers follow their references, they are not presented in the figures. It has been observed that, to reduce the energy consumption of the vehicle, the energy optimal control decreases the speed of the vehicle. However,

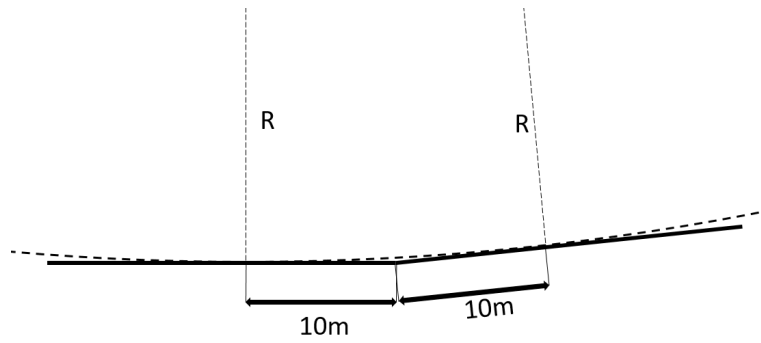


Figure 3.4: An example of slope smoothing at edges

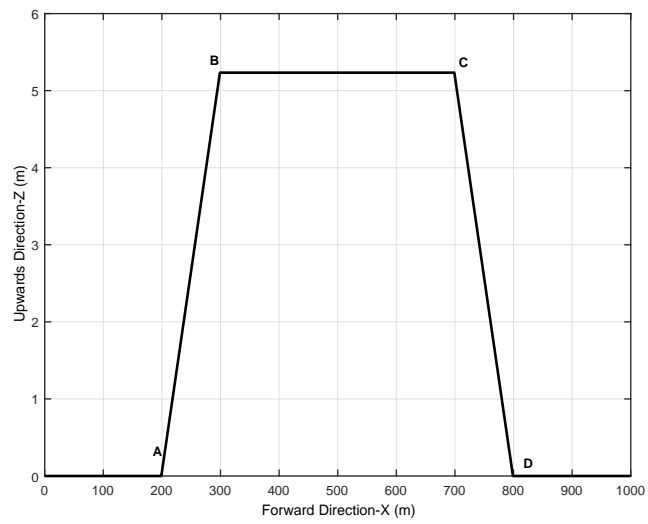


Figure 3.5: Marks for the start and stop points of the sloped sections

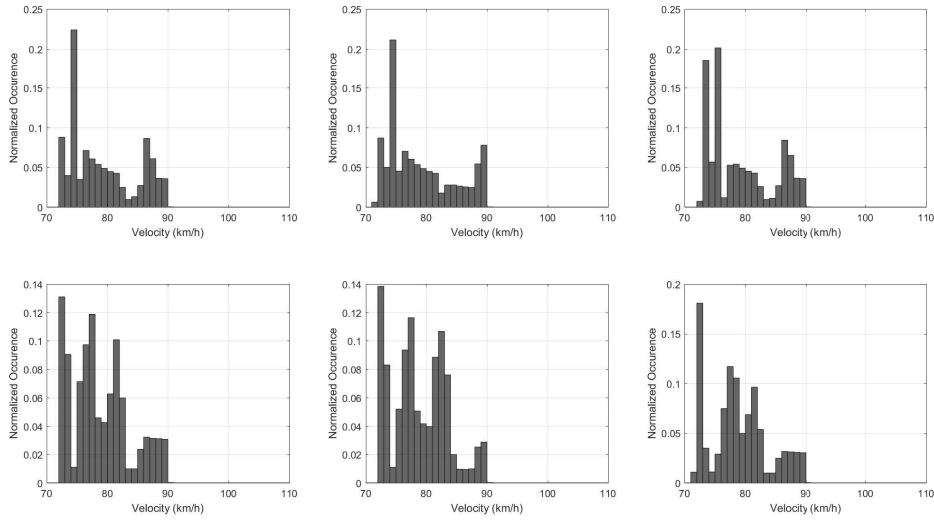


Figure 3.6: Histogram of the speed profiles of vehicle under energy optimal controller for various scenarios (top left: Scenario-01, top middle: Scenario-05, top right: Scenario-09, bottom left: Scenario-13, bottom middle: Scenario-17, and bottom right: Scenario-21)

note that the vehicle speed does not stick to lower speed limit defined for the energy optimal controller which is 70 km/h. This is because, as the speed of the vehicle becomes smaller, the amount of time to complete the road gets greater, and such an increase in time may result in more energy consumption. The energy optimal controller, therefore, generates speed profiles optimized for the vehicle constraints and the road topology. Note that the histograms show that the speeds of the vehicles under the energy optimal controller have components greater than the reference speed 90 km/h very rarely to reduce the acceleration and consecutive power consumption. In Table 3.3, average speeds of the vehicle under energy optimal controller are presented for all the scenarios. It has been observed that the average speeds are always below the reference speed defined for the optimal controller. Note that there is always a trade-off between the reduction in energy consumption and the effect of the constraint keeping the speed of the vehicle close to the reference speed.

Driving/braking torque commands applied to the wheels throughout Scenario 20 under cruise controllers with different reference speeds and the energy optimal controller are shown in Fig. 3.7. Remember that the vehicle is front drive with four wheels can have independent braking commands, in other words, the rear wheels are only used in braking and only excited with negative torque commands. It has been observed that the energy optimal controller demands more negative driving commands from front wheels and greater braking commands from all the wheels compared to the cruise controllers. Energy management strategy with greater regenerative braking results in admissible extension to duration for completing the given path compared to the standard cruise controller with 90 km/h speed reference which is initial speed

Table3.3: Average speeds of the vehicles under energy optimal controllers (km/h)

Scenario ID	01	02	03	04	05	06	07	08
Average Speed	79.24	79.79	78.78	78.54	79.13	79.58	79.65	78.56
Scenario ID	09	10	11	12	13	14	15	16
Average Speed	79.27	78.63	78.74	78.09	78.88	79.90	78.73	79.40
Scenario ID	17	18	19	20	21	22	23	24
Average Speed	78.89	79.79	78.30	79.24	78.92	79.26	78.53	79.10

for energy optimal controller as well. Furthermore, note that since the road profile is longitudinal only and there is no change in road friction coefficients throughout the scenario, the torque commands are symmetrical for left and right side wheels.

Friction forces applied on the wheels at their contact points with the ground are shown in Fig. 3.8 for a vehicle performing Scenario 19. Step 13 of the algorithm presented avoids the wheels to skid, and it has been observed that none of the wheels gets closer to the static friction limits of the wheels which is around 2 kN. Scenario 19 and Scenario 20 have close definitions in Table 3.2. Note the similarities in Figures 3.7 and 3.8 that since the wheels avoid slippage, the driving/braking commands are transferred directly to tire friction forces and generate traction. Furthermore, note that since the road profile is longitudinal only and there is no change in road friction coefficients throughout the scenario, the friction forces applied on the wheels are symmetrical for left and right side wheels.

In Fig. 3.9, change in  $SoC$  of vehicle batteries under the energy optimal controller and cruise controllers with different reference speeds for Scenarios 9-12 are demonstrated. It has been observed that during regenerative braking, batteries of the vehicle are charged. The superiority of the energy optimal controller compared to the cruise controllers is found to be clear. Note that to preserve some capacity in the battery that can be charged with regenerative braking, the initial state-of-charge of the package is taken as 90%.

Energy consumption ( $EC$ ) of the vehicle is calculated according to (3.7). The energy efficiency ( $EE$ ) of the energy optimal controller with respect to the cruise controller with different reference speed is calculated with (3.8). In Table 3.4,  $EC$ s of the vehicle under cruise controllers with different speed references and the energy optimal controller and the  $EE$ s of the energy optimal controller with respect to the others are presented. It has been observed that energy consumptions of the vehicle under the energy optimal controller are the smallest in all the scenarios and the efficiencies compared to the cruise controllers are up to 80%.

$$EC = SoC_{initial} - SoC_{final} \quad (3.7)$$

$$EE = \frac{EC_{Cruise\ Controller} - EC_{Optimal\ Controller}}{EC_{Cruise\ Controller}} \quad (3.8)$$

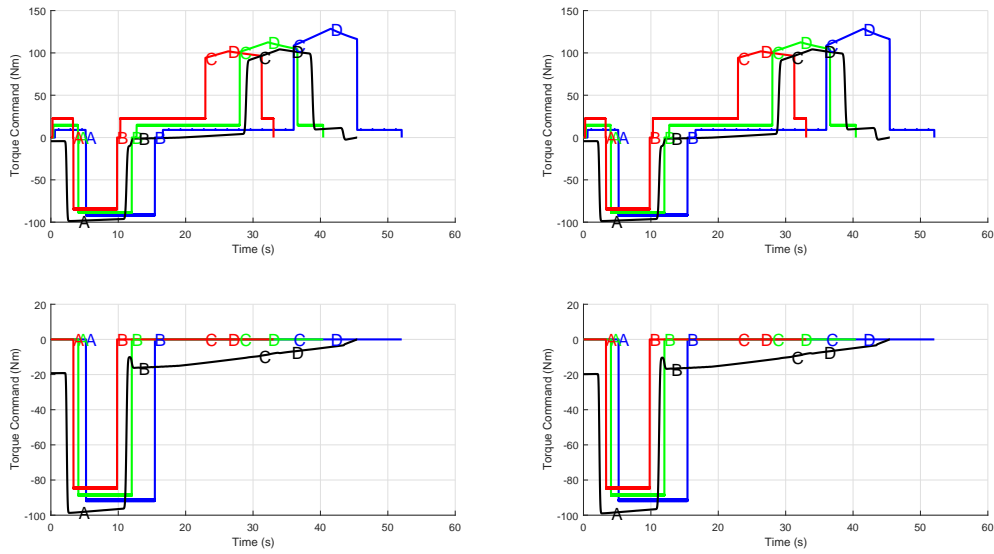


Figure 3.7: Torque commands applied to the wheels for Scenario 20 (red: cruise controller with 110 km/h speed reference, green: cruise controller with 90 km/h speed reference, blue: cruise controller with 70 km/h speed reference and black: energy optimal controller; top left: front left wheel, top right: front right wheel, bottom left: rear left wheel and bottom right: rear right wheel)

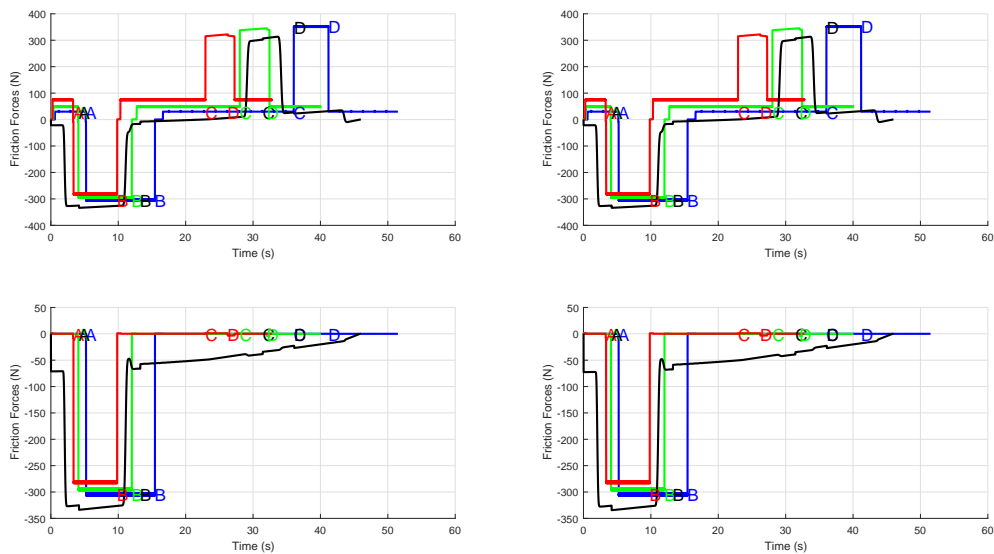


Figure 3.8: Longitudinal friction forces applied to the wheels for Scenario 19 (red: cruise controller with 110 km/h speed reference, green: cruise controller with 90 km/h speed reference, blue: cruise controller with 70 km/h speed reference and black: energy optimal controller; top left: front left wheel, top right: front right wheel, bottom left: rear left wheel and bottom right: rear right wheel)

Table3.4:  $EC$ s of the vehicle under different controllers ( $kJ$ ) and  $EE$ s of the energy optimal controller with respect to cruise controllers (%)

Scenario ID	$EC_{CC,70}$	$EC_{CC,90}$	$EC_{CC,110}$	$EC_{OC}$	$EE_{CC,70}$	$EE_{CC,90}$	$EE_{CC,110}$
Scenario-01	8.58	6.73	5.53	1.20	86.01	82.17	78.30
Scenario-02	8.58	6.73	5.53	1.18	86.25	82.47	78.66
Scenario-03	9.02	6.80	5.58	2.34	74.06	65.59	58.06
Scenario-04	8.71	6.80	5.58	2.32	73.36	65.88	58.42
Scenario-05	8.59	6.75	5.55	2.37	72.41	64.89	57.30
Scenario-06	8.59	6.75	5.55	2.35	72.64	65.19	57.66
Scenario-07	8.59	6.75	5.55	3.58	58.32	46.96	35.50
Scenario-08	8.59	6.75	5.55	3.38	60.65	49.93	39.10
Scenario-09	7.31	5.72	4.68	1.18	83.86	79.37	74.79
Scenario-10	7.31	5.72	4.73	1.13	84.54	80.24	75.85
Scenario-11	7.45	5.80	4.68	2.32	68.86	60.00	50.95
Scenario-12	7.45	5.80	4.73	2.27	69.53	60.86	52.01
Scenario-13	8.61	6.74	5.54	1.32	84.67	80.41	76.17
Scenario-14	8.72	6.81	5.59	1.50	82.80	77.97	73.17
Scenario-15	8.61	6.74	5.54	1.19	86.18	82.34	78.52
Scenario-16	8.72	6.81	5.58	1.50	82.80	77.97	73.12
Scenario-17	7.38	5.75	4.70	1.07	85.50	81.39	77.23
Scenario-18	7.49	5.82	4.75	1.50	79.97	74.23	68.42
Scenario-19	7.38	5.75	4.70	0.66	91.06	88.52	85.96
Scenario-20	7.49	5.79	4.75	0.15	80.37	74.61	69.05
Scenario-21	8.61	6.75	5.55	2.47	71.31	63.41	55.50
Scenario-22	8.61	6.75	5.55	2.27	73.52	66.22	58.92
Scenario-23	8.61	6.75	5.55	2.29	73.40	66.07	57.74
Scenario-24	8.61	6.75	5.55	3.28	61.90	51.41	40.90

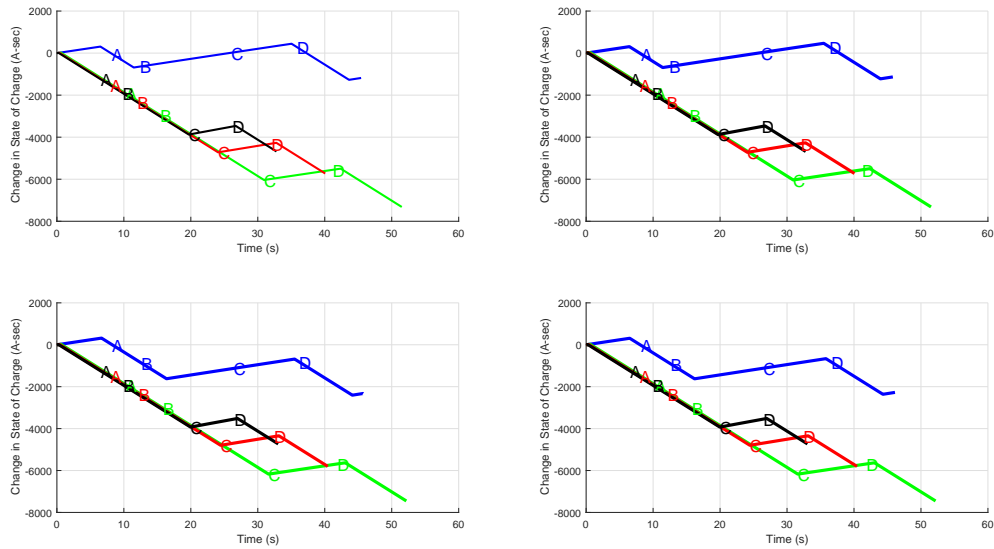


Figure 3.9: Change in state of charge of vehicle battery package (black: cruise controller with 110 km/h speed reference, red: cruise controller with 90 km/h speed reference, green: cruise controller with 70 km/h speed reference and blue: energy optimal controller; top right: Scenario-09, top left: Scenario-10, bottom right: Scenario-11 and bottom left: Scenario-12)

In Table. 3.5, number of iterations spent in finding the energy optimal control solution for the scenarios is presented. For a computer, with Intel Core i7-6700 HQ CPU, 2.60 Ghz, and 16 GB Ram, and x64 bit Windows 7, an iteration takes 20 seconds to complete.

### 3.4 Skidding Compensation

In this section, for the scenarios given in Table 3.2, the sloped sections are considered as icy road sections with  $\mu = 0.19$  [8]. It has been observed that both the optimal

Table3.5: Number of iterations to find the energy optimal solution

Scenario ID	01	02	03	04	05	06	07	08
Iterations	1340	1302	1288	1290	1312	1302	1297	1352
Scenario ID	09	10	11	12	13	14	15	16
Iterations	1320	1327	1290	1321	1340	1279	1360	1298
Scenario ID	17	18	19	20	21	22	23	24
Iterations	1353	1298	1352	1349	1339	1320	1326	1299

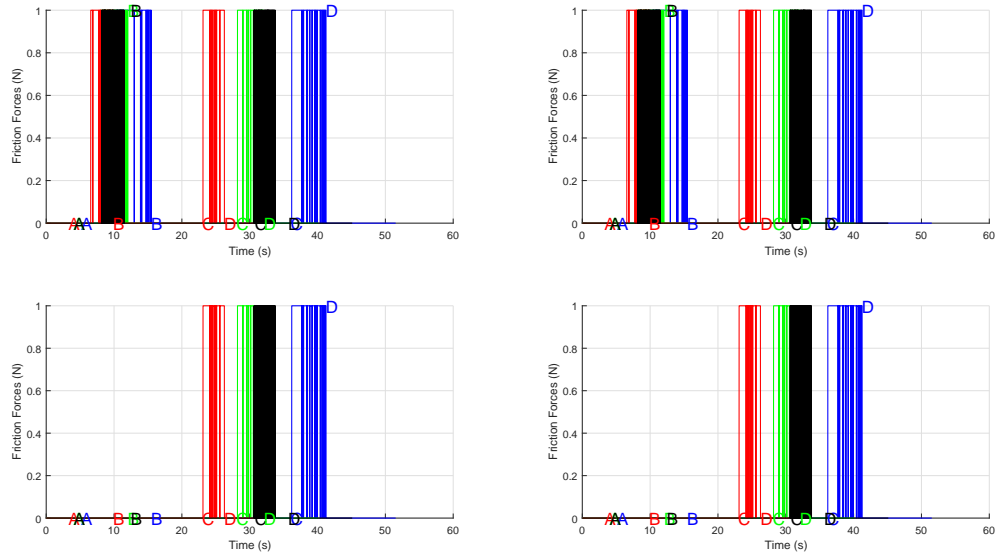


Figure 3.10: Skidding conditions of the wheels under different controllers in icy sloped version of Scenario-01 (red: cruise controller with 110 km/h speed reference, green: cruise controller with 90 km/h speed reference, blue: cruise controller with 70 km/h speed reference and black: energy optimal controller; top left: front left wheel, top right: front right wheel, bottom left: rear left wheel and bottom right: rear right wheel)

controller and the cruise controllers with different speed references drive the vehicle with wheels in slippage during the icy sloped sections. The wheel skidding conditions for Scenario-01 is presented in Fig. 3.10.

It has been observed that rear wheels are in slippage during braking along the downhill on icy road, while the front wheels are in slippage both during driving along the uphill and braking along the downhill on icy road sections. Note that the vehicle is front drive; hence, as the controller generates a positive driving command along the uphill section, the rear wheels are left unexcited. The observation on wheel skidding conditions show that, even if the road is icy, the wheels enter slippage condition when there is torque command applied to them.

In this study, a skidding compensation logic is proposed to minimize the amount of skidding. According to the aforementioned results, a wheel enters into slippage when non-zero torque command is applied on it; hence, the skidding compensation logic tries to reduce the magnitude of the torque commands applied to the wheels when they are under skidding, and compensates these command along the sections prior to the skidding part, [4]. The proposed skidding compensation is illustrated in Fig. 3.11.

Skidding compensation logic transfers the torque commands to be applied to the wheels during their slippage to the previous time instants for reducing slippage and compensating its action. The approach can be interpreted as increasing speed of the vehicle before an icy uphill road to complete the section with the available kinetic energy and no further need to apply drive commands during this icy part, or decreasing

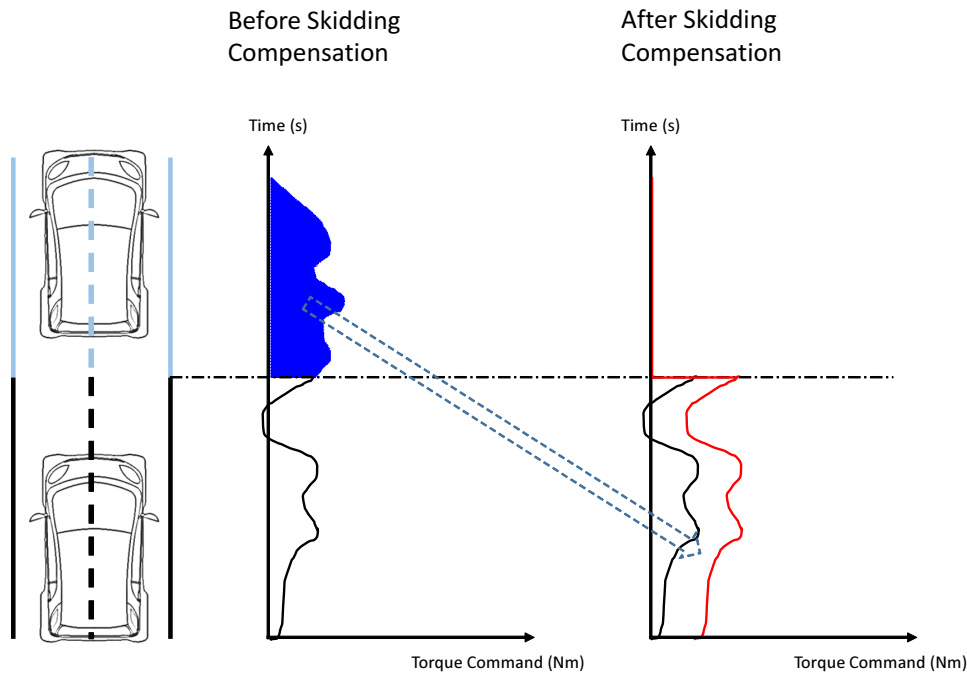


Figure 3.11: Skidding compensation logic transfers the command to be applied during wheel slippage to the instants prior to the skidding section

the speed before an icy downhill to complete the section with a speed in the limits and no further need to apply brake commands during the icy part. The energy optimality is observed to be affected less than 1% with skidding compensation being enabled. The results can also be considered as a validation of insensitivity of the optimal controller to local changes in wheel skidding conditions.

The validity of the skidding compensation is depicted in the results presented in Table 3.6. The first three columns following the header column shows the efficiency of the energy optimal controller compared to the cruise controllers with different reference speed according to (3.8). The following column shows the change power consumption of the vehicle under energy optimal controller with and without skidding compensation, and the columns to the end show the percentage of reduction in the instants where the wheels are in slippage when the skidding compensation is enabled.

According to the results, it has been shown that, the energy optimal controller preserves its superiority in energy management along roads with icy sections compared to the cruise controllers with different reference speeds. Furthermore, the proposed skidding compensation does not yield any change in energy consumption of the vehicle; while, it enables reduction in skidding occurrences of the wheels, fulfilling its objective.

Table3.6: Efficiency of the energy optimal controller compared to the cruise controllers in (%) and changes in power consumption of the vehicle under optimal control with and without skidding compensation logic, and the reduction in slippage on the wheels with skidding compensation logic enabled(%)

Scenario ID	$EE_{70}$	$EE_{90}$	$EE_{110}$	$EC_{OC}$	$SC_{FL}$	$SC_{FR}$	$SC_{RL}$	$SC_{RR}$
Scenario-01	86.13	83.32	78.48	0.00 E-0	07.37	07.37	09.50	09.50
Scenario-02	86.36	82.62	78.84	-1.38 E-3	05.41	05.41	07.39	07.39
Scenario-03	73.82	66.47	59.14	4.15 E-3	05.25	05.25	06.88	06.88
Scenario-04	73.94	66.62	59.32	2.77 E-3	06.14	06.14	08.15	08.15
Scenario-05	72.88	65.48	57.64	-1.38 E-3	08.21	08.21	10.15	10.15
Scenario-06	72.99	65.63	58.20	-2.77 E-3	10.02	10.02	12.52	12.52
Scenario-07	66.38	61.39	53.36	1.38 E-3	05.63	05.63	08.13	08.13
Scenario-08	67.20	63.17	57.85	1.38 E-3	07.55	07.55	11.24	11.24
Scenario-09	83.86	79.37	74.79	-1.38 E-3	05.91	05.91	07.22	07.22
Scenario-10	84.54	80.24	75.85	1.38 E-3	08.22	08.22	09.87	09.87
Scenario-11	69.13	60.34	51.37	-1.38 E-3	07.74	07.74	09.48	09.48
Scenario-12	66.85	61.85	50.08	-2.77 E-3	09.23	09.23	12.22	12.22
Scenario-13	83.26	78.64	74.01	0.00 E-0	10.12	10.12	14.70	14.70
Scenario-14	84.14	78.41	73.70	-4.15 E-3	08.78	08.78	14.73	14.73
Scenario-15	84.28	79.97	75.63	0.00 E-0	09.56	09.56	15.17	15.17
Scenario-16	83.26	78.56	73.84	-4.15 E-3	07.13	07.13	16.08	16.08
Scenario-17	84.40	80.00	75.53	4.15 E-3	06.37	06.37	14.27	14.27
Scenario-18	80.37	74.74	69.05	-5.53 E-3	05.76	05.76	16.48	16.48
Scenario-19	90.08	87.30	84.47	-2.77 E-3	11.17	11.17	17.22	17.22
Scenario-20	80.64	75.09	69.47	0.00 E-0	13.04	13.04	19.10	19.10
Scenario-21	70.51	62.52	54.41	-1.38 E-3	07.48	07.48	09.64	09.64
Scenario-22	69.89	60.71	51.96	2.77 E-3	07.48	07.48	09.88	09.88
Scenario-23	72.73	65.33	57.84	-1.38 E-3	06.31	06.31	08.69	08.69
Scenario-24	71.78	63.99	55.39	0.00 E-0	05.68	05.68	07.76	07.76

### 3.5 Sensitivity Analysis

In this section, a sensitivity analysis on the energy consumption of the vehicle under the energy optimal controller has been performed. Note that the solutions attained by energy optimal control solution is a sequence of control commands to be applied at fixed time instants, i.e. at each sampling time of 0.01 s. In the sensitivity analysis, these control sequences obtained for the nominal vehicle and scenario parameters are preserved, but the parameters of the vehicle or the scenario are disturbed. Hence, the control sequence to be applied at fixed time instants may not correspond to the exact position of the road where they will be applied in the new parameters case. In order to preserve this information, similar to what is done in the solution approach for the energy optimal controller, a transformation between position and time domains is performed. The optimal control sequence is associated with the positions along the road which is sectioned with a high resolution. Similar approach is followed for cruise controller command outputs to achieve a fair comparison.

In Section 3.3, results are presented for an autonomous vehicle with no driver or passenger inside. In the sensitivity analysis, the following four configurations are considered: only driver case (*Configuration-1*), driver and a passenger seated on front right (*Configuration-2*), driver and a passenger seated on rear right (*Configuration-3*, taxi configuration), and driver and 3 passengers (*Configuration-4*). The parameters are stated in Table 2.1.

According to the different configurations in the sensitivity analysis, mass of the vehicle, location of  $CoG$ , inertia of the vehicle are changed. The results are presented for the average of the all Scenarios 1-24. Note that mass of passenger/driver over mass of chassis is changing between 6.25% to 25%. The change in energy consumption of the vehicle under optimal controller is always less than 4%, however. The magnitude of the change in total energy consumption is smaller compared to the change of mass in the configurations. The sensitivity of the optimal control solution for the defined scenarios towards different passenger configurations are small in magnitude indeed. In Table 3.7, changes in total energy consumption of the vehicle under standard cruise controllers with different reference speeds are presented as well. Note that the magnitude of these changes are smaller yet comparable with those of the energy optimal controller. In the results, it is shown that with increasing mass, total energy consumption of the vehicle under cruise controllers are increasing. Yet, the energy optimal controller has achieved to decrease the energy consumption of the vehicle in different passenger configurations. The controller benefits from regenerative braking smarter as the total mass to be carried alters for the same initial  $SoC$ . Note that however, the increase in effectiveness is limited compared to the change in total mass of the vehicle, as expected.

All the simulations are held on an electric vehicle with initial  $SoC$  of 90%. The battery is not fully charged to allow further charging via regenerative braking. Simulations above are repeated for initial  $SoC$  – 75% and  $SoC$  – 50% cases as well. In Table 3.8, changes in energy consumptions of the vehicle under standard cruise controllers and the energy optimal controller for different initial  $SoC$  cases averaged for all the scenarios in Table 3.2 are presented. The calculation of changes in total energy consumption of the vehicle follows (3.9).

Table3.7: Corresponding change in total  $EC$  of the vehicle under different controllers (%) for different configurations (%), average of all scenarios

Configuration ID	$\Delta_{mV,\%}$	$\Delta_{EC,\%CC,70}$	$\Delta_{EC,\%CC,90}$	$\Delta_{EC,\%CC,110}$	$\Delta_{EC,\%OC}$
<i>Configuration-1</i>	6.25	0.47	0.30	0.26	-0.83
<i>Configuration-2</i>	12.50	0.82	0.59	0.34	-2.50
<i>Configuration-3</i>	12.50	0.86	0.64	0.39	-2.55
<i>Configuration-4</i>	25.00	1.40	0.89	0.54	-4.17

Table3.8: For different initial  $SoC$  values changes in total energy consumptions of the vehicle under different controllers, average of all scenarios

$\Delta_{EC}$	$\Delta_{EC_{Initial\ SoC,75\%}}$	$\Delta_{EC_{Initial\ SoC,50\%}}$
$\Delta_{EC,\%CC,70}$	7.55	7.52
$\Delta_{EC,\%CC,90}$	6.61	6.54
$\Delta_{EC,\%CC,110}$	5.70	5.59
$\Delta_{EC,\%OC}$	248.75	244.59

$$\Delta_{EC,\%} = \frac{EC_{Initial\ SoC,100\%} - EC_{Initial\ SoC}}{EC_{Initial\ SoC,100\%}} \quad (3.9)$$

According to results in Table 3.8, all the controllers reduces the energy consumption of the vehicle for initial  $SoC$  of battery,75% and 50% cases. However, the energy consumption of the vehicle under energy optimal controller reduces drastically for lower initial  $SoC$  values. In fact, average improvement in energy management is greater than 100% for energy optimal controller indicating that the vehicle starts to use regenerative braking so effectively that it stores energy to battery for lower initial  $SoC$  values compared to the energy consumption in 100%  $SoC$  initiation, according to (3.9). In other words, the effectiveness of the energy optimal controller becomes significantly visible for lower initial  $SoC$  of the battery package. This noticeable result validates as the energy consumption limitations become tighter, the performance of the vehicle under the energy optimal controller is incomparably better than those of the cruise controller.

### 3.6 Conclusions and Discussions

In this chapter, the mathematical model presented in Chapter 2 is used to design an energy optimal controller. In the selected scenarios with roads including uphill and downhill sections with different slopes and lengths, the optimal controller performance is compared with cruise controllers with various speed references. The

superiority of the optimal control approach is demonstrated through these extensive simulations. The optimal control problem is a free-final time problem. On the other hand, the distance to be travelled is fixed. A numerical method based on mapping the control inputs from the time domain to position domain has been developed and utilized to satisfy the fixed distance constraint. The proposed method is one of the main contributions of this study. It has been shown that the energy efficiency is achieved with no violations on speed constraints, wheel torque limits and battery constraint, with a travel time comparable with cruise controllers.

The uphill and downhill motion is also studied along icy roads. The high energy efficiency of the optimal control approach compared to the cruise controller with different speed references is validated on icy road sections as well. A skidding compensation function is proposed to reduce the amount of slippage, and it has been observed that the energy efficiency is preserved. The proposed skidding compensation technique is verified through simulations and presented as one of the major contributions of this study.

A sensitivity analysis is also performed. It has been shown that as a representative of different combinations of passengers, the sensitivity of the energy optimal controller on the mass change and distribution is smaller in magnitude. It has also been demonstrated that for different initial values of the state-of-charge of the battery, the energy efficiency of the vehicle under the energy optimal controller becomes significantly improved as compared to the standard cruise controllers. This noticeable result validates that as the battery characteristics dominates the energy storage capability during regenerative braking, the performance of the vehicle under the energy optimal controller is incomparably better than those of the cruise controller. The analysis itself can be considered as a benchmark for all the controllers proposed to the literature.

The performance of the optimal controllers is not directly compared to the policies available in the literature due to the differences in the fidelities of the mathematical models. The simplified models ignoring lateral dynamics, air drag, road conditions, battery models and torque constraints and possible skidding conditions prevent establishing an accurate comparison basis. Instead, in this study, a numeric comparison between energy optimal controller and standard cruise controllers for different speed references is performed. The cruise controllers with different speed references are used to generate an insight about energy efficiency of the proposed method. There can be better cruise controllers in literature; but the concept has been proven by constant speed cruise controllers. The results are considered to be used as reference outcomes for future experimental validation of the optimal control theory based energy management policies.

In addition to numerical comparison with standard cruise controller, qualitative comparisons between this study and those available in the literature are performed as presented in Table 3.9. The studies are compared in terms of their model complexity: consideration of wheel skidding conditions, consideration of sloped roads, and consideration of the nonlinear vehicle dynamics. Furthermore, as additional comparison merits, it is taken into consideration whether the earlier studies include detailed power consumption models or sensitivity analyses as well.

The studies in the literature closest to the present study are given in Table 3.9. Mainly,

Table3.9: Comparison against methods in the literature

Method	Wheel Slippage	Motion on Slopes	Nonlinear Dynamics	Power Cons. Model	Sensitivity Analysis
This study	✓	✓	✓	✓	✓
Sciarretta'15 [73]	×	×	×	✓	×
Pennycott'14 [66]	×	✓	×	×	×
Dib'14 [23]	×	×	×	✓	×
Chen'12 [17]	×	✓	×	×	×

the studies based on off-line energy optimization methods include simpler vehicle dynamics, and they discard wheel skidding kinematics. Pennycott, et al., and Chen, et al. include road sections with slopes in their studies. Sciarretta, et al., and Dib, et al. take power consumption battery dynamics into account during their optimal control studies.

The literature comparison is held between this study and the others following off-line optimization approaches. On-line methods are left out of this comparison, since it is unfair to compare on-line methods with off-line methods. The on-line methods use rather simplified mathematical models and can reach a local optimal solution due to their assumptions required to satisfy runtime computation limits. The off-line methods, on the other hand, can reach to a global optimal solution, yet they cannot be implemented in practice, especially when the road conditions alter rapidly. However, the off-line optimization results can be used to generate rule sets and references for on-line controllers.



## CHAPTER 4

### VEHICLE CORNERING

In this chapter, vehicle cornering under constant Ackerman's steering law is investigated. The average power consumption of the vehicle, and the amount of time vehicle corners the circular arc are selected as objectives of energy and time optimal control problems. Applying wheel torque, vehicle speed and battery power constraints to the problem, the performances of the optimal controllers are evaluated in simulations. In terms of battery charge and time consumption measures, the behaviour of the vehicle under optimal controllers are compared with those under cruise controllers. The simulation results confirm the effectiveness of the optimal controllers against standard cruise controllers.

A Pareto-front analysis is carried out with multi-objective energy and time minimization using NSGA-II algorithm. The analysis provides a multi-objective solution of the vehicle cornering problem with a compromise between travel time and energy consumption of the vehicle that enables vehicle to complete cornering with minimum energy consumption within the given speed limits. The optimality of the Pareto-front results are discussed. Furthermore, a sensitivity analysis is performed and it is confirmed that the optimal control solution is insensitive to the different passenger seating arrangements.

#### 4.1 Introduction

In this chapter, energy and time optimal control policies are proposed for electric vehicles by using optimal control techniques for the cornering behaviour often encountered in the urban traffic. The vehicle cornering is assumed to obey well-known Ackermann's steering law, dynamics of which can be found in [30] in details.

Cornering behaviour and steering control has been studied for vehicles extensively. Sharp, et al. describe a mathematical model for an auto mobile based on the Newton-Euler equations. The equations do not take any specific modification for skidding of the wheels. The authors propose an optimal discrete time controller with a horizon, for which the nonlinear vehicle model is linearised. An evaluation of path tracking performance is provided in simulated scenarios, [76]. Ahmadi, et al. propose an adaptive nonlinear control scheme for a vehicle under steering command sequences and evaluates the path tracking performance. The model is based on the Newton-Euler equations with no skidding assumption. The control scheme has cascaded loops; one

of them is for cancelling the non-linearities in the error dynamics, and the other one is for tracking the curved road through an inverse dynamics model, [5].

Cossalter, et al. generate a method using two-point optimal control boundary value problem to evaluate vehicle manoeuvrability. Physical constraints like tire adherence and road boundaries are taken into consideration for the motion of a vehicle controlled with an ideal driver performing optimal manoeuvres. The vehicle model is specialized for yaw motion of the vehicle and the penalty function is adjusted to optimize invulnerability, [21]. Thommyppilai, et al. model the car drivers, and use a linear optimal control theory in vehicle cornering. In the simulations, on their linearised vehicle model, trim states are defined and gain-scheduling adaptive control laws are shown to be advantageous against fixed control schemes in terms of path tracking performances, [80].

A detailed literature survey on time optimal control policies for vehicle cornering can be found in [77]. Velenis, et al. use Bellman's principle of optimality to generate minimum time velocity profiles for a vehicle, modelled as a point mass. The semi-analytical method includes acceleration limits along a specified path in the problem definition, [84]. The authors extent their approach to a half-car model in [83].

Tavarnini, et al. use a symbolic-numerical indirect method for nonlinear optimal control technique to solve minimum time car manoeuvring problem. For different road surfaces optimal driver control results are evaluated, [79]. Rucco, et al. study minimum time vehicle cornering problem with a nonlinear optimal control technique. The authors include a rigid car model, planar track, lane boundaries, and enforce normal force constraints on the tires as well as steering and tire limits. Similar to our study, a 90-degree turning scenario is simulated, [71].

Hendrikx, et al. use the distance travelled along the centre line of the road as an independent variable in their optimal control approach based on the gradient descent algorithm. Simulations are based on inverse dynamics of car handling including calculations of the driver actions to perform the manoeuvres in the shortest time. The authors have presented a solution to the lane changing problem, [35]. Fuijoka, et al. generate a numeric solution for the optimal time problem along a road with a given 3D description. A sequential conjugate gradient restoration algorithm is applied to an oversimplified point mass vehicle model, [28].

Gerdtts, et al. use the moving horizon technique and solve a sequence of local optimal control problems with suitable continuity conditions. The reference trajectory attained in this way is turned out to have a high accuracy in reproduction of the optimal trajectory, [29]. Timings, et al. use convex optimization to calculate minimum manoeuvre time, and linearise the nonlinear vehicle model at each time step. The authors use model predictive control and minimize the deviations from the centre-line. The steering constraints and minimization of the cost function enhances the non-optimal linearised steering actions, [81].

The energy and time management strategies proposed in this study are based on the classical optimal control theory with constraints on vehicle speed, wheel torques and applicable battery power. The constrained optimal control problems are defined and solved for an electric vehicle, where regenerative braking is possible to improve the energy management. The optimal controller performances are shown to be more

effective compared to standard cruise controllers, as expected.

Furthermore, the energy and time optimal control objectives are used to carry out a Pareto-front analysis with multi-objective energy and time minimization using NSGA-II (Non-Dominating Sorting Genetic Algorithm) algorithm. The analysis provides a multi-objective solution to the vehicle cornering problem with a compromise between travel time and energy consumption of the vehicle that enables vehicle to complete cornering with minimum energy consumption within the given speed limits. The optimality of the Pareto-front is validated with classical optimal control solution for the problem with weighted energy and time optimality objectives.

The study aims to generate the following contributions to the literature available on the optimality problem in vehicle cornering motion:

- The optimal control problem is discussed on vehicle mathematical model which is sufficiently detailed to be applicable for any gross motion. In addition to the motion model, battery model and regenerative braking capability of the electric drive are included.
- The classical optimal control is shown to be a valid and applicable technique for time and energy optimization for vehicle motion. Time and energy optimality problems are both handled in a single solution structure.
- Both time and energy optimal control problems are free-final time problems. On the other hand, the distance to be covered is chosen to be fixed. A numerical method based on mapping the control inputs from the time domain to the position domain has been developed and utilized to satisfy the fixed distance constraint.
- It has been shown with NSGA-II genetic algorithm that there is a Pareto-front between time and energy optimization problems. The optimality of this Pareto-front is validated with classical optimal control approach.
- A sensitivity analysis is performed and it is confirmed that the optimal control solution is insensitive to the different passenger seating arrangements.

In Section 4.2, the energy and time optimal control problems are defined based on the 3-DoF gross motion model of the vehicle. In several cornering scenarios, the optimal control problems are solved with application of Pontryagin's minimal principle taking the constraints on the vehicle speed, the wheel driving torques and the battery power into account. In Section 4.3, the optimal control solutions are presented and they are compared with the results obtained for a vehicle under standard cruise controllers. In Section 4.4, The Pareto-front analysis is carried out for multi-objective optimization and the optimality of the results are discussed with optimal control results obtained for weighted time and energy objectives. In Section 4.5, a sensitivity analysis is performed and it is confirmed that the optimal control solution is insensitive to the different passenger seating arrangements.

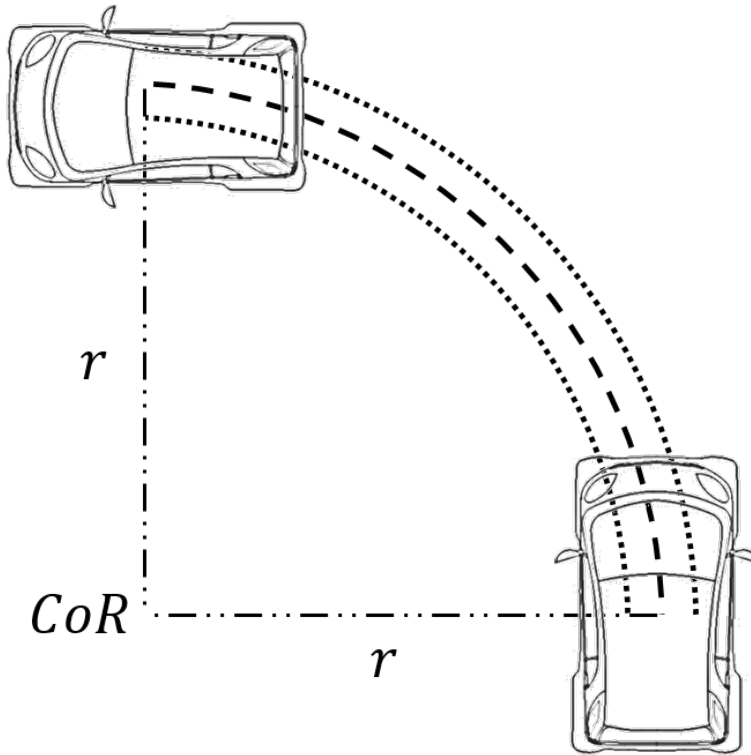


Figure 4.1: Motion representation for vehicle cornering

## 4.2 Optimal Controller Design

In this study, the behaviour of the vehicle cornering around a *CoR* with constant Ackermann's steering law is investigated. The motion of the vehicle through the cornering scenarios is illustrated in Fig. 4.1.

The optimal control approach and algorithm is presented in Section 3.2. The algorithm is presented with a visualization as a reminder in Fig. 4.2 as well.

The energy and time optimal control problem can be written as in (4.1) and (4.2), respectively. Note that both of the problems have the boundary conditions and constraints in terms of the state only and the final time is free. The problem definition for vehicle cornering motion is the same as that of uphill/downhill motion defined in (3.3).

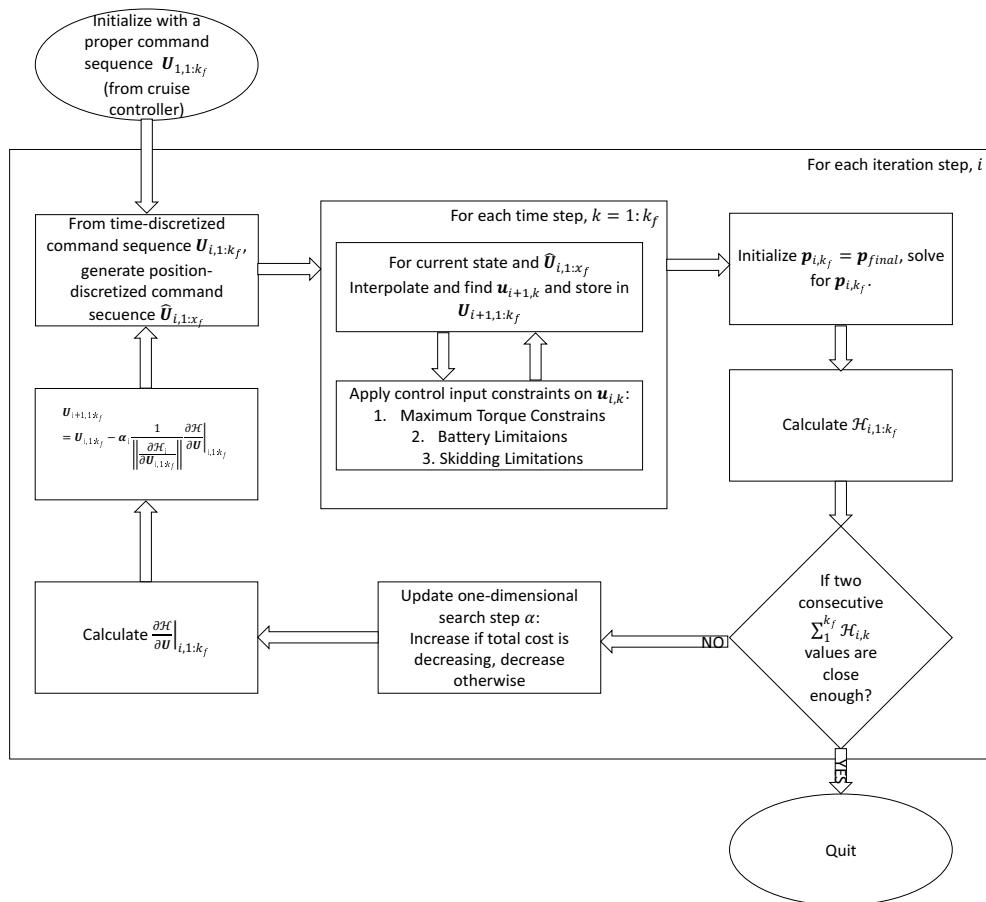


Figure 4.2: Optimal controller design algorithm

*minimize*

$$J_e \left( \sum_w M_{wc,y}^{(w)} \right) = \sum_{t_0}^{t_f} \left( \begin{array}{ll} M_{w_{flc},y}^{(w_{fl})} \omega_{w_{fl},y} + M_{w_{frc},y}^{(w_{fr})} \omega_{w_{fr},y} & \text{if } \sum_w M_{wc,y}^{(w)} \geq 0 \\ -\min(M_{w_{flc},y}^{(w_{fl})} \omega_{w_{fl},y} + M_{w_{frc},y}^{(w_{fr})} \omega_{w_{fr},y} + M_{w_{rlc},y}^{(w_{rl})} \omega_{w_{rl},y} + M_{w_{rrc},y}^{(w_{rr})} \omega_{w_{rr},y}, RPCB) & \text{if } \sum_w M_{wc,y}^{(w)} < 0 \end{array} \right)$$

*subject to*

$$\dot{\mathbf{x}} = \mathbf{f}(\mathbf{x}, SoC, M_{wc,y}^{(w)})$$

$$v_{v,x_{min}}^{(o)} \leq v_{v,x}^{(o)} \leq v_{v,x_{max}}^{(o)}$$

$$M_{w_{flc},y}^{(w_{fl})} \omega_{w_{fl},y} + M_{w_{frc},y}^{(w_{fr})} \omega_{w_{fr},y} \leq FPCB$$

$$M_{wc,y}^{(w)} \leq MTC$$

$$|\bar{u}_{vw_k}^T \bar{F}_{gw_k}^{(w_k)}| < \mu_{s,w_k} \bar{u}_z^T \bar{F}_{gw_k}^{(w_k)}$$

(4.1)

*minimize*

$$J_t(t_f) = \sum_{t_0}^{t_f} 1$$

*subject to*

$$\dot{\mathbf{x}} = \mathbf{f}(\mathbf{x}, SoC, M_{wc,y}^{(w)}) \tag{4.2}$$

$$v_{v,x_{min}}^{(o)} \leq v_{v,x}^{(o)} \leq v_{v,x_{max}}^{(o)}$$

$$M_{w_{flc},y}^{(w_{fl})} \omega_{w_{fl},y} + M_{w_{frc},y}^{(w_{fr})} \omega_{w_{fr},y} \leq FPCB$$

$$M_{wc,y}^{(w)} \leq MTC$$

$$|\bar{u}_{vw_k}^T \bar{F}_{gw_k}^{(w_k)}| < \mu_{s,w_k} \bar{u}_z^T \bar{F}_{gw_k}^{(w_k)}$$

The optimal control problems are defined for a path of a specified length; hence, the initial state is known, and final state can be specified in terms of position. Other than state boundary conditions, optimal control problems have free final time. According to Pontryagin's minimum principle a solution satisfying the control input constraints is found. State constraints follow the artificial state method explained in [49]. Therefore, Hamiltonians at discrete time step,  $k$ , can be written as in (4.3) and (4.4) for energy and time optimal control problems, respectively.

$$\mathcal{H}_k = \left( \begin{array}{ll} M_{w_{flc},y}^{(w_{fl})} \omega_{w_{fl},y} + M_{w_{frc},y}^{(w_{fr})} \omega_{w_{fr},y} & \text{if } \sum_w M_{wc,y}^{(w)} \geq 0 \\ -\min(M_{w_{flc},y}^{(w_{fl})} \omega_{w_{fl},y} + M_{w_{frc},y}^{(w_{fr})} \omega_{w_{fr},y} + M_{w_{rlc},y}^{(w_{rl})} \omega_{w_{rl},y} + M_{w_{rrc},y}^{(w_{rr})} \omega_{w_{rr},y}, RPCB) & \text{if } \sum_w M_{wc,y}^{(w)} < 0 \end{array} \right) + \mathbf{p}^T \mathbf{f}(\mathbf{x}, SoC, M_{wc,y}^{(c)}) + \mathbf{p}_l \left[ \left( v_{v,x_{min}}^{(o)} \leq v_{v,x}^{(o)} \right)^3 \left( v_{v,x_{max}}^{(o)} \leq v_{v,x}^{(o)} \right)^3 \right] \tag{4.3}$$

$$\mathcal{H}_k = 1 + \mathbf{p}^T \mathbf{f}(\mathbf{x}, SoC, M_{wc,y}^{(c)}) + \mathbf{p}_l \left[ (v_{v,x_{min}}^{(o)} \leq v_{v,x}^{(o)})^3 (v_{v,x_{max}}^{(o)} \leq v_{v,x}^{(o)})^3 \right] \quad (4.4)$$

In (4.3) and (4.4),  $\mathbf{p}$  denotes the co-state and  $\mathbf{f}(\mathbf{x}, SoC, M_{wc,y}^{(c)})$  denotes the nonlinear state update function. The velocity constraints are taken into consideration in the form given in (4.3) and (4.4) with a Lagrange multiplier  $\mathbf{p}_l$ .

Note that as depicted in Fig. 4.2, derivative of the Hamiltonian function defined in (4.3) with respect to the control input is calculated. When the control input is positive, the vehicle is consuming energy, when it is negative, due to regenerative braking properties of the electric motors, some amount of energy can be stored back to the batteries. Note that Hamiltonian is discontinuous when the control input  $\mathbf{u}$  becomes zero. This discontinuity can be solved with an adjustment in the definition of the Hamiltonian. Instead of using two disjoint functions for positive and negative control inputs, their averaged sum weighted with a continuous function, such as  $\tan^{-1}(\cdot)$  can be used. The modified Hamiltonian can be expressed as in (4.5). Together with this modification, in this study an energy optimal control algorithm is proposed. Similar discontinuity problem does not exist for time optimal control Hamiltonian definition.

$$\begin{aligned} \mathcal{H}_k = & \left( 0.5 + \frac{1}{\pi} \tan^{-1} \left( \eta \sum_w M_{wc,y}^{(w)} \right) \right) \left( M_{w_{fl},y}^{(w_{fl})} \omega_{w_{fl},y} + M_{w_{fr},y}^{(w_{fr})} \omega_{w_{fr},y} \right) \\ & - \left( -0.5 + \frac{1}{\pi} \tan^{-1} \left( \eta \sum_w M_{wc,y}^{(w)} \right) \right) \left[ \min \left( M_{w_{fl},y}^{(w_{fl})} \omega_{w_{fl},y} + M_{w_{fr},y}^{(w_{fr})} \omega_{w_{fr},y} \right. \right. \\ & \left. \left. M_{w_{rl},y}^{(w_{rl})} \omega_{w_{rl},y} + M_{w_{rr},y}^{(w_{rr})} \omega_{w_{rr},y}, RPCB \right) \right] \\ & + \mathbf{p}^T \mathbf{f}(\mathbf{x}, SoC, M_{wc,y}^{(c)}) + \mathbf{p}_l \left[ (v_{v,x_{min}}^{(o)} \leq v_{v,x}^{(o)})^3 (v_{v,x_{max}}^{(o)} \leq v_{v,x}^{(o)})^3 \right] \end{aligned} \quad (4.5)$$

In (4.5),  $\eta$  stands for the smoothing factor, and it has been chosen sufficiently large so that the smoothed Hamiltonian approximates the discontinuous one. In Fig. 4.3, for different values of  $\eta$  and control commands, the normalized differences between the modified Hamiltonian given in (4.5) and the discontinuous Hamiltonian given in (4.3) is presented. The vehicle speed is chosen to be 90 km/h, the wheel speeds are calculated accordingly, and other components in Hamiltonian equations are taken to be the same.

It has been observed in Fig. 4.3 that for  $\eta$  greater than 1, the normalized difference between modified and discontinuous Hamiltonian functions are less than 1E-4, which is negligible. Since the modified Hamiltonian has smoother characteristics compared to the discontinuous one, the convergence of the solution is faster with the modified Hamiltonian function.

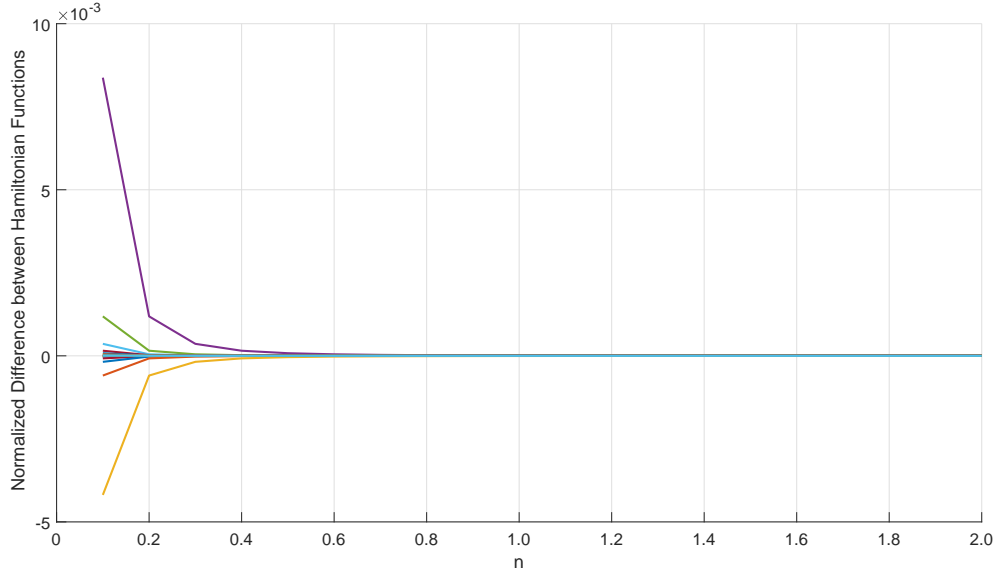


Figure 4.3: Normalized difference between modified and discontinuous Hamiltonian functions for different values of  $\eta$

### 4.3 Results

Parameters of the model used in the simulations are given in Table 2.1. The model parameters are approximate average values of the electric vehicles in market.

The test scenarios are selected to satisfy the minimum cornering radius for the corresponding vehicle speed. Hence, the cruise controllers do not have to alter their speed and preserve their control behaviour throughout the cornering. The vehicle speed reference for the cruise controller is selected as 50 km/h. The speed range of vehicle under cruise controller is defined as 49 - 51 km/h. The optimal controllers are enabled to command the vehicle through a speed range of 45 to 55 km/h. There are 6 scenarios as presented in Table 4.1. Both cruise controller and the optimal controllers are functions of driving/braking torque commands. The steering command is applied as the cornering initiates according to Ackermann's steering law for the radii given in the second column of the table. The trajectory is presented in Fig. 4.1.

The energy and time optimal controllers with Hamiltonian definitions in (3.6) and (4.4), respectively are designed in accordance with the aforementioned algorithm. The energy efficiency of the vehicle under an optimal controller is calculated with the ratio of the energy consumption of the vehicle under the optimal control against that under the standard cruise controller. Energy consumption is calculated with (4.6), and energy efficiency is calculated with (4.7) as percentage of the relative improvement in energy consumption of the vehicle. The equation will yield positive results greater than 100%, meaning that in some cases, the vehicle under energy optimal controller can regenerate energy while the vehicle under cruise controller consumes.

Table 4.1: Test scenarios

Scenario ID	Rotation Radius (m)
Scenario-01	50
Scenario-02	60
Scenario-03	70
Scenario-04	80
Scenario-05	90
Scenario-06	100

$$EC = SoC_{initial} - SoC_{final} \quad (4.6)$$

$$EE = \frac{EC_{Cruise\ Controller} - EC_{Optimal\ Controller}}{EC_{Cruise\ Controller}} \quad (4.7)$$

The cruise controller is selected as constant speed controller with reference speed of 50 km/h. The initial speed of the vehicle for the optimal controllers are selected to the same according to problem definition, yet they can be chosen any value between the speed limits of 45 km/h to 55 km/h. For different initial speeds of the vehicle, energy and time consumptions of the vehicle are calculated. For the initial speeds close to upper speed limits, time optimal controller is failed generate solutions with the given speed limits, similarly for the initial speed close to the lower limit, energy optimal controller cannot results into a feasible solution. The effect of selection of different initial speeds to the optimal controller problems are presented in Table. 4.2.

According to results it has been observed that the energy consumption of the vehicle under energy optimal controller reaches a minimum and stays at this minimum as the initial speed of the vehicle becomes greater than or equal to 50 km/h. For initial speed greater than 50 km/h, energy consumption of the vehicle under energy optimal controller does not change, only the time consumption gets smaller. Similarly, time consumption of the vehicle under time optimal controller does not change much for the initial speeds less than or equal to 50 km/h, but the energy consumption does. Hence, 50 km/h initial vehicle speed is chosen to be the best selection that optimizes the vehicle motions under both energy and time optimal controllers. As the initial speed is selected as 50 km/h, for the different scenario, the energy consumption performances of the optimal controllers are presented in Table 4.3.

Since there is a speed limitation of  $\pm 5$  km/h around 50 km/h reference speed, a comparison on absolute time consumptions of the vehicle to complete the cornering motion under different controllers is misleading. Instead, extremes of the durations for vehicle to complete the road within the given speed range are calculated as  $t_{max}$  and  $t_{min}$ . Time performance of a controller is equated to 0% if the consumed time to complete the road under this controller is equal to  $t_{max}$ , and 100% if it is equal to  $t_{min}$ . The results are presented in Table 4.4 and Fig. 4.4.

Table4.2: Energy consumptions  $EC$  and time consumptions  $TC$  of the vehicles under energy optimal controller  $EOC$  and time optimal controller  $TOC$  for different initial vehicle speeds for SC-01 ( $NS$  indicates no solution)

Initial Speed ( $km/h$ )	$EC_{EOC}(J)$	$TC_{EOC}(s)$	$EC_{TOC}(J)$	$TC_{TOC}(s)$
45	$NS$	$NS$	950	5.26
46	$NS$	$NS$	940	5.26
47	350	6.18	930	5.25
48	-250	6.14	920	5.25
49	-290	6.13	920	5.24
50	-280	5.91	910	5.24
51	-280	5.79	900	5.22
52	-270	5.68	890	5.20
53	-270	5.58	860	5.16
55	-260	5.47	$NS$	$NS$
55	-250	5.37	$NS$	$NS$

Table4.3: Energy performances of the optimal controllers,  $EOC$ : Energy Optimal Controller,  $TOC$ : Time Optimal Controller,  $EC$ : Energy consumption in  $J$ ,  $EE$ : Energy efficiency

Scenario ID	$EC_{CC}(J)$	$EC_{EOC}(J)$	$EC_{TOC}(J)$	$EE_{EOC}(\%)$	$EE_{TOC}(\%)$
Scenario-01	1.10E+3	-0.28E+3	0.79E+3	125.45	28.18
Scenario-02	1.31E+3	-0.34E+3	0.96E+3	125.95	26.72
Scenario-03	1.53E+3	-0.41E+3	1.18E+3	126.80	22.88
Scenario-04	1.74E+3	-0.47E+3	1.38E+3	127.01	20.69
Scenario-05	1.95E+3	-0.52E+3	1.00E+3	126.67	48.72
Scenario-06	2.17E+3	-0.58E+3	1.81E+3	126.73	16.59

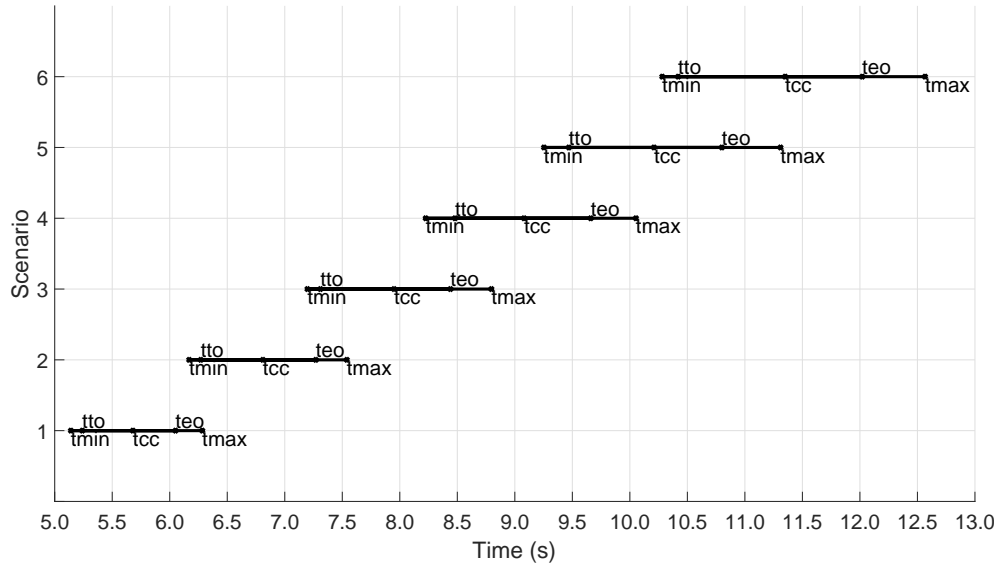


Figure 4.4: Time consumptions of the controllers:  $t_{min}$ : minimum time to complete the road (with the maximum speed in the range),  $t_{max}$ : maximum time to complete the road (with the minimum speed in the range),  $t_{cc}$ : time to complete the road under cruise controller,  $t_{eo}$ : time to complete the road under energy optimal controller,  $t_{to}$ : time to complete the road under time optimal controller

Table4.4: Time consumption performances of the optimal controllers,  $EOC$ : Energy Optimal Controller,  $TOC$ : Time Optimal Controller,  $TC$ : Time consumption in  $s$ ,  $TE$ : Time efficiency

Scenario ID	$TC_{CC}(s)$	$TC_{EOC}(s)$	$TC_{TOC}(s)$	$TE_{EOC}(\%)$	$TE_{TOC}(\%)$
Scenario-01	05.68	05.91	05.24	-20.13	38.52
Scenario-02	06.81	07.10	06.27	-21.15	39.39
Scenario-03	07.95	08.51	07.31	-35.01	40.02
Scenario-04	09.08	09.76	08.48	-37.20	32.83
Scenario-05	10.21	10.93	09.42	-35.01	35.99
Scenario-06	11.35	12.19	10.59	-36.76	40.70

In Fig. 4.4, for each scenario,  $t_{max}$ ,  $t_{min}$  values and performances of the optimal controllers and the cruise controller are demonstrated. Time efficiency values are calculated according to the improvements attained in the time consumed to finalize the given path relative to the standard cruise controller. Note that, while the time optimal controller results into a time minimized solution, the energy optimal controller has worse travel time results as compared to the cruise controllers.

In Fig. 4.5, positions of the vehicle under cruise controller and energy and time optimal controllers are presented for Scenario-01. In the colour-bar, the acceleration of the vehicle under the controllers are presented as well. It has been observed that magnitudes of the vehicle accelerations are around the same order for the vehicles under the considered controllers. However, energy optimal controller generates the lowest accelerations to minimize the energy consumption, while the time optimal controller requires the highest acceleration to maximize the speed. Similar results have been obtained for the other scenarios as well.

In Fig. 4.6, speeds of the vehicle under standard cruise controller, energy optimal controller and time optimal controller are depicted for Scenario-01. All the controllers have the same initial state in position and velocity and the same boundary conditions in the final position. By intuition, it is expected that vehicle shall reach the upper speed limit of 55 km/h in time-optimal drive and the lower speed limit of 45 km/h in energy optimal drive immediately and preserve those speeds. However, due to constraints on power supply capacity of the battery, maximum torque to be applied on the wheels and the skidding prevention requirement, the vehicle speeds do not approach the extreme terminal values. Furthermore, note that for energy optimal control solution, sticking to the lower speed limit and applying full braking to charge the battery via regeneration, will result in greater amount of time for the vehicle to complete the cornering. The amount of energy consumed throughout this time will become comparable with the saved energy. Hence, the optimal control problem for the vehicle has no such trivial solution. The optimal control policies generate the commands to yield vehicle motion that optimize the objectives within the vehicle constraints, road profile and power dynamics of the battery package. In Table 4.5, average speeds of the vehicle under energy and time optimal controllers are presented for all the scenarios. It has been observed that the average speeds are always below the reference speed defined for the energy optimal controller and always above it for the time optimal controller. Note that there is always a trade-off between the reduction in energy or time consumption and the effect of the constraint keeping the speed of the vehicle close to the reference speed.

In Fig. 4.7, driving/braking torque commands applied to the wheels under standard cruise controller, energy optimal controller and time optimal controller are depicted for Scenario-01. According to the results, it has been observed that the energy optimal control policy applies the lowest torque commands to the wheels in average and the time optimal control policy applies the highest. These characteristics yield energy minimization and reduction in time to complete the given path in the energy optimal and the time optimal controllers, respectively. Note that according to Ackerman's steering law, the speeds of the front wheels during the cornering motion have small differences, which in turn, results in small differences between the torque commands applied to the front wheels. A similar discussion is valid for the rear wheels. The close equivalence in the torque profiles of the wheels in different sides of an axle is

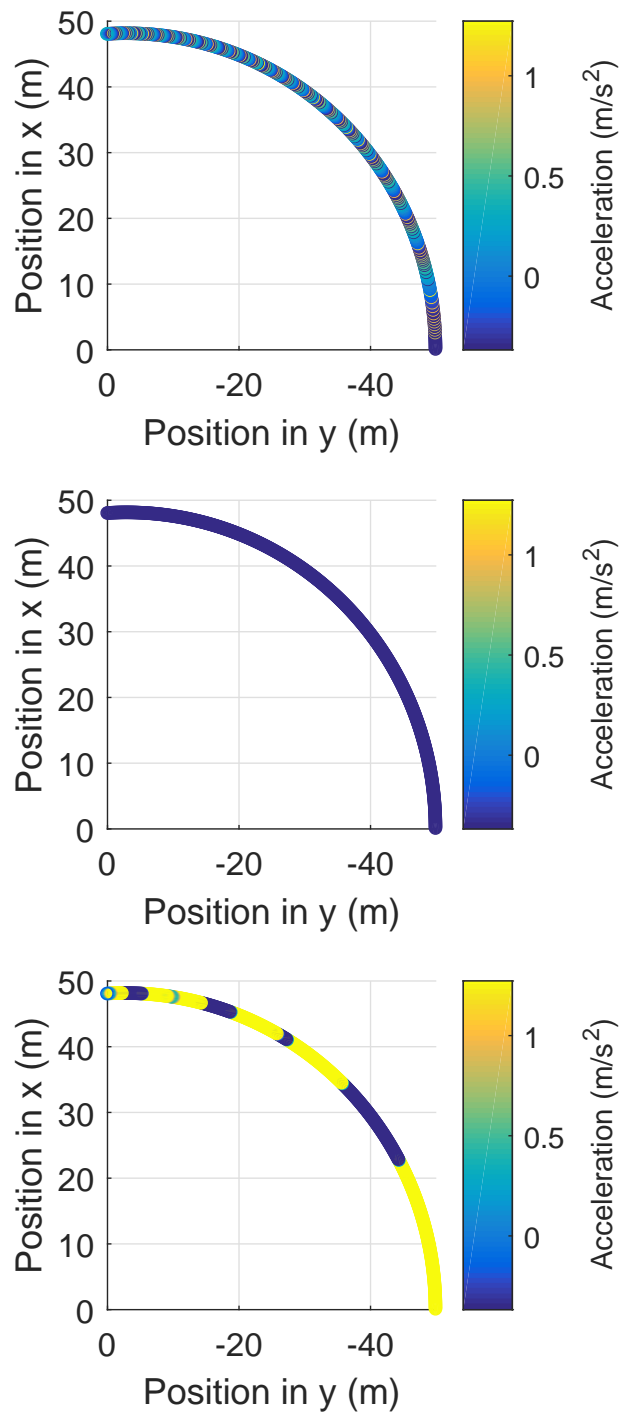


Figure 4.5: Positions and accelerations of the vehicle under different controllers (top: cruise controller, middle: energy optimal controller and bottom: time optimal controller)

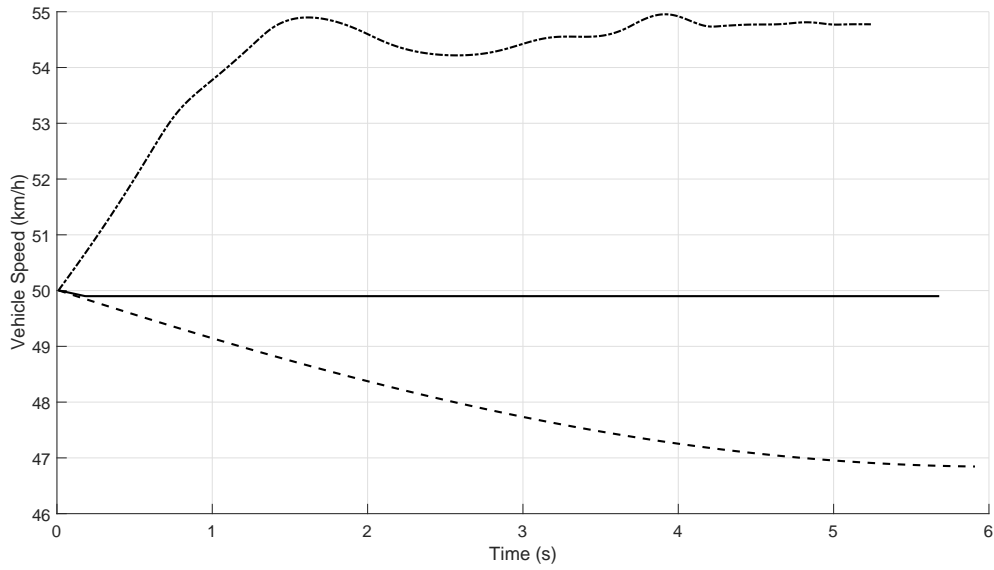


Figure 4.6: Speed of the vehicle under different controllers (solid line: cruise controller, dashed line: energy optimal controller and dash-dotted line: time optimal controller)

Table 4.5: Average speeds of the vehicles under energy and time optimal controllers (km/h)

Scenario ID	Vehicle Speed under TOC	Vehicle Speed under EOC
01	53.96	47.84
02	54.11	47.79
03	54.15	46.51
04	53.34	46.35
05	54.02	46.56
06	53.39	46.39

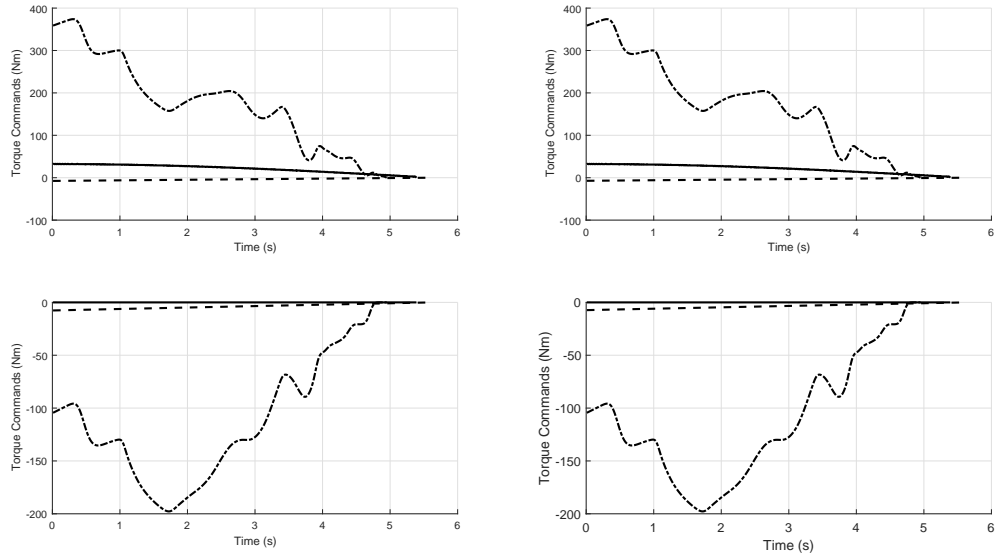


Figure 4.7: Torque commands applied to the vehicle under different controllers (solid line: cruise controller, dashed line: energy optimal controller and dash-dotted line: time optimal controller; top left: front left wheel, top right: front right wheel, bottom left: rear left wheel and bottom right: rear right wheel)

due to this nature of Ackerman’s steering law.

Fig. 4.8 presents the friction forces on the wheels of the vehicle under the cruise controller, the energy optimal controller and the time optimal controller obtained in Scenario-01. It has been observed that the friction forces do not exceed static friction limits for each wheel as shown in dashed lines in Fig. 4.8. The net friction on the wheel is in the direction of the net velocity of the contact point between the wheel and the ground. The friction forces on longitudinal and lateral directions of wheel are projected to the direction of the net velocities of their contact points with ground.

In Table. 4.6, number of iterations spent in finding the energy and time optimal control solutions for the scenarios are presented. For a computer, with Intel Core i7-6700 HQ CPU, 2.60 Ghz, and 16 GB Ram, and x64 bit Windows 7, average time to complete an iteration step is also given in the table.

#### 4.4 Pareto Front Analysis

In Section 4.2, time optimal and energy optimal control policies are introduced, and in Section 4.3, the results attained with these control policies over six scenarios are presented, and the results are compared against standard cruise controllers. It has been observed that the energy optimal control policy returns an energy efficient drive at a cost of decrease in the time efficiency and vice versa for the time optimal control policy. However, note that achieving the cornering with low speed does not always mean an energy efficient drive; since, the lower the vehicle speed, the longer the vehicle

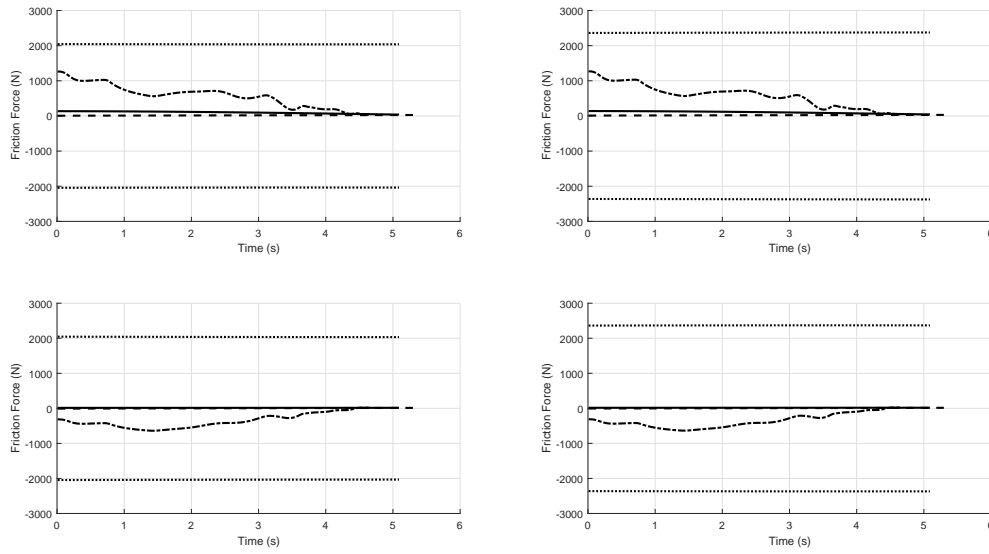


Figure 4.8: Friction forces on the wheels of the vehicle under different controllers (solid line: cruise controller, dashed line: energy optimal controller and dash-dotted line: time optimal controller; top left: front left wheel, top right: front right wheel, bottom left: rear left wheel and bottom right: rear right wheel)

Table4.6: Number of iterations to find the energy and time optimal solutions

Scenario ID	Iterations EOC	Iterations TOC	Single Iteration Time (s)
01	1843	1745	22.53
02	1828	1726	26.56
03	1882	1712	30.12
04	1851	1755	33.96
05	1862	1769	36.47
06	1816	1741	41.56

completes the road, and the energy consumed in these instants becomes comparable with the energy saving with regenerative braking. Hence, there is a compromise between time and energy optimality. In this section, with help of multi-objective control, a Pareto-front for energy and time optimization for vehicle cornering will be searched.

A genetic algorithm (GA) is used to generate torque commands. Note that the time-discretized control commands,  $U$  has variable size for different drives due to varying total travel time. Instead, position-discretized control commands,  $\hat{U}$  is used as optimization vector. Two objectives defined in 4.1 and 4.2 for energy and time optimization are employed in multi-objective optimization problem. Computations have been performed to determine the Pareto-optimal solutions. The characteristics of the multi-objectives generates a solution along the Pareto-front that has the minimum energy consumption among those with the same time consumption, or it has the minimum time consumption among the energy consumption equivalent solution set.

NSGA-II algorithm [22] is used to find the Pareto-optimal solutions. The algorithm defines a crowding distance and uses a crowded comparison to sort the population according to their non-domination rank. A binary tournament selection is used to select from the parent population. The offspring population generated after mutation and recombination is then mixed with the parent population. The elitism is preserved through this new mixed population. Thereafter, a sorting according to the non domination rank of the individuals are used to generate the new parent population, and the algorithm continues the iterations. For further details, please refer to [22].

The solutions not completing the corner, or not satisfying the limitations on vehicle speed, wheel torque and battery are eliminated throughout the GA iterations by setting both of the objectives to a big number.

The energy and time optimal solutions are given as members of the initial population. The results for multi-objective Pareto-front analysis is depicted in Fig. 4.9. Some solution on the Pareto front are marked with different colours to be used in comparisons for speed and torque profiles. Similar results are obtained for other scenarios as well.

According to Fig. 4.9, for any point along the Pareto-front, a multi-objective optimal controller performance exists. Above the Pareto-front, there are non-optimal solutions for the vehicle cornering problem. Below the Pareto-front, solution is not feasible for the given limits on vehicle speed, battery characteristics, and applied torque to the wheels under constant Ackermann's steering for the given scenarios.

In Fig. 4.10, the speeds of the vehicle for the selected non-dominating solutions of multi-objective energy and time optimization problems for Scenario-01 are presented. The colour codes are the same as those in Fig. 4.9. According to the results in Fig. 4.9 and Fig. 4.10, for the given speed range limits, minimum energy vehicle cornering behaviour can be obtained. As a result of the Pareto-front analysis, in accordance with the traffic regulations or any other user requirements, the time and energy optimal driving policies can be generated for various speed limits and cornering radii.

In Fig. 4.11, the driving/braking torque commands applied to the wheels under the control of the selected non-dominating solutions of multi-objective energy and time optimization problems for Scenario-01 are presented. The colour codes are the same

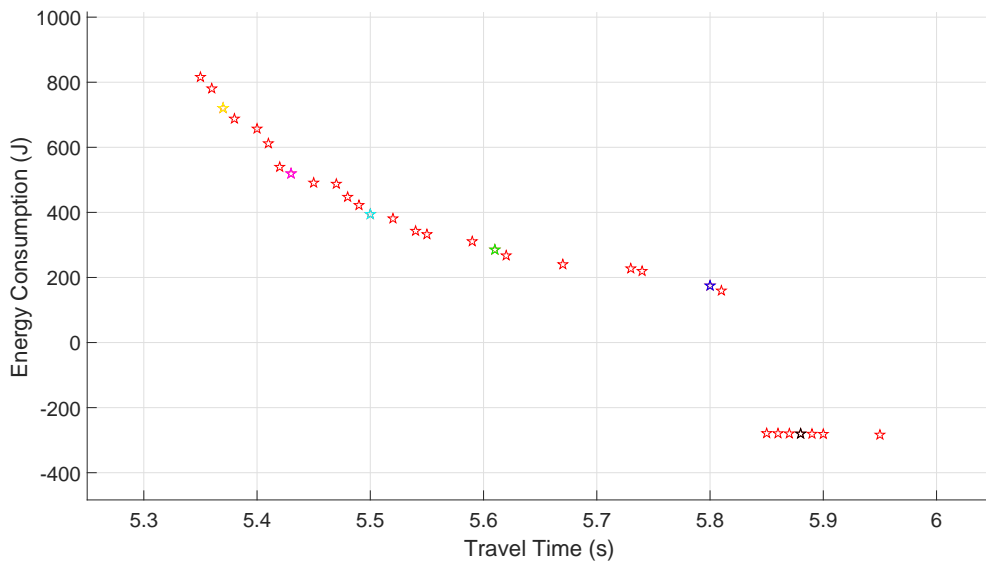


Figure 4.9: Pareto-front analysis of multi-objective energy and time optimization with NSGA-II algorithm

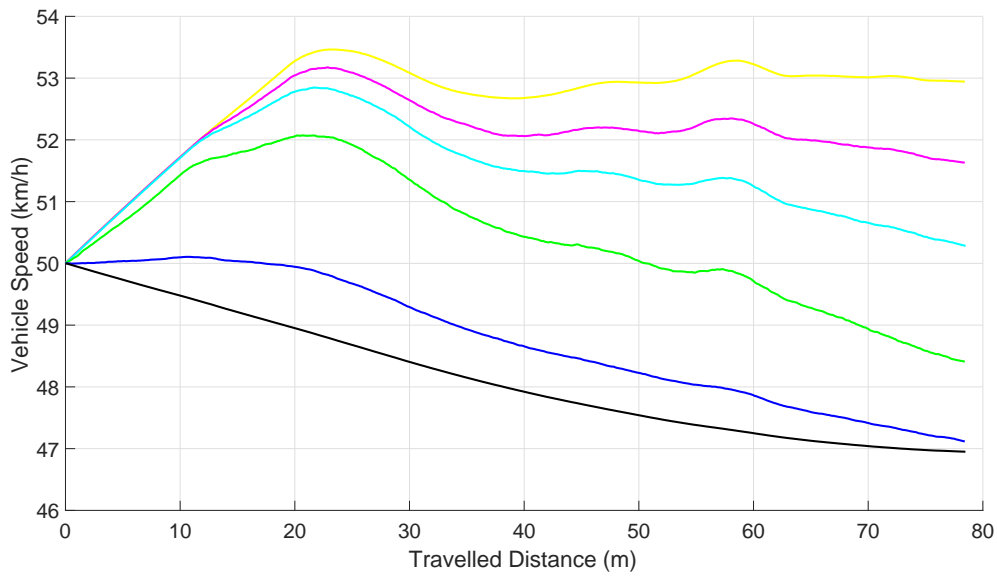


Figure 4.10: Speed profiles for the steps along Pareto-front of time and energy multi-objective controller (colour codes matches with Fig. 4.9)

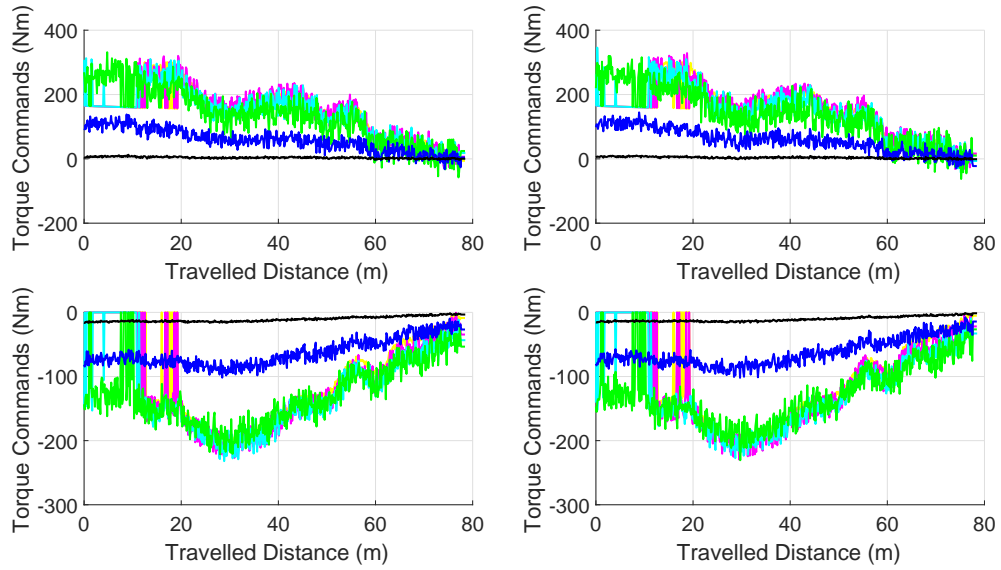


Figure 4.11: Torque commands applied to the wheels along Pareto-front of time and energy multi-objective controller (colour codes matches with Fig. 4.9; top left: front left wheel, top right: front right wheel, bottom left: rear left wheel and bottom right: rear right wheel)

as those in Fig. 4.9. The general characteristics of the torque commands applied to the wheels can be used as an selection criterion of the operating point along the Pareto-front.

In Table. 4.7, number of iterations spent in finding the Pareto-front for the scenarios are presented. The population size in the Genetic Algorithm is selected as 100. For a computer, with Intel Core i7-6700 HQ CPU, 2.60 Ghz, and 16 GB Ram, and x64 bit Windows 7, average time to complete an iteration step is also given in the table. In the table, the number of solution candidates tested by NSGA-II is presented as well. It has been observed that as the rotation radius becomes greater, the number of solutions checked and the number of NSGA-II iterations increase.

In Fig. 4.12, the Pareto-front obtained for Scenario-01 is presented together with the solutions of weighted energy and time optimality objectives solved with classical optimal control approach. The time and energy optimality results for weighted objectives is turned out to be unevenly distributed along the Pareto-front. For instance, the blue marker in Fig. 4.12 shows the results where the objective is 0.84 energy efficient, 0.16 time efficient, while, the solution with green marker has objective weighting of 0.90 energy and 0.10 time. The other weightings are, 0.94 energy, 0.06 time for black marker, and 1 energy 0 time for cyan marker.

The results demonstrated in Fig. 4.12, show that the non-dominating solutions are as optimal as the results obtained with weighted objectives solved with classical optimal control approach. This outcome gives an insight about the optimality of the Pareto-front. Furthermore, for the problems where the weighted-objective optimal control solutions are unevenly distributed, the Pareto-front analysis with multi-objective op-

Table4.7: Number of iterations to find the Pareto-front

Scenario ID	Iterations	Single Iteration Time (s)	Number of Solutions Tested
01	118	122.03	57001
02	123	124.74	66501
03	156	128.91	78501
04	201	133.44	101001
05	225	148.51	117001
06	277	155.96	139001

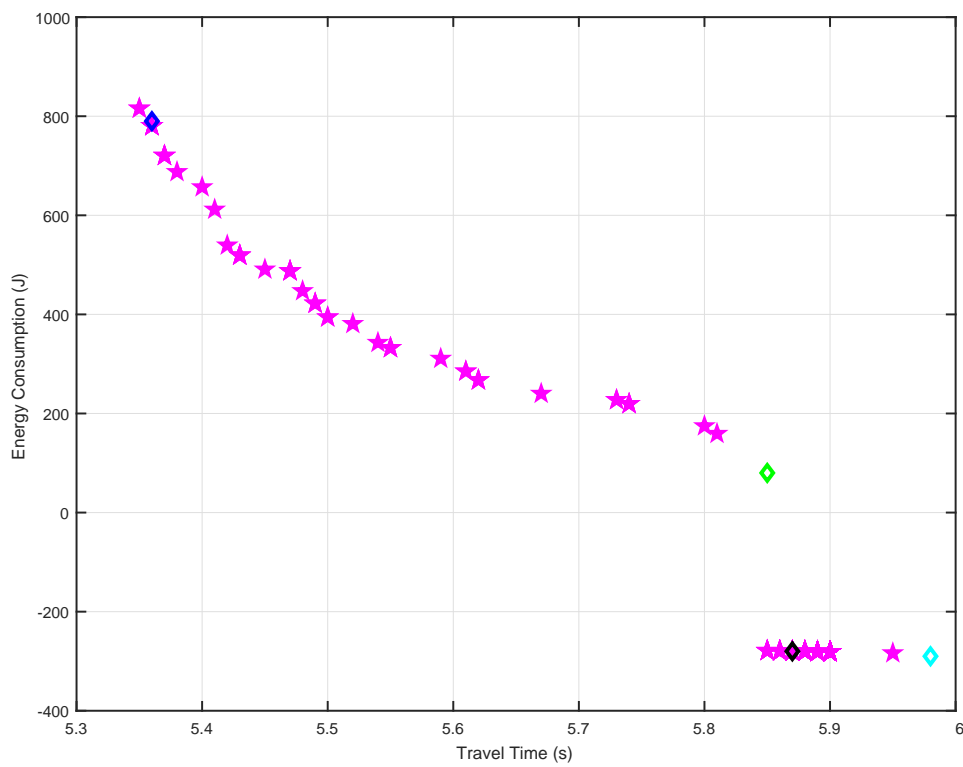


Figure 4.12: Pareto-Front for Time and Energy Multi-Objective Optimization and Weighted Optimal Control Results

timization provides more detailed results. Note that, the solution of optimal control problems require more time and computational power compared to non-dominating solution analysis with NSGA-II algorithm.

#### 4.5 Sensitivity Analysis

In this section, a sensitivity analysis on the energy and time consumptions of the vehicle under the optimal controllers has been held. Note that the solutions attained by energy and time optimal control criteria are sequences of control commands to be applied at fixed time instants, i.e., at each sampling time of 0.01 s. In the sensitivity analysis, these control sequences obtained for the nominal vehicle and scenario parameters are preserved, but the parameters of the vehicle or the scenario are disturbed. Hence, the control sequences to be applied at fixed time instants may not correspond to the exact positions of the road where they will be applied in the new parameters case. In order to preserve these information, similar to what is done in the solution approach for the optimal controllers, a transformation between position and time domains is performed. The optimal control sequences are associated with the positions along the road which is sectioned with a high resolution. Similar approach is followed for cruise controller command outputs to achieve a fair comparison.

In Section 4.3, the results are attained for an autonomous vehicle with no driver or passenger inside. In the sensitivity analysis, the following four configurations are considered: only the driver case (*Configuration-1*), the driver and a passenger seated on the front right seat (*Configuration-2*), the driver and a passenger seated on rear right seat (*Configuration-2*, taxi configuration), and the driver and 3 passengers (*Configuration-4*). The parameters are stated in Table 2.1.

According to the different configurations in the sensitivity analysis, the mass of the vehicle, the location of *CoG*, the inertia of the vehicle are changed. The sensitivity analysis shows that the optimal control strategies are insensitive to the parameter changes. Although the speed profiles and torque command profiles are changing for different configurations, the final energy consumption and travel time costs are attained to be the optimal ones. In Fig. 4.13 and Fig. 4.14, for different passenger arrangements defined in the configurations, the velocity and torque outcomes of the energy and time optimal solutions in Scenario-01 are presented, respectively.

#### 4.6 Conclusions and Discussions

In this chapter, vehicle motion and power consumption models are used to design energy and time optimal controllers based on classical optimal control theory. The vehicle speed boundaries for the optimal controllers are chosen as  $50 \pm 5$  km/h. The energy consumption and travel time performances of the optimal controllers are compared with the standard cruise controllers for various cornering scenarios.

The time and energy management problem is defined for electric vehicles including battery and wheel torque constraints. The problem may be subjected to specified

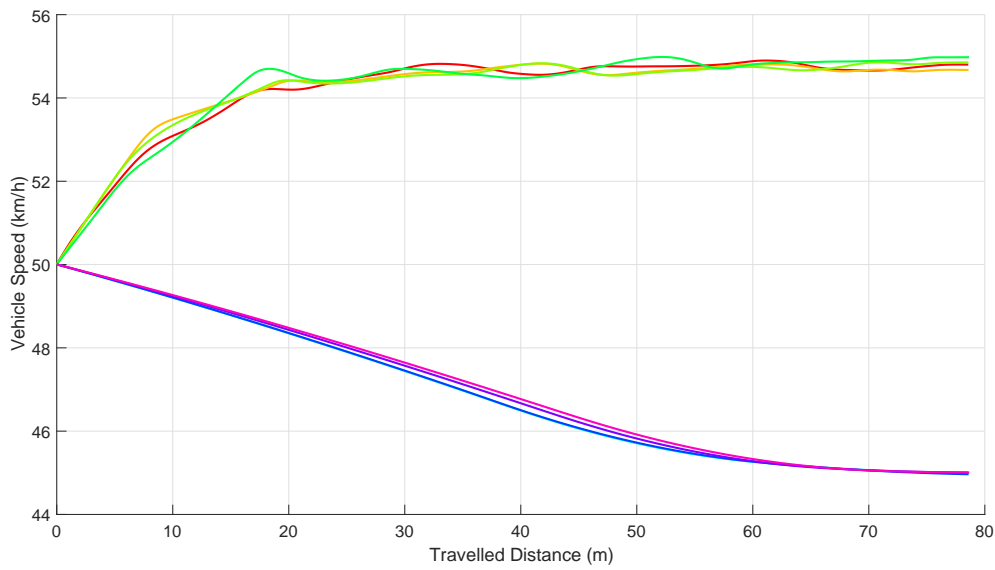


Figure 4.13: Speed profiles of the vehicle under optimal control strategies for different passenger configurations (red: *Configuration-1* and time optimal, orange: *Configuration-2* and time optimal, light green: *Configuration-3* and time optimal, green: *Configuration-4* and time optimal, turquoise: *Configuration-1* and energy optimal, blue: *Configuration-2* and energy optimal, violet: *Configuration-3* and energy optimal, and purple: *Configuration-4* and energy optimal)

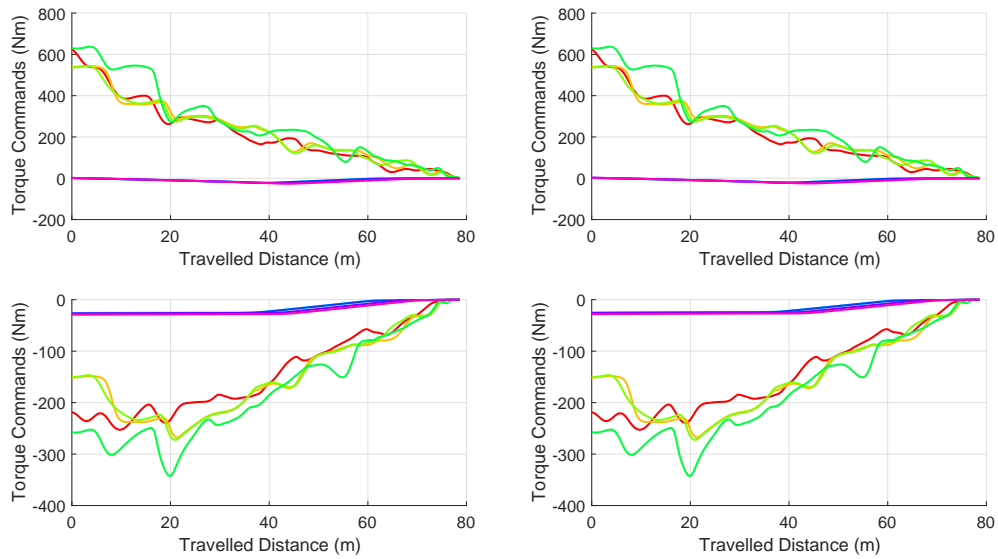


Figure 4.14: Torque commands applied to the wheels of the vehicle under optimal control strategies for different passenger configurations; (red: *Configuration-1* and time optimal, orange: *Configuration-2* and time optimal, light green: *Configuration-3* and time optimal, green: *Configuration-4* and time optimal, turquoise: *Configuration-1* and energy optimal, blue: *Configuration-2* and energy optimal, violet: *Configuration-3* and energy optimal, and purple: *Configuration-4* and energy optimal; top left: front left wheel, top right: front right wheel, bottom left: rear left wheel and bottom right: rear right wheel)

speed constraints as well. A solution algorithm employing Pontryagin's minimum principle is presented. The optimal control problem is free final time with boundary conditions defined as a function of state variables only.

The study aims to generate the following contributions to the literature available on the optimality problem in vehicle cornering motion:

- The optimal control problem is discussed on vehicle mathematical model which is sufficiently detailed to be applicable for any gross motion. In addition to the motion model, battery model and regenerative braking capability of the electric drive are included.
- The classical optimal control is shown to be a valid and applicable technique for time and energy optimization for vehicle motion. Time and energy optimality problems are both handled in a single solution structure.
- Both time and energy optimal control problems are free-final time problems. On the other hand, the distance to be covered is chosen to be fixed. A numerical method based on mapping the control inputs from the time domain to the position domain has been developed and utilized to satisfy the fixed distance constraint.
- It has been shown with NSGA-II genetic algorithm that there is a Pareto-front between time and energy optimization problems. The optimality of this Pareto-front is validated with classical optimal control approach.
- A sensitivity analysis is performed and it is confirmed that the optimal control solution is insensitive to the different passenger seating arrangements.

The proposed energy optimal controller gives an insight about the limits of energy management in the electric vehicles benefiting from regenerative braking and performing cornering. In this study, a cruise controller is utilized to give a reference merit for this comparison. There may exist better cruise controller policies for vehicle cornering.

## CHAPTER 5

### VEHICLE HANDLING

In this chapter, vehicle cornering around roads with low friction coefficients is studied and an autopilot design is proposed to satisfy desired handling performance. A novel hierarchical optimization approach is presented to generate off-line solutions for electric vehicles cornering along roads with different friction coefficients and radii of curvature. Vehicle motion as the output of this optimization process, together with the vehicle states and control commands at each sampling time are generated and stored for different selected scenario parameters with various rotation radii and friction coefficients. A vehicle status definition is presented as a function of vehicle states that contains the most informative data to evaluate the vehicle handling performance. The vehicle statuses at each decision instant among these off-line optimized data are clustered with the k-means clustering technique. These are associated with the control commands applied. A cluster centre-control command corresponds to a rule that produces the unique control command to be applied as a function of vehicle status. The autopilot is constructed by a convex combination of these rules. This basic idea of autopilot design has been extended for motion along a specific rotation radii and friction coefficients; the control commands corresponding to arbitrary scenario parameters are obtained by a runtime scheduling of the weighted-interpolation among the control commands corresponding to different scenario parameters.

Vehicles under autopilots with different number of clusters are tested in cornering motions along the icy roads, and according to the vehicle handling performances, the number of clusters is tuned. The autopilot design is compared with the off-line optimized control command sequences along the same test scenarios. It has been observed that performance of a vehicle under autopilot control does not differentiate from those under off-line optimized control commands in terms of vehicle states, vehicle handling performances and energy consumptions more than 5%. The performance of the autopilot proposal is also tested with different scenarios, and the approach based on runtime scheduling of the weighted-interpolation between the control commands corresponding to different scenario parameters is verified.

#### 5.1 Introduction

Vehicle cornering is one of the most intriguing problems in vehicle control, especially along the curvatures with low friction coefficients. Establishing a stable vehicle motion as well as a desired path tracking performance along the curvature is a compli-

cated problem on icy roads. During wheel slippage, control transmission between the torque applied to the wheel and the consequent traction capacity is reduced. Effects of the steering commands and the resultant handling performance are even more difficult to inspect.

Electric vehicles, with their environmental-friendly characteristics and usage of high-efficient electric motor technology, are one of the most promising alternative for private transportation. However, the problem of vehicle handling along curvatures with low friction coefficients turns out to be even more complicated for electric vehicles, due to their limitations in power consumption and electric motor torque capabilities.

There are significant number of studies conducted to optimize vehicle handling. The non-linear problem is linearised with some saturation effects and tried to be solved to improve the path tracking performance as in [76]. Alternatively, non-linear controllers are used directly to settle the problem. In [5], the authors propose a control scheme in a cascaded loop; one of them is for cancelling the non-linearities in the error dynamics, and the other one is for tracking the curved road with an inverse dynamics model.

The complexity of the problem can be overcome with simplifying the motion model to a yaw-only motion model, and a two-point boundary value optimal control problem can be solved to optimize vehicle manoeuvrability, [21]. Model reduction via linearisation prior to the application of optimal control rules are also proposed. In [80], for instance, the authors show in simulations that on their linearised vehicle model with trim states, gain-scheduling adaptive control laws are advantageous against the fixed control schemes in terms of path tracking performances. In addition to the controllers based on optimal control theory,  $H_\infty$  controller on linearised vehicle model to improve handling [41], and neural network traction control algorithms to improve vehicle steer-ability throughout the cornering motion [31] are also studied. In addition to these methods, four-wheel steering systems [85] and direct yaw moment control systems [3] are proposed to improve vehicle handling as well. Various studies are available in the literature to optimize direct yaw moment control [25, 10].

The skidding prevention problem is treated with different solution philosophies. Anti-lock brake systems (ABS) handles skidding during braking [62], while traction control systems (TCS) addresses the problem during acceleration [88]. These controllers reduce the torque applied on the wheels under slippage due to low road friction coefficient, to prevent skidding or to reduce the skidding range with certain performances [47]. Another approach to vehicle handling problem along icy roads is to evaluate the problem as a trajectory tracking problem. In [20], a discrete-time sliding mode control is proposed as a solution. In order to improve the degraded performance of ABS especially for the scenarios including icy roads, in [51], a fuzzy model reference learning control technique is presented. Additionally, studies maximizing the traction forces up to the limits of skidding with wheel slippage observers [58] or methods avoiding unstable vehicle dynamics based on measurements of steering torque, vehicle side-slip and tire-road friction coefficients [7] are proposed to improve vehicle handling along roads with low friction coefficients.

In this study, the problem of vehicle cornering around roads with low friction coefficients is addressed and an autopilot design is proposed. A hierarchical optimization

approach to generate a vehicle motion with desired handling performance and an autopilot design based on runtime decision making through an evaluation of the rules extracted from these optimized solutions are presented.

A two-level optimization logic to construct the motions of the vehicles cornering along icy roads with desired vehicle handling error is illustrated. The outer layer optimization algorithm first tries to solve the easiest problem which is cornering along an asphalt road, and the first solution proposal is the simplest which is applying a constant control command throughout the entire road. If a solution with desired vehicle handling performance is achieved with optimizing this solution proposal, then the friction coefficient is decreased gradually, and as skidding starts, the problem is modified to more difficult ones by dividing the road iteratively into increasing number of sections. In each section, a different optimal control command is found. In any of these iterations, if the solution cannot reach the desired performance, in one of the sections, that section is divided further into two sections. Hence, the number of control commands to be optimized is increased. This is defined as more complex solution in the context, since the number of command vectors to be optimized becomes larger. As the outer optimization layer selects the current friction coefficient and optimizes the solution complexity, the inner layer optimizes the control command vectors one vector at a time to minimize the handling error. Assuming that the control command space is divided into cells, an optimization technique focusing a search cone on the direction of the cell whose handling cost minimum, has been proposed. The optimization algorithms are counted among the main contributions of this study.

A vehicle status definition is proposed as a function of vehicle states that contains the most informative data to evaluate vehicle handling performance, such as the deviation from the curvature, the vehicle velocity, and the angular difference between the velocity and the line tangent to the curvature. The optimization results are used to generate a motion where vehicle status vectors and control command vectors at each sampling time can be stored. A clustering is performed on the vehicle status space, following the well known k-means clustering technique. For each cluster centre, a control command vector is assigned. Different cluster sets are generated for different rotation radii and friction coefficients. A cluster corresponds to a rule that defines the command to be applied as a function of the vehicle status. These rules are used in runtime decision making process of the autopilot.

The proposed autopilot calculates its current vehicle status and makes a decision about the command vector to be applied at that instant from the control commands associated with each cluster centre. This assignment is inversely proportional to the relative distances of the current vehicle status to those at the cluster centres. The control commands to be applied for motion along a specific rotation radius and friction coefficient are obtained by runtime scheduling of the weighted-interpolation between the control commands corresponding to different scenario parameters. The implementation of clustering based decision making process, and its application on electric vehicles cornering around roads with different friction coefficients, can be considered as one of the main contributions of this study.

The autopilot design is verified in comparisons to off-line optimization results in terms of vehicle handling performances and energy consumption of the vehicle, and the number of clusters is tuned in these tests. The performance of the autopilot

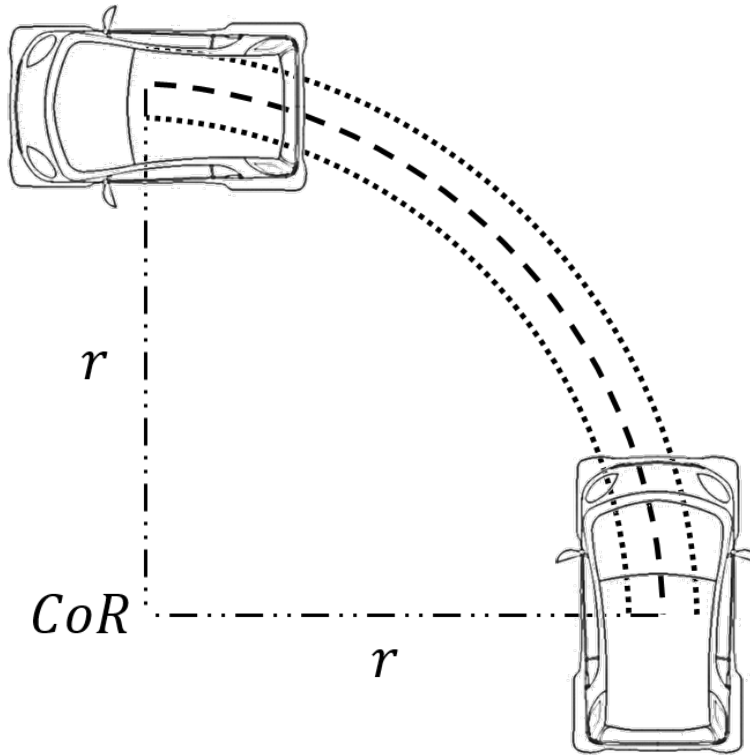


Figure 5.1: Motion representation for vehicle handling problem

proposal is also tested with different scenarios, and the approach based on runtime scheduling of the weighted-interpolation between the control commands corresponding to different scenario parameters is verified.

In Section 5.2, the solution approach is proposed. In Sections 5.3-5.3.2, the multi-level optimization logic to generate solutions for vehicles cornering an icy road with desired vehicle handling error is presented. In Section 5.4, off-line optimization results are evaluated, the rules to be employed in autopilot design are generated with k-means clustering. In Section 5.5.1, the approach used in tuning the number of clusters is introduced. In Section 5.5.2, for the parameters determined, the autopilot results are compared with off-line optimization results as a verification of the solution approach, and in Section 5.5.3, for different test scenarios, the vehicle handling performances of an electric car under the proposed autopilot design are presented.

## 5.2 Solution Approach

This study addresses the vehicle handling problem for cornering motion along roads with low friction coefficient, such as icy roads. The motion of the vehicle is presented in Fig. 5.1. As depicted in the illustration, a margin along the curvature can be defined, where it is assumed that the vehicle motion inside this margin has satisfactory handling performance.

The *cornering during slippage autopilot* design is founded on a runtime decision making process according to current vehicle status. A vehicle status definition is proposed as a function of vehicle states that contains the most informative data to evaluate the handling performance. An off-line optimization is performed to generate vehicle motion with adequate handling performance. The off-line optimization for cornering around a certain radius along roads with low friction is obtained with first finding an optimized solution for asphalt road ( $\mu = 0.72$  [8]), and then reducing the friction coefficient to icy road ( $\mu = 0.19$  [8]). The optimized motion is stored in pairs of vehicle status vectors and the corresponding control command vectors for each decision instant.

The vehicle status vectors throughout the motion are later clustered with well-known k-means clustering. The control command vector to be applied in each of the cluster centre is calculated as the weighted sum of control commands corresponding to each vehicle status sample in that cluster, where the weights are taken inversely proportional to the Euclidean distances between the vehicle status of the sample and the vehicle status at the cluster centre. Hence, a representative control command to be applied at a representative vehicle status is obtained for each cluster, which is then interpreted as a rule in decision making process. The clustering is performed for different scenarios with different friction coefficients and rotation radii; thus, cluster sets are obtained for these different scenarios.

The generated rules are used in runtime decision making process. At each decision instant, this process evaluates the current vehicle status, and proportional to the Euclidean distances to each cluster centre, the control command according to the scenario under consideration is calculated. The control command to be applied for motion along a specific rotation radius and friction coefficient is obtained by runtime scheduling of the weighted-interpolation between the control commands corresponding to different scenarios with different friction coefficients and rotation radii.

The autopilot design is verified in tests considering the off-line optimization outputs as ground truth. The number of clusters are tuned in these verification tests. Tuned parameters are used in solution approach, and scenarios with different friction coefficients and rotation radii are tested to demonstrate the autopilot performance. The overall solution approach is depicted in Fig. 5.2.

### 5.3 Optimization Algorithms

The vehicle motion with desired handling performance during cornering is optimized with a hierarchical optimization process. The hierarchy is composed of two layers: an outer layer is for guiding the solution to answer the desired problem, and an inner layer is for generating a solution with a non-gradient based optimization algorithm to minimize the vehicle handling cost for a given problem.

The outer layer initiates its optimization with a simple solution for relatively easy problem: a constant command is applied throughout the entire cornering motion along an asphalt road. The difficulty of the problem increases as the skidding starts due to low friction coefficient; hence, the solution gets complex which is defined as applying

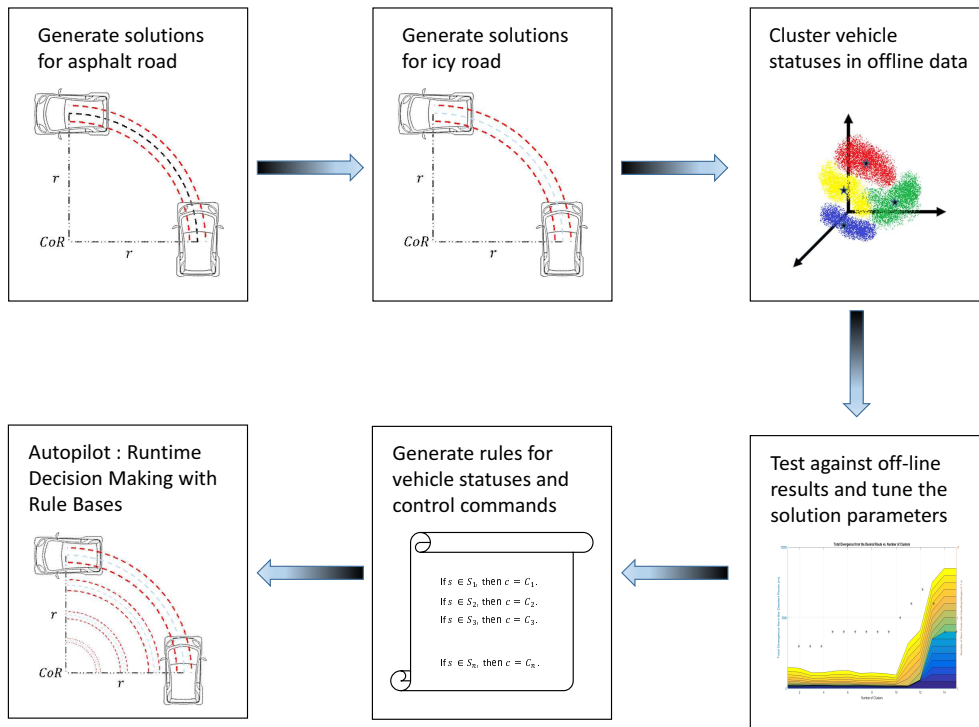


Figure 5.2: Solution approach for vehicle handling problem

different control commands at different sections of the road.

The inner layer is for optimizing the control command vector to minimize the handling error. The vehicle motion model comprises Newton-Euler equations for the chassis and the wheels. In cases of wheel slippage, the relation between linear and angular velocities and accelerations of the wheels does not hold, and skidding dynamics become in act. Depending on these modes of the wheels and including the non-holonomic conditions due to Ackerman's steering law, the motion model is complicated. In each solution step, to find the traction forces and accelerations of the vehicle, all the structural forces are also calculated. The accuracy of the model preserved in return of computational complexity. Hence, instead of a gradient-based optimization algorithm, one following a non-gradient based approach is designed in the inner layer.

### 5.3.1 Outer Layer Optimization: from easy problem to difficult problem, from simple solution to complex solution

Determining a sequence of control command vectors for the vehicle cornering along an icy road ( $\mu = 0.19$ ) with desired handling performance is the ultimate aim of the outer layer optimization algorithm, yet this problem is difficult to solve due to skidding conditions. This goal is achieved through iterations of solving the problem for cornering the roads with slightly higher friction coefficients. Hence, the outer layer

optimization logic is initiated with a control command vector to perform cornering with desired handling performance along asphalt roads ( $\mu = 0.72$ ), which is the solution of a relatively easy problem.

As the initial solution to this relatively easy problem, a single command vector of size five, consisting of four torque commands applied to the wheels and the steering command, is selected. This is the simplest solution proposal with complexity of one, where complexity is defined as the number of road sections where control command vector is constant. If the solution complexity does not yield the desired handling performance, the solution proposal is changed to more complex one. The replicas control command vector to be applied at a road section is considered as two different vectors to be applied in two halves of this section, and then these two vectors are optimized separately by the inner layer optimization algorithm. Hence, the problem to be solved is attacked with the solution proposal with minimum complexity.

Such an approach to solve a difficult problem which probably requires a complex solution, starting with defining an easier version of the problem probably requiring a simpler solution, is one of the main contributions of this study. Note that, an attempt to solve the difficult problem directly, may yield significant amount of time, and for the case of the vehicle cornering along icy roads, may generate tumbling of vehicle creating a feeling that the problem has no solution at all. The approach in the outer layer optimization logic is illustrated in Fig. 5.3.

### 5.3.2 Inner Layer Optimization: non-gradient based optimization algorithm

The vehicle handling problem is defined in (5.1), which minimizes the cost of deviation from a desired arc or a determined margin around this arc. Since the road description is a quarter circle with radius  $r$ , the determined margin can be defined in terms of the radius as  $\delta r$ . Here note that, the vehicle motion dynamics, the power consumption dynamics, the wheel torque limits should also be included in the problem as constraints. Furthermore, in order to enforce the vehicle to complete the defined path within a time budget, the velocity of the vehicle can be constrained. Moreover, the intuition of an acceptable vehicle motion requires the vehicle prevent tumbling, in other words, normal forces on the wheels should always be positive.

$$\begin{aligned}
& \text{minimize} \\
& \text{Cost} \triangleq \sum_{t=0}^{t_f} (\bar{r}_{oc}^{(o)} - r)^2 \quad \text{if } \|\bar{r}_{oc}^{(o)} - r\| > \delta r \\
& \text{subject to} \\
& \dot{\mathbf{x}} = \mathbf{f}(\mathbf{x}, SoC, M_{wc,y}^{(w)}) \\
& v_{v,x_{min}}^{(o)} \leq v_{v,x}^{(o)} \leq v_{v,x_{max}}^{(o)} \\
& M_{w_{fl}c,y}^{(w_{fl})} \omega_{w_{fl},y} + M_{w_{fr}c,y}^{(w_{fr})} \omega_{w_{fr},y} \leq FPCB \\
& \forall w_k \quad M_{wc,y}^{(w)} \leq MTC \\
& \forall w_k \quad \bar{u}_z^T \bar{F}_{gw_k}^{(w_k)} > 0
\end{aligned} \tag{5.1}$$

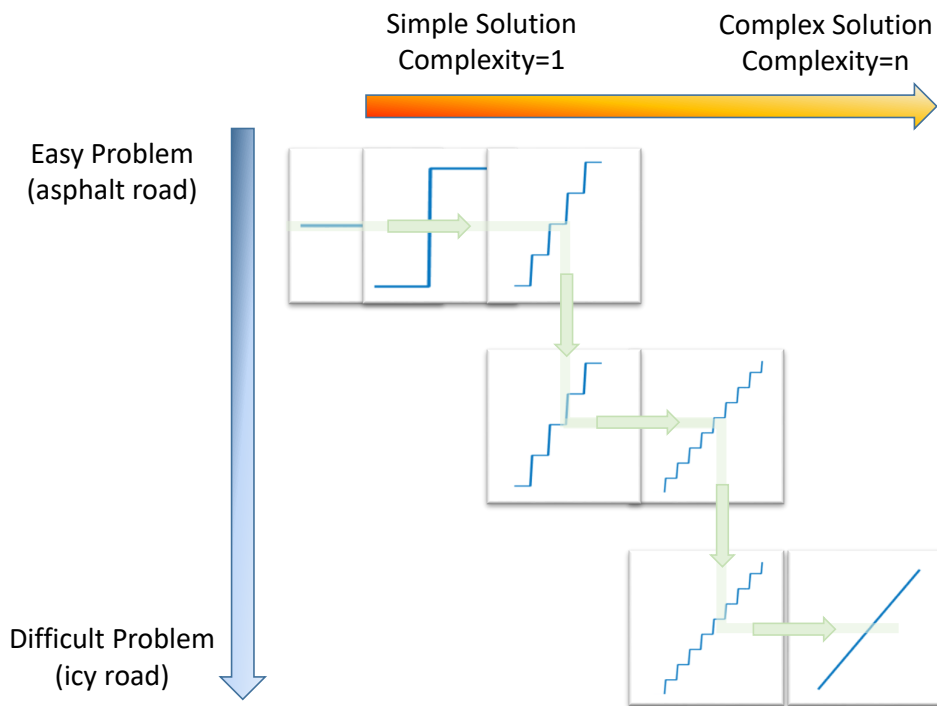


Figure 5.3: The outer layer optimization logic

Table5.1: Outer layer optimization algorithm

---

01:	<b>Procedure:</b> Outer Layer Optimization Algorithm
02:	<b>Initialization :</b>
03:	Generate road with $\mu = \mu_{init}$ and $r = r_{init}$ .
04:	Generate a solution with some arbitrary fixed control commands with <i>Complexity</i> = 1 ( <i>SolutionSetSize</i> = <i>Complexity</i> × 5).
05:	Calculate <i>CurrentCost</i> = <i>Cost</i> .
06:	<b>Inner Loop :</b>
07:	For each complexity, <i>k</i> :
08:	Solve $\min_{\text{Solution}(k)} \text{Cost}$ .
09:	If <i>CurrentCost</i> ≠ 0, then go to Step <i>Complexity Increase</i> .
10:	If <i>CurrentCost</i> = 0, then go to Step <i>Outer Loop</i> .
11:	<b>Complexity Increase :</b>
12:	Update <i>Complexity</i> = <i>Complexity</i> × 2 and <i>SolutionSetSize</i> = <i>Complexity</i> × 5.
13:	Update Solution, by duplicating each block of size 5 in Solution.
14:	Go to Step <i>Inner Loop</i> .
15:	<b>Outer Loop :</b>
16:	Update $\mu$ and $r$ .
17:	If $\mu = \mu_{final}$ and $r = r_{final}$ , then return.
18:	Generate road, and go to Step <i>Inner Loop</i> .
19:	<b>end procedure</b>

---

In (5.1),  $FPCB$  stands for forward power capacity of the battery package to be extracted from Fig. 2.7, and  $MTC$  defines the maximum torque capacity of the wheels. The cost function defined in (5.1) is a squared sum of the position deviations throughout the cornering. The motion model incorporated with the non-linear battery model is too complicated to calculate this cost analytically. Note that depending on the slippage conditions for each wheel, the governing equations for the vehicle motion switches between different conditions, and this behaviour further complicates the model. Therefore, a non-gradient based optimization algorithm is preferred to minimize the cost. The problem parameters such as the friction coefficient is selected by the outer optimization layer, which optimizes the solution complexity as well. There are many non-gradient based optimization methods available in literature; genetic algorithms, simplex methods [64], particle swarm optimization [46], or Hooke and Jeeves method [37] are proposed as solutions based on cost optimization without a gradient calculation.

In the inner layer, an optimization algorithm is proposed to minimize the handling cost. The control command space of five dimensions: four torque and one steering input, is divided into cells. The middle points of these cells are assumed to represent the entire cell. Hence, for a given control command vector, there are always neighbouring cells, for example, there are  $3^5 - 1 = 242$  possible new solutions that can be checked within an 1-neighbourhood; and  $5^5 - 1 = 3124$  in 2-neighbourhood of the current solution proposal.

In each iteration, the optimization algorithm searches the alternative with a minimum cost inside its neighbourhood. A search cone along the direction of two consecutive optimization iterations is generated. The costs of the solution candidates inside this cone will be checked. If a solution with better cost performance is found inside this cone, the current status is updated with this candidate. The direction towards this candidate is stored as the direction of the centre line of the search cone for the upcoming iteration. Furthermore, in an iteration, if a better solution is found, a narrower search cone is used in the next iteration, and if otherwise, the search cone is enlarged. The approach has a strong analogy with adaptively adjusting the one dimensional search step in gradient-based optimization techniques. The proposed optimization logic and its application to optimize vehicle handling in a cornering problem is considered to be one of the main contributions of this study. An example of the search cone optimization is presented for 3 variables and 1-neighbourhood case in Fig.5.4.

Note that since the candidates inside the neighbourhood of the current state are solved and stored, in the next iteration, only performances of the candidates that are not solved in previous iterations are computed. The number of calculations in this algorithm is equal to that of searching all possible candidates around the current state, only in the worst case i.e,  $\alpha = \pi$ . Otherwise, the number of computations is always smaller than exhaustive search. Furthermore, focusing in the direction towards the candidate with the best cost at each optimization step, and eliminating the other candidates, increase the convergence rate of the algorithm compared to those of other non-gradient based optimization algorithms.

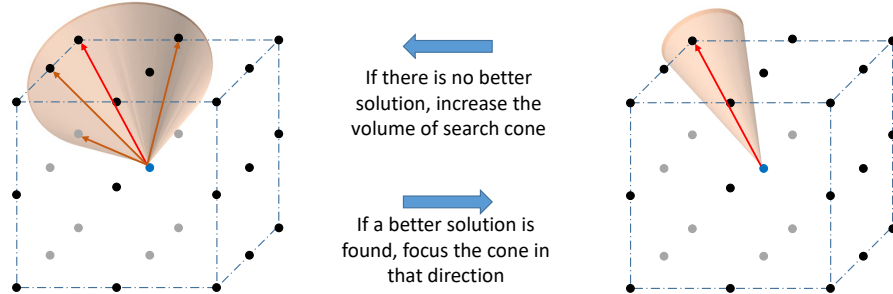


Figure 5.4: The inner layer optimization logic

Table5.2: Non-gradient based optimization algorithm: search cone optimization

- 
- 01: **Procedure:** Optimization of  $x$ , with initial condition of  $x_{init}$
- 02: **Initialization :**
- 03: Calculate cost of current state  $x$ , and store as  $CurrentCost$ .
- 04: Define cone angle as  $\alpha = \pi$ , set cone angle update rate  $0 < \beta < 1$ .
- 05: Define initial direction as  $\Delta x = \Delta x_{init}$ .
- 06: Create  $CandidatePool = \emptyset$ .
- 07: **Iterations :**
- 08: Generate solution candidates which are  $\alpha$  neighbourhood of  $x$  as  $\hat{x}_k$ .
- 09: Select solution candidates that are not inside the  $CandidatePool$ .
- 10: Calculate Costs of each solution candidate,  $Costs_k$ .
- 11: If  $\min_k Costs_k < CurrentCost$ , update  $CurrentCost = \min_k Costs_k$ ,  
 $\Delta x = x_k - x$ ,  $x = x_k$ , update  $\alpha = \alpha \times \beta$ .
- 12: Else Update  $\alpha = \alpha \beta$ .
- 13: Put all the candidates solved into the pool, update  $CandidatePool$ .
- 14: If  $CurrentCost < Threshold$ , return; else, go to Step *Iterations*.
- 15: **end procedure**
-

## 5.4 Status Clustering and Rule Generation

In this study, an autopilot design for electric vehicles cornering around low-friction roads; i.e. icy road ( $\mu = 0.19$ ) is proposed. Vehicle motions are first optimized off-line to achieve a desired handling performance. A vehicle status definition is proposed as a function of vehicle states that contains the most informative data to evaluate the handling performance. Vehicle statuses and control commands applied at each decision instant are stored to be used as data set in rule generation. The rule sets used in the runtime decision making process are generated via clustering the vehicle statuses and calculating associated control commands.

The vehicle status is defined as  $\Theta = [p_d, v, \theta]^T$ ;  $p_d$ : radial position deviation normalized with rotation radius ( $r$ ),  $v$ : velocity of the vehicle,  $\theta$ : angle of velocity of the vehicle with respect to tangent of the desired route, as depicted in Fig. 5.5. The hierarchical optimization procedure gives a result of control command vector(s) to be applied at different road sections that optimizes the vehicle handling for the scenario with a certain rotation radius and friction coefficient. When this command sequence is applied, at each sampling time defined as decision instants, the control commands, the vehicle states and hence the vehicle statuses are obtained. Even solution of a single scenario, generates hundreds of such data.

The vehicle status sets at each decision instant are clustered with a centroid-based clustering technique: k-means clustering [56]. In k-means, the number of clusters is a parameter to be specified in advance. Other than centroid based clustering, there are distribution-based clustering and density based clustering techniques are available in the literature [34]. In this study, to ease computation and keep the focus on the autopilot design rather than clustering techniques, k-means clustering is preferred. In k-means clustering, the vehicle status samples represented in the space of  $\Theta = [p_d, v, \theta]^T$  are clustered into  $k$  classes, according to the Euclidean distances between the samples. The samples that are close enough to each other generate a cluster.

For  $k$  clusters, the clustering process associates each vehicle status to a cluster and generates  $k$  cluster centres. Similar to vehicle statuses, the control commands are stored at each decision instant. For each cluster, a control command vector corresponding to the cluster centre is calculated with weighted sum of the control commands of each sample in that cluster. The weighting is inversely proportional to the Euclidean distance between the vehicle status of the sample and that of the cluster centre. A thresholding can be performed as well to ease the computation by eliminating the contributions of the control commands associated with the vehicle statuses that are far away from the cluster centre, see (5.2).

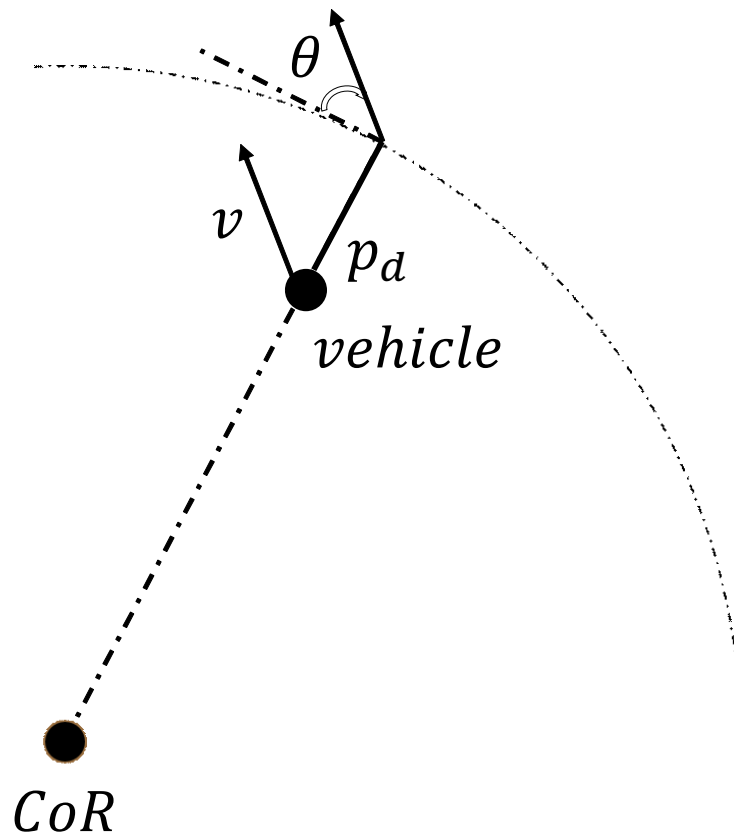


Figure 5.5: Definitions of vehicle statuses,  $\Theta = [p_d, v, \theta]^T$ ;  $p_d$ : radial position deviation normalized with rotation radius ( $r$ ),  $v$ : velocity of the vehicle,  $\theta$ : angle of velocity of the vehicle with respect to tangent of the desired route

$$\begin{aligned}
\bar{C}_{\mathbb{C}_k} &= \sum_{j=1}^{N_{\mathbb{C}_k}} \gamma_k \xi_j^k \bar{C}_j \\
\xi_j^k &= 1/D_j^k \\
\gamma_k &= \sum_{j=1}^{N_k} 1/\xi_j \\
D_j^k &= \|\Theta_j - \Theta_{\mathbb{C}_k}\|
\end{aligned} \tag{5.2}$$

In (5.2),  $\mathbb{C}_k$  indicates the  $k$ -th cluster,  $\bar{C}_{\mathbb{C}_k}$  is the representative control command vector of the cluster  $\mathbb{C}_k$ ,  $\bar{C}_j$  is the control command vector of  $j$ -th vehicle status vector clustered in cluster  $\mathbb{C}_k$ .  $\xi_j^k$  is the weight of the  $j$ -th vehicle status vector,  $\gamma_k$  is the normalization factor of  $\mathbb{C}_k$ , and  $N_{\mathbb{C}_k}$  is the number of vehicle status vectors in this cluster.  $\xi_j^k$  is inversely proportional to the distance of the  $j$ -th vehicle status vector to the cluster centroid vehicle status.  $\Theta_j$  defines the location of the  $j$ -th vehicle status vector in vehicle status space, and similarly,  $\Theta_{\mathbb{C}_k}$  is the location of the cluster centroid in the vehicle status space.

Hence, for each cluster, a characterizing vehicle status at the cluster centroid, and a characterizing control command vector to be applied at this cluster centroid are attained. A cluster corresponds to a rule that defines the command to be applied as a function of the vehicle status. These rules are used in runtime decision making process of the autopilot. Similar rule sets can be acquired for other scenarios with different rotation radii and friction coefficients.

#### 5.4.1 Autopilot Design: Runtime Decision Making

The autopilot design is based on runtime decision making process based on the rule sets generated from the off-line optimization results. At each decision instant  $t$  in runtime, the vehicle status vector  $\Theta_t$  is extracted from the vehicle state. The corresponding control command to be applied,  $\bar{C}_t$  is calculated with interpolating between commands to be applied at cluster centroids,  $\bar{C}_{\mathbb{C}_k}$ , weighted inversely proportional with the distance of the current vehicle status to each of the cluster centroid,  $D_j^k = \|\Theta_j - \Theta_{\mathbb{C}_k}\|$ . The clustering and command generation in the autopilot are performed for each cluster set attained for a selected rotation radius and friction coefficient. Finally, control commands to be applied for motion along a specific rotation radius and friction coefficient are obtained by runtime scheduling of the weighted-interpolation between the control commands corresponding to different scenario parameters.

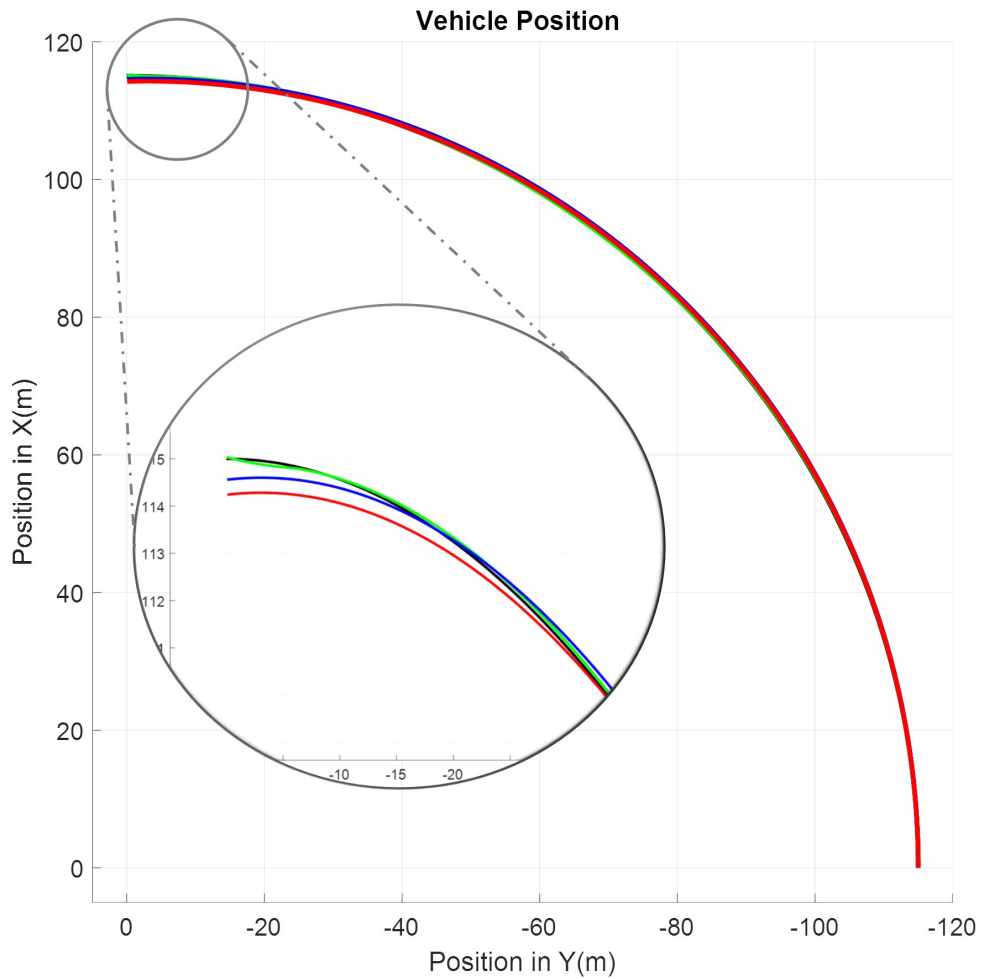


Figure 5.6: Vehicle cornering under control of autopilots with different number of clusters for scenario  $r = 115m, \mu = 0.19$  (green:  $k=20$ , blue:  $k=10$  and red:  $k=5$ )

## 5.5 Results

### 5.5.1 Tuning Cluster Parameters

The major drawback for k-means clustering is the need to define the number of clusters beforehand. To determine the number of clusters, for different cases the performance of the autopilot for different rotation radii and friction coefficients are evaluated. For example, the off-line optimization result for  $r = 115m, \mu = 0.19$ , icy road, is selected as the training data, and with different number of clusters  $k$ , the vehicle status samples are clustered. The performances of autopilot design with different number of clusters is presented in Fig. 5.6. Similar tests are repeated for  $r = 110m, \mu = 0.19$ , icy road, and outcomes are illustrated in Fig. 5.7.

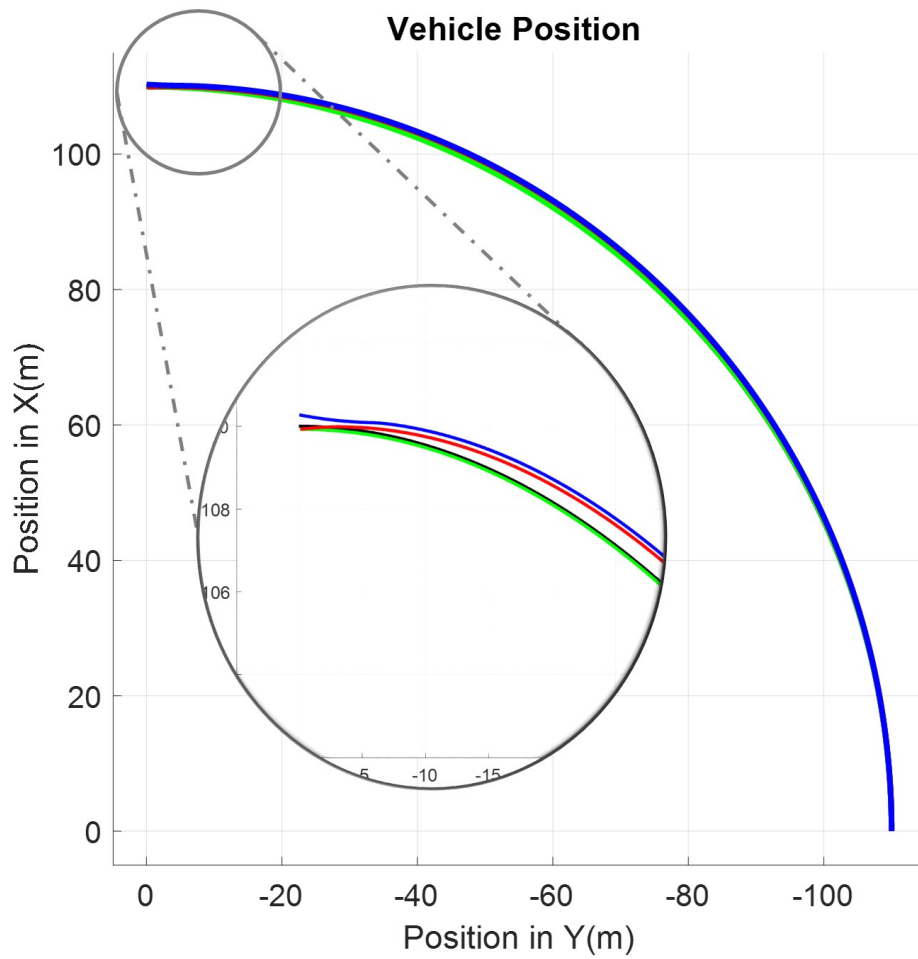


Figure 5.7: Vehicle cornering under control of autopilots with different number of clusters for scenario  $r = 110m, \mu = 0.19$  (green:  $k=20$ , blue:  $k=10$  and red:  $k=5$ )

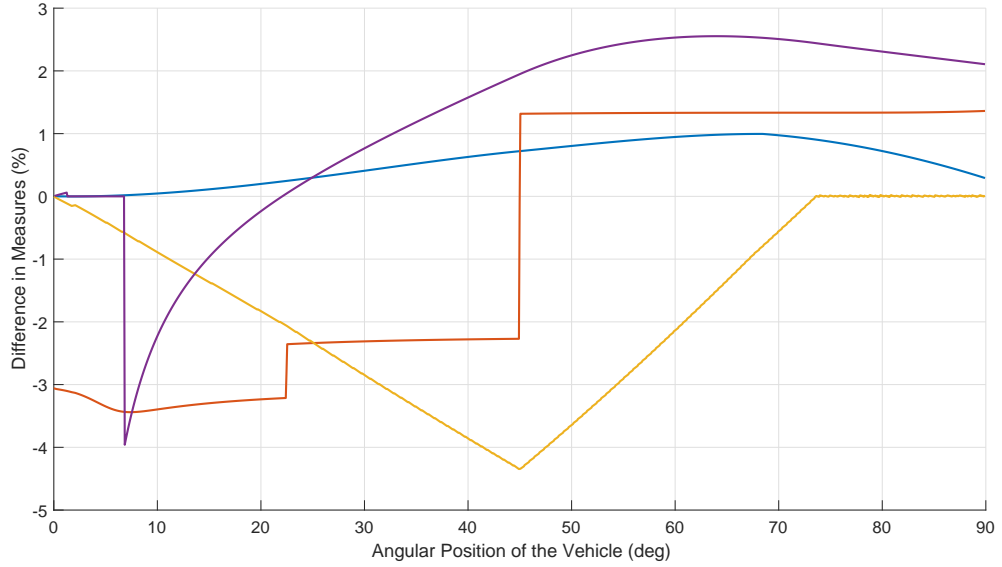


Figure 5.8: Autopilot results compared with off-line optimization results, for  $r = 115m$ ,  $\mu = 0.19$ , normalized differences on various features (blue: position error, red: rotation radius commands, yellow: velocity of the vehicle and violet: power consumption of the vehicle)

The results depict that, the minimum divergence from the rotation radius is attained when the number of clusters is selected as 20. It is observed that the number of clusters greater than 20 does not yield significant improvement in vehicle handling.

### 5.5.2 Autopilot Performance Compared against Off-line Optimization Results

Parameters of the model used in the simulations are given in Table 2.1. The model parameters are approximate average values of the electric vehicles in market.

Number of clusters being selected as 20, the autopilot design is tested against the optimization results for various rotation radii and friction coefficients. Below in Figs. 5.8 and 5.9, the design validation tests for  $r = 115m$ ,  $\mu = 0.19$ , icy road, and  $r = 110m$ ,  $\mu = 0.19$ , icy road, are presented. The comparisons give differences between absolute position errors, rotation radius commands, vehicle velocities and changes in *SoC* of the battery package under autopilot control and under the control commands optimized off-line, in percentage.

The results show that, the changes in measures of vehicle depicted in the figures under control of the autopilot are not greater than 5% compared to those in optimized control commands. The handling performance is satisfactory for the vehicle under autopilot control as well; in other words, with vehicle handling margin of  $\delta r = 1m$ , the vehicle under autopilot generates zero cost according to the cost definition in (5.1). The power consumption of the vehicle does not alter significantly either. This can be interpreted as a verification of the autopilot proposal.

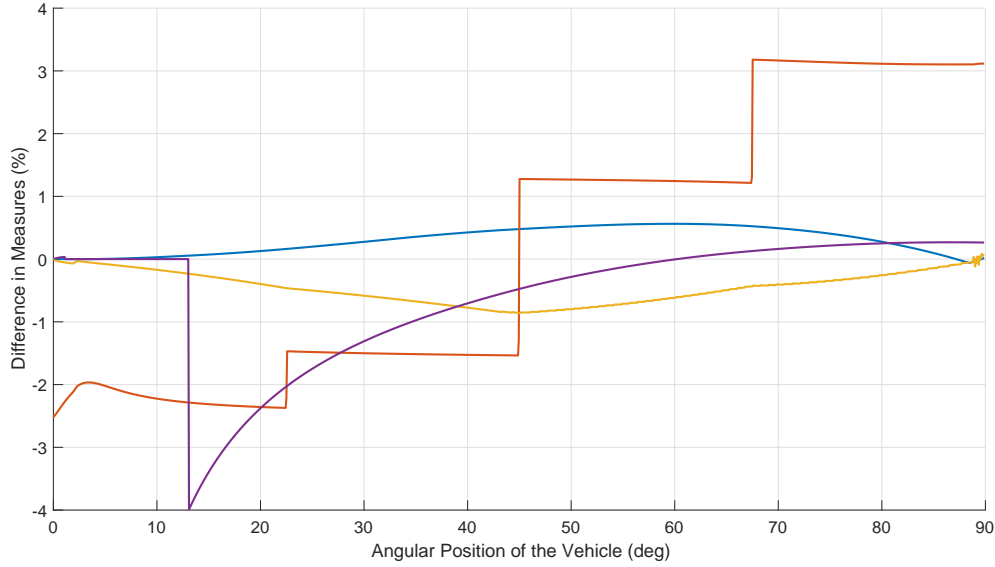


Figure 5.9: Autopilot results compared with off-line optimization results, for  $r = 110m, \mu = 0.19$ , normalized differences on various features (blue: position error, red: rotation radius commands, yellow: velocity of the vehicle and violet: power consumption of the vehicle)

### 5.5.3 Autopilot Performances in Test Scenarios

The off-line optimization data have been used to generate rules for runtime decision making process. It is not possible to attain off-line optimization data for every scenario; hence, for various rotation radii and friction coefficients, the rules obtained for different off-line optimization will be interpolated. As depicted in previous results, for  $r = 115m, \mu = 0.19$ , icy road, and  $r = 110m, \mu = 0.19$ , icy road, number of clusters are selected as 20, and by clustering the rules to be used in decision making process are acquired and tested against off-line optimization data. In this part,  $r = 112m, \mu = 0.19$  is tested. The results are depicted in Fig. 5.10. In the test, ground truth is depicted in black. The behaviour of the vehicle with decisions being made based on rules only from  $r = 115m, \mu = 0.19$  is in blue, only from  $r = 110m, \mu = 0.19$  is in red, and based on runtime scheduling of the weighted-interpolation of these two rule sets is in green. It has been observed that the latter approach presents far better handling performance compared to that of decision making based on rules generated from a single scenario.

In Fig. 5.11, the position deviation from the perfect arc, the rotation radius commands, the deviations in velocity of the vehicle from the reference  $50km/h$  speed and the changes in state-of-charge of the battery as an indication of power consumption of the vehicle under control of autopilot designs, based on rules from single rotation radius,  $r = 110m, \mu = 0.19$  and  $r = 115m, \mu = 0.19$  and runtime scheduling of the weighted-interpolation of the two are presented, for the vehicle moving along icy road  $r = 112m, \mu = 0.19$ . It has been observed that, total position deviation of the vehicle from the desired route, as the definition of the vehicle handling is the smallest in the

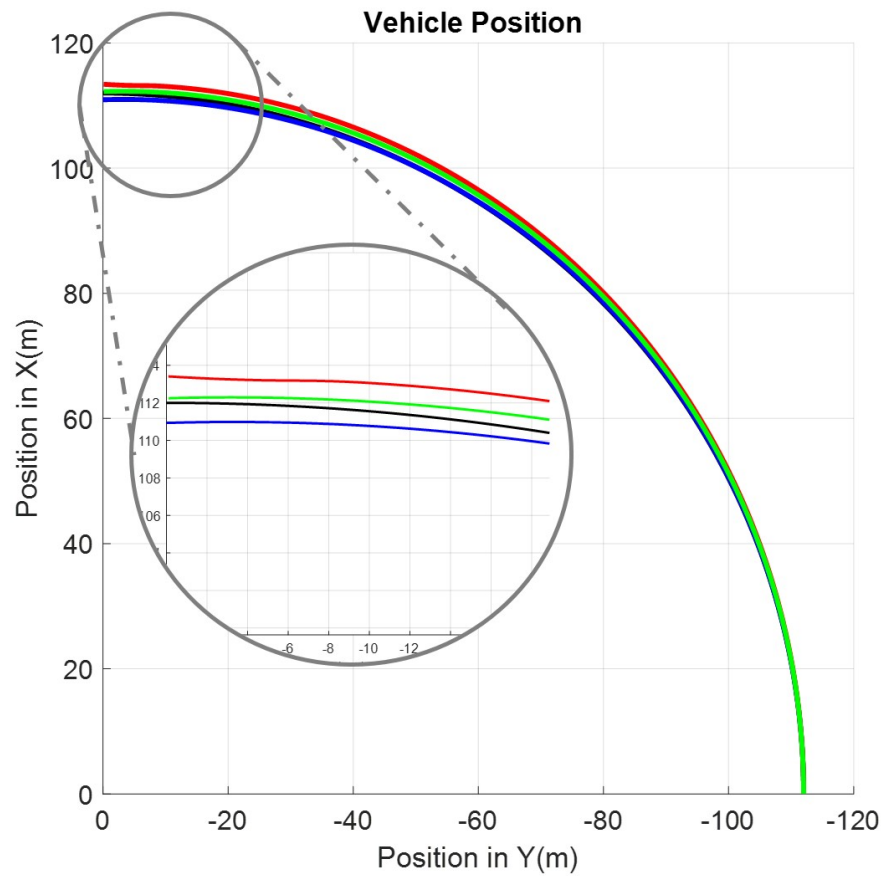


Figure 5.10: Autopilot performance for  $r = 112m, \mu = 0.19$  with runtime scheduling of the weighted-interpolation the rule bases from different rotation radii (black: ground truth, blue: rule bases of  $r = 115m, \mu = 0.19$  only, red: rule bases of  $r = 110m, \mu = 0.19$  only and green: runtime scheduling of the weighted-interpolation of the rule bases)

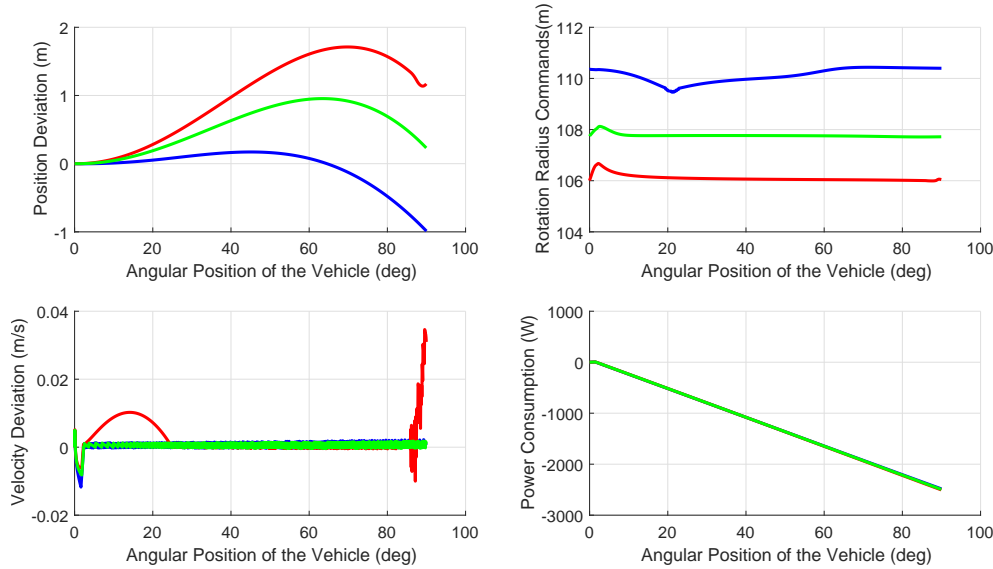


Figure 5.11: Autopilot performance measures for  $r = 112m, \mu = 0.19$  with runtime scheduling of the weighted-interpolation of the rules from different rotation radii, normalized differences on various features (blue: rule bases of  $r = 115m, \mu = 0.19$  only, red: rule bases of  $r = 110m, \mu = 0.19$  only and green: runtime scheduling of the weighted-interpolation of the rule bases)

case of runtime scheduling autopilot design. Furthermore, it has been demonstrated that the runtime scheduling of the weighted-interpolation of the commands obtained different radii sticks to the reference speed tighter compared to the others.

In order to test the effects of runtime scheduling of the weighted-interpolation between control commands generated from off-line optimization data for the same rotation radius but different friction coefficients, the following road is generated. As depicted in Fig. 5.12, the quarter circled road has gradually decreasing friction coefficient. In real life, instead of sharp changes, such gradual changes in friction coefficient are more common.

In varying friction coefficient road test, rules from 20 clusters for  $r = 110m, \mu = 0.19$ , icy road,  $r = 110m, \mu = 0.24$ , wet road, and  $r = 110m, \mu = 0.72$  dry asphalt road each are generated based on off-line optimization results. The results are depicted in Fig. 5.13. It has been observed that, the runtime scheduling of the weighted-interpolation of the rules generates the only autopilot design that vehicles completes the test road with varying friction coefficient. The autopilots based on rules from clustering the optimization data from only a single friction coefficient scenario cannot achieve to be valid throughout the scenario.

Measures similar to those in Fig. 5.11, are presented for the varying friction coefficient scenario as well in Fig. 5.14. It has been observed that, the runtime scheduling of the weighted-interpolation of the rules makes the vehicle approach to a converging error in position deviation from the desired route. The deviation from the reference

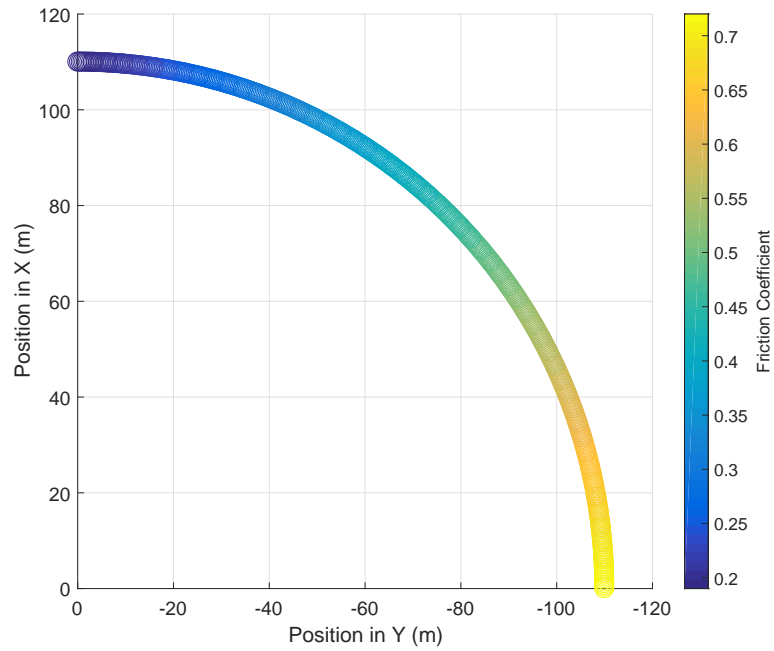


Figure 5.12: Test road with gradually decreasing friction coefficient

velocity is the smallest as well.

## 5.6 Conclusion

In this chapter, the problem of vehicle cornering around roads with low friction coefficients is addressed and an autopilot design is proposed. A hierarchical optimization approach to generate a vehicle motion with desired handling performance and an autopilot design based on runtime decision making through an evaluation of the rules extracted from these optimized solutions are presented. A two-layer optimization logic to generate motions of a vehicle cornering an icy road with desired handling error is presented. The outer layer optimization algorithm first tries to solve the easiest problem which is cornering along the asphalt road. The first solution proposal is the simplest which is generating a constant command vector to be applied throughout the entire road. If a solution with desired vehicle handling performance is achieved, then problem gradually updated with more difficult ones and the friction coefficient is decreased and the skidding initiates as a consequence. In any of these iterations, if the solution cannot reach the desired performance, and the solution proposal is updated with more complex ones. The replicas control command vector to be applied at a road section is considered as two different vectors to be applied in two halves of this section, and then these two vectors are optimized separately.

As the outer optimization layer selects the current friction coefficient and optimizes the solution complexity, the inner layer optimizes the control command vectors to minimize the handling error. Assuming that the control command space is divided

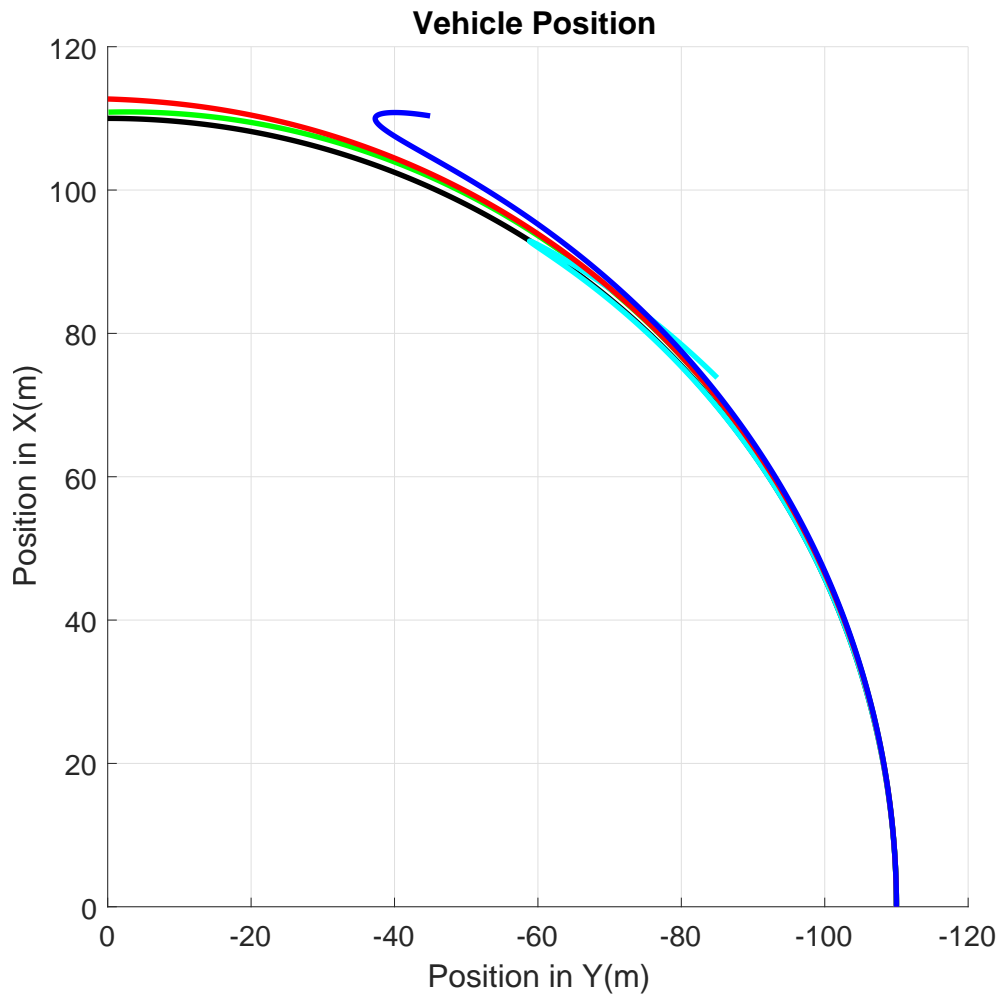


Figure 5.13: Autopilot performance for  $r = 110m, \mu = 0.72 - 0.19$  with runtime scheduling of the weighted-interpolation of the rules from different friction coefficients (black: ground truth, red: rule bases of  $r = 110m, \mu = 0.19$  only, blue: rule bases of  $r = 110m, \mu = 0.24$  only, cyan: rule bases of  $r = 110m, \mu = 0.72$  only, and green: runtime scheduling of the weighted-interpolation of the rule bases)

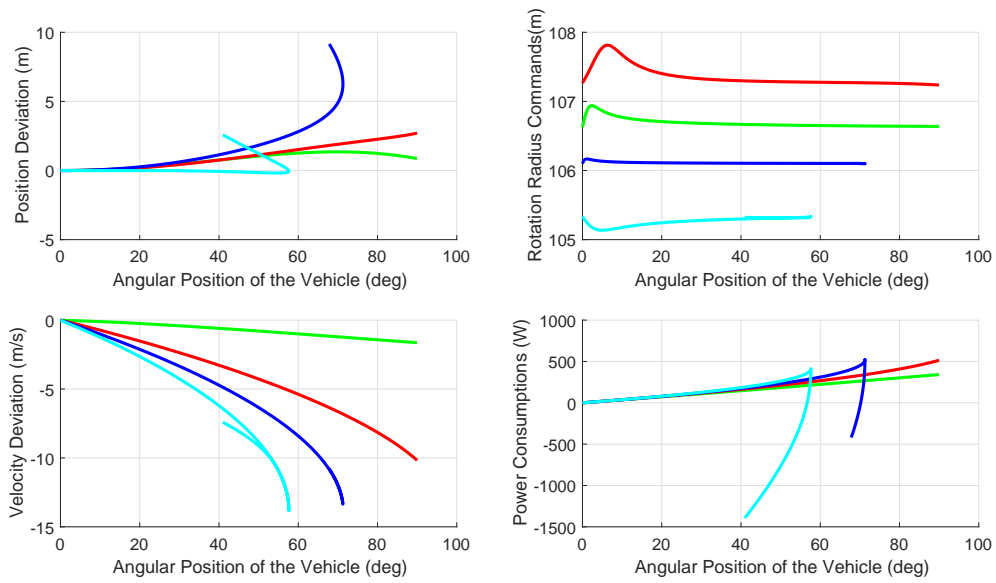


Figure 5.14: Autopilot performance measures for  $r = 110m, \mu = 0.72 - 0.19$  with runtime scheduling of the weighted-interpolation of the rules from different friction coefficients, normalized differences on various features (red: rule bases of  $r = 110m, \mu = 0.19$  only, blue: rule bases of  $r = 110m, \mu = 0.24$  only, cyan: rule bases of  $r = 110m, \mu = 0.72$  only, and green: runtime scheduling of the weighted-interpolation of the rule bases)

into cells, an optimization technique focusing a search cone towards the direction of the cell whose cost minimum, has been proposed. In this non-gradient based optimization method, the volume of the search cone is decreased if the current optimization direction minimizes the cost, or increased otherwise, similar to the adjustments performed in search step, in one dimensional search algorithms. The optimization algorithms are counted among the main contributions of this study. The optimization algorithms are counted among the main contributions of this study.

The optimization results are used to generate vehicle states and control commands applied at each sampling instant throughout a single scenario. A vehicle status is defined as  $\Theta = [p_d, v, \theta]^T$ ;  $p_d$ : radial position deviation normalized with rotation radius ( $r$ ),  $v$ : velocity of the vehicle,  $\theta$ : angle of velocity of the vehicle with respect to tangent of the desired route. A clustering is performed on the vehicle status space, based on well known k-means clustering technique. For each cluster centre, a control command vector is calculated. A cluster corresponds to a rule that defines the command to be applied as a function of the vehicle status. The clustering is performed for different scenarios with different friction coefficients and rotation radii; thus, cluster sets are obtained for these different scenarios.

The generated rules are used in runtime decision making process. At each decision instant, this process evaluates the current vehicle status, and proportional to the Euclidean distances to each cluster centre, the control command according to the scenario under consideration is calculated. The control command to be applied for motion along a specific rotation radius and friction coefficient is obtained by runtime scheduling of the weighted-interpolation between the control commands corresponding to different scenarios with different friction coefficients and rotation radii. The implementation of clustering based decision making process, and its application on electric vehicles cornering around roads with different friction coefficients, can be considered as one of the main contributions of this study.

The autopilot design is verified in comparisons to off-line optimization results in terms of vehicle handling performances and energy consumption of the vehicle. The results show that, the vehicle under control of autopilot design has similar motion characteristics as the vehicle under control of optimized control commands. The handling performance is satisfactory for the vehicle under autopilot control as well. The power consumption of the vehicle does not alter significantly either. This can be interpreted as a verification of the autopilot proposal. The number of clusters is tuned in these tests. The results depict that, the minimum divergence from the rotation radius is attained when the number of clusters is selected as 20. It is observed that the number of clusters greater than 20 does not yield significant improvement in vehicle handling.

The runtime scheduling of the weighted-interpolation of the rules obtained from optimization results for different scenarios with different rotation radii and friction coefficient is also tested to be successful. According to the results, autopilot design based on the runtime scheduling of the weighted-interpolation of the rules obtained for different friction coefficients is the only solution that vehicle completes a road with friction coefficient varying from asphalt road to icy road.

## CHAPTER 6

### CONCLUSIONS

Auto-mobiles are in our life for more than a century, and the main stream technology in auto-mobile propulsion is based on conventional internal combustion engines. However, our bondage with combustion engine driven auto-mobiles left its scar in the environment, and depleted our resources rapidly. As a clean alternative in public transportation, electric vehicles seem to be the most promising technology.

The widespread usage of electric cars, however, is limited with current battery technology, and the distances to be travelled with a fully charged battery are not as long as the conventional vehicles. The energy and time optimization are crucial problems for electric vehicles in addition to the other available problems for any vehicle, such as handling. Battery characteristics, constraints related to electric motor technologies complicates the solutions of these problems in electric vehicles.

This thesis addressed the challenges in electric vehicles: energy optimality, time optimality, and handling optimality. To generate optimal solutions to these problems, first necessary familiarity with electric vehicles were acquired. A high fidelity mathematical model for electric vehicles was introduced. Wheel skidding kinematics and battery dynamics were incorporated into the mathematical model.

Energy and time optimality problems were solved with approaches based on classical optimal control theory. A solution method for these two-point boundary value problems with defined state boundaries and free final time was developed and the obtained solutions were compared with the cruise controllers with various speed references. The optimal control solutions were observed to benefit from regenerative braking more effectively, as in the scenarios studied along the roads with uphill and downhill sections. The superiority of the optimal control was demonstrated to be valid on icy uphill and downhill sections as well.

A skidding compensation logic was proposed to reduce wheel slippage. The optimal control solution, however, seems to be insensitive to such a compensation. The sensitivity of the energy optimal controller on passenger seating configurations and initial state-of-the-charge of the battery were turned out to be smaller in magnitude compared to the changes in altering parameters. The results exhibited an evidence that the solution with optimal control reach the global optimum. Superiority of the energy optimal controller against the cruise controllers became more evident in the scenarios where the battery is far from being fully charged.

The vehicle cornering problem for electric vehicles were evaluated in terms of both energy and time optimality. Significant improvements in both objectives compared to the cruise control solutions were obtained with classical optimal control approach. A Pareto-front analysis were carried out with multi-objective energy and time minimization. The analysis provided a multi-objective solution to the vehicle cornering problem with a compromise between travel time and energy consumption that enables the vehicle to travel over the corner with minimum energy consumption within the given speed limits. The optimality of the Pareto-front results were discussed. Furthermore, a sensitivity analysis were performed to confirm that the optimal control solution is insensitive to the different passenger seating arrangements.

The vehicle cornering around roads with low friction coefficients were studied as well and an autopilot design was proposed to satisfy desired handling performance. A novel hierarchical optimization approach was presented to generate off-line solutions for cornering along roads with different friction coefficients and radii of curvature. Vehicle motion as the output of this optimization process, together with vehicle states and control commands at each sampling time were stored for different selected scenario parameters with various rotation radii and friction coefficients. The vehicle statuses as a function of vehicle states were clustered with the k-means clustering technique, and they were associated with the control commands applied. A cluster centre-control command corresponds to a rule that produces the unique control command to be applied as a function of vehicle status. The autopilot was constructed by a convex combination of these rules. This basic idea of autopilot design has been extended for motion along a specific rotation radii and friction coefficients; the control commands corresponding to arbitrary scenario parameters are obtained by a runtime scheduling of the weighted-interpolation among the control commands corresponding to different scenario parameters.

The autopilot design was compared with the off-line optimized control command sequences along the test scenarios, and it was observed that performance of a vehicle under autopilot control does not differentiate from those under off-line optimized control commands in terms of vehicle states, vehicle handling performances and energy consumptions more than 5%. The performance of the autopilot proposal was also tested with different scenarios, and the approach based on runtime scheduling of the weighted-interpolation between the control commands corresponding to different scenario parameters was verified.

The following contributions to the available literature is proposed in this thesis:

1. A high fidelity vehicle model incorporated with wheel skidding kinematics and power consumption dynamics was developed and used in all the simulations. The energy optimality problem for vehicles moving along roads with icy or asphalt uphill/downhill sections, the energy, time and multi-objective optimal control problem for vehicle cornering and the vehicle handling problem for cornering along icy roads were all simulated on this detailed mathematical model.
2. In solution algorithms of optimal control problems, a numerical method based on mapping the control inputs from the time domain to position domain was proposed to deal with these free-final time two point boundary value problems.
3. A skidding compensation approach was proposed to reduce the incidences of

wheel slippage. The skidding compensation logic was shown to be effective in reducing the slippage and it was observed that the energy optimality of the solution is preserved.

4. The superiority of the optimal control theory based solution for the energy management problem of electric vehicles was shown with comparisons against standard cruise controllers both in asphalt and icy roads.
5. Low sensitivity of the energy optimal controller with respect to passenger arrangements and initial state-of-charge of the battery in electric vehicles were demonstrated for motions along roads with uphill and downhill sections.
6. Low sensitivities of both energy and time optimal controllers with respect to passenger arrangements were demonstrated for vehicle cornering motions.
7. It was shown with NSGA-II genetic algorithm that there is a Pareto-front between time and energy optimization problems for vehicle cornering. The optimality of this Pareto-front was validated with classical optimal control approach.
8. As solution to the vehicle handling problem in cornering along icy roads, an optimization technique was proposed. The approach finds the probably complex solution that may vary between different sections of the curvature, of the relatively difficult problem, cornering around icy roads. The method attacks the problem by first trying to solve the relatively easier problems, cornering around higher friction roads. The proposed solution is simple at first, fixing the commands throughout the entire curvature and optimizing the commands. If a solution is not found, the road is sectioned by two-fold with different command are assigned and optimized. As the number of the sections increases, the number of variables to be optimized becomes larger; hence, the solution gets complex. When the desired handling performance is obtained, the friction coefficient is decreased until the icy road conditions are reached. Eventually the skidding starts, and the problem becomes complicated, yet a solution proposal was always obtained.
9. An optimization technique to minimize position deviation from the desired route, was presented. The method searches the candidates around a neighbourhood of a current best solution bounded within a search cone. The centreline of this search cone is generated from the difference between two consecutive optimization steps, and its volume is adjusted according to the changes in the cost throughout these iterations.
10. An autopilot for vehicle cornering around icy roads is proposed based on runtime decision making process. The rule sets to be used in the process are generated by clustering the vehicle statuses obtained in off-line optimization and associating control command to these clusters. A cluster centre-control command corresponds to a rule that produces the unique control command to be applied as a function of vehicle status. This basic idea of autopilot design has been extended for motion along a specific rotation radii and friction coefficients; the control commands corresponding to arbitrary scenario parameters are obtained by a runtime scheduling of the weighted-interpolation among the control commands corresponding to different scenario parameters.

In this thesis, based on classical optimal control theory, energy optimal control solutions for vehicles moving along roads including uphill and downhill sections, that may be icy or not, were derived. The superiority of the optimal controller compared to the standard cruise controllers with various speed references, and the insensitivity of the optimal controller to the changes in mass distribution of the vehicles according to different passenger configurations and initial state of charge of the battery depicted that the approach is valid. The optimal control solutions can be used as foundation of an autopilot design. Similar to the one designed in Chapter 5: Vehicle Handling, autopilots based on runtime decision making according to the rules generated by the optimal control solutions can be proposed.

In real life, unlike that is assumed in Chapter 4: Vehicle Cornering, the roads with such constant cornering radius does not exist. The road designs obey the so called *clothoid* pattern, [2, 40]. As a future work, energy and time optimal control structures based on optimal control theory can be applied to the vehicles cornering such a *clothoid* curvature. Furthermore, the energy, time and multi-objective optimal control solutions proposed in this study, can be extended to the lane changing problem. Note that there are two consecutive cornering, in opposite directions in a lane changing problem. Additionally, in order to benefit from advantages of optimal control solutions in real-life application, autopilot designs based on rule extraction from off-line optimization data and using them in runtime convex combination of the rules can be proposed.

In this thesis, in Chapter 5: Vehicle Handling, cornering motion along roads with different and especially low friction coefficients were studied and an autopilot design was proposed. The proposed autopilot can be further extended to overtaking the vehicle moving in front as along roads with low friction coefficients. Furthermore, the scenarios where only the wheels on one side, left or right, are on icy section of the road, the performance of the autopilot can be tested.

This thesis was focused on some optimal control problems, and the solutions were evaluated only in simulation environment. The experimentation of the methods on vehicles requires not only taking some measurements from a vehicle moving along some road section, but also the capability and permission to intervene into control commanding hardware of the vehicle. The lack of such resources and permissions retained us from the experimental proof of the approaches introduced.

## REFERENCES

- [1] *Panasonic Lithium Ion NCR18650 Datasheet*, 2012.
- [2] A. Aashto. Policy on geometric design of highways and streets. *American Association of State Highway and Transportation Officials, Washington, DC*, 1(990), 2001.
- [3] M. Abe, N. Ohkubo, and Y. Kano. A direct yaw moment control for improving limit performance of vehicle handling - comparison and cooperation with 4ws-. *Vehicle System Dynamics*, 25(sup1):3–23, 1996.
- [4] K. Ahiska, M. K. Ozgoren, and M. K. Leblebicioglu. Energy optimal controller for electric vehicles on partially icy roads with heuristic skidding compensation. In *Control, Automation and Systems (ICCAS), 2015 15th International Conference on*, pages 101–106, Oct 2015.
- [5] J. Ahmadi, A. K. Sedigh, and M. Kabganian. Adaptive vehicle lateral-plane motion control using optimal tire friction forces with saturation limits consideration. *IEEE Transactions on Vehicular Technology*, 58(8):4098–4107, Oct 2009.
- [6] C. Alaoui. *Electric vehicle energy management system*. PhD. thesis, Department of Electrical Engineering, University of Massachusetts Lowell, 2001.
- [7] C. E. Beal and J. C. Gerdes. Model predictive control for vehicle stabilization at the limits of handling. *IEEE Transactions on Control Systems Technology*, 21(4):1258–1269, July 2013.
- [8] P. Blau. *Friction Science and Technology*. CRC Press, 2009.
- [9] M. Blundell and D. Harty. *The Multibody Systems Approach to Vehicle Dynamics*. Butterworth-Heinemann, Oxford, 2004.
- [10] M. Canale, L. Fagiano, A. Ferrara, and C. Vecchio. Vehicle yaw control via second-order sliding-mode technique. *IEEE Transactions on Industrial Electronics*, 55(11):3908–3916, Nov 2008.
- [11] C. Canudas de Wit, H. Olsson, K. J. Astrom, and P. Lischinsky. A new model for control of systems with friction. *IEEE Transactions on Automatic Control*, 40(3):419–425, Mar 1995.

- [12] C. Canudas de Wit, P. Tsiotras, E. Velenis, M. Basset, and G. Gissinger. Dynamic friction models for road/tire longitudinal interaction. *Vehicle System Dynamics*, 39(3):189–226, 2003.
- [13] L. Caracciolo, A. de Luca, and S. Iannitti. Trajectory tracking control of a four-wheel differentially driven mobile robot. In *Robotics and Automation, 1999. Proceedings. 1999 IEEE International Conference on*, volume 4, pages 2632–2638, 1999.
- [14] C. C. Chan. The state of the art of electric, hybrid, and fuel cell vehicles. *Proceedings of the IEEE*, 95(4):704–718, April 2007.
- [15] D. J. Chang and E. K. Morlok. Vehicle speed profiles to minimize work and fuel consumption. *Journal of Transportation Engineering*, 131(3):173–182, 2005.
- [16] Y. Chen, X. Li, C. Wiet, and J. Wang. Energy management and driving strategy for in-wheel motor electric ground vehicles with terrain profile preview. *IEEE Transactions on Industrial Informatics*, 10(3):1938–1947, Aug 2014.
- [17] Y. Chen and J. Wang. Fast and global optimal energy-efficient control allocation with applications to over-actuated electric ground vehicles. *IEEE Transactions on Control Systems Technology*, 20(5):1202–1211, Sept 2012.
- [18] Y. Chen and J. Wang. Adaptive energy-efficient control allocation for planar motion control of over-actuated electric ground vehicles. *IEEE Transactions on Control Systems Technology*, 22(4):1362–1373, July 2014.
- [19] D. Corona and B. D. Schutter. Adaptive cruise control for a smart car: A comparison benchmark for mpc-pwa control methods. *IEEE Transactions on Control Systems Technology*, 16(2):365–372, March 2008.
- [20] M. L. Corradini, T. Leo, and G. Orlando. Experimental testing of a discrete-time sliding mode controller for trajectory tracking of a wheeled mobile robot in the presence of skidding effects. *Journal of Robotic Systems*, 19(4):177–188, 2002.
- [21] V. Cossalter, M. D. Lio, R. Lot, and L. Fabbri. A general method for the evaluation of vehicle manoeuvrability with special emphasis on motorcycles. *Vehicle System Dynamics*, 31(2):113–135, 1999.
- [22] K. Deb. *Multi-Objective Optimization Using Evolutionary Algorithms*. John Wiley & Sons, Inc., New York, NY, USA, 2001.
- [23] W. Dib, A. Chasse, P. Moulin, A. Sciarretta, and G. Corde. Optimal energy management for an electric vehicle in eco-driving applications. *Control Engineering Practice*, 29:299 – 307, 2014.
- [24] M. Eshani, Y. Gao, and A. Emadi. *Modern electric, hybrid electric, and fuel cell vehicles: Fundamentals, theory, and design*. Boca Raton: CRC Press, 2010.

- [25] E. Esmailzadeh, A. Goodarzi, and G. Vossoughi. Optimal yaw moment control law for improved vehicle handling. *Mechatronics*, 13(7):659 – 675, 2003.
- [26] M. Ferdowsi. Plug-in hybrid vehicles - a vision for the future. In *2007 IEEE Vehicle Power and Propulsion Conference*, pages 457–462, Sept 2007.
- [27] A. E. Fuhs. *Hybrid vehicles and the future of personal transportation*. Boca Raton: CRC Press, 2009.
- [28] T. Fujioka and M. Kato. Numerical analysis of minimum-time cornering. In *International Symposium on Advanced Vehicle Control (1994: Tsukuba-shi, Japan)*, pages 260–265, 1994.
- [29] M. Gerds, S. Karrenberg, B. Muller-Bessler, and G. Stock. Generating locally optimal trajectories for an automatically driven car. *Optimization and Engineering*, 10(4):439–463, 2008.
- [30] T. D. Gillespie. Fundamentals of vehicle dynamics. Technical report, SAE Technical Paper, 1992.
- [31] A. Haddoun, M. E. H. Benbouzid, D. Diallo, R. Abdessemed, J. Ghouili, and K. Srairi. Analysis, modeling and neural network traction control of an electric vehicle without differential gears. In *2007 IEEE International Electric Machines Drives Conference*, volume 1, pages 854–859, May 2007.
- [32] N. Hamzah, Y. M. Sam, H. Selamat, and M. K. Aripin. Ga-based sliding mode controller for yaw stability improvement. In *Control Conference (ASCC), 2013 9th Asian*, pages 1–6, June 2013.
- [33] P. M. Hart. *An Antilock-Braking Systems (ABS) Control: A Technical Review*. Draft Report, 2003.
- [34] J. A. Hartigan. *Clustering Algorithms*. John Wiley & Sons, Inc., New York, NY, USA, 1975.
- [35] J. P. M. Hendrikx, T. Meijlink, and R. F. C. Kriens. Application of optimal control theory to inverse simulation of car handling. *Vehicle System Dynamics*, 26(6):449–461, 1996.
- [36] K. Hofstetter, C. Grohs, J. Eberhardsteiner, and H. Mang. Sliding behaviour of simplified tire tread patterns investigated by means of fem. *Computers & Structures*, 84(17 - 18):1151 – 1163, 2006. Formulations and Computational Models for Finite Strains.
- [37] R. Hooke and T. A. Jeeves. Direct search solution of numerical and statistical problems. *Journal of the Association for Computing Machinery*, 8(2):212–229, April 1961.

- [38] Y. H. Hosam el deen. *Computer control of vehicle skidding on slippery roads*. PhD. thesis, Department of Electrical and Computer Engineering, University of Wisconsin-Madison, 1986.
- [39] M. Ivarsson, J. Aslund, and L. Nielsen. Look-ahead control consequences of a non-linear fuel map on truck fuel consumption. *Proceedings of the Institution of Mechanical Engineers, Part D: Journal of Automobile Engineering*, 223(10):1223–1238, 2009.
- [40] A. Jeffrey, editor. *Handbook of Mathematical Formulas and Integrals (Third Edition)*. Academic Press, Burlington, third edition edition, 2004.
- [41] T. A. Johansen, J. Kalkkuhl, J. Ludemann, and I. Petersen. Hybrid control strategies in abs. In *American Control Conference, 2001. Proceedings of the 2001*, volume 2, pages 1704–1705, 2001.
- [42] S. Kachroudi, M. Grossard, and N. Abroug. Predictive driving guidance of full electric vehicles using particle swarm optimization. *IEEE Transactions on Vehicular Technology*, 61(9):3909–3919, Nov 2012.
- [43] M. A. S. Kamal, M. Mukai, J. Murata, and T. Kawabe. Ecological driver assistance system using model-based anticipation of vehicle-road-traffic information. *IET Intelligent Transport Systems*, 4(4):244–251, December 2010.
- [44] M. A. S. Kamal, M. Mukai, J. Murata, and T. Kawabe. Ecological vehicle control on roads with up-down slopes. *IEEE Transactions on Intelligent Transportation Systems*, 12(3):783–794, Sept 2011.
- [45] M. A. S. Kamal, M. Mukai, J. Murata, and T. Kawabe. Model predictive control of vehicles on urban roads for improved fuel economy. *IEEE Transactions on Control Systems Technology*, 21(3):831–841, May 2013.
- [46] J. Kennedy and R. Eberhart. Particle swarm optimization. In *Neural Networks, 1995. Proceedings., IEEE International Conference on*, volume 4, pages 1942–1948, Nov 1995.
- [47] P. Khatun, C. M. Bingham, N. Schofield, and P. H. Mellor. An experimental laboratory bench setup to study electric vehicle antilock braking/ traction systems and their control. In *Vehicular Technology Conference, 2002. Proceedings. VTC 2002-Fall. 2002 IEEE 56th*, volume 3, pages 1490–1494 vol.3, 2002.
- [48] H. Khayyam, S. Nahavandi, and S. Davis. Adaptive cruise control look-ahead system for energy management of vehicles. *Expert Systems with Applications*, 39(3):3874 – 3885, 2012.
- [49] D. E. Kirk. *Optimal control theory: an introduction*. Courier Corporation, 2012.

- [50] K. M. Kritayakirana. *Autonomous Vehicle Control at the Limits of Handling*. PhD. thesis, Department of Mechanical Engineering, Stanford University, California, 2012.
- [51] J. R. Layne, K. M. Passino, and S. Yurkovich. Fuzzy learning control for antiskid braking systems. *IEEE Transactions on Control Systems Technology*, 1(2):122–129, Jun 1993.
- [52] S. Li, K. Li, R. Rajamani, and J. Wang. Model predictive multi-objective vehicular adaptive cruise control. *IEEE Transactions on Control Systems Technology*, 19(3):556–566, May 2011.
- [53] S. E. Li, Z. Jia, K. Li, and B. Cheng. Fast online computation of a model predictive controller and its application to fuel economy/-oriented adaptive cruise control. *IEEE Transactions on Intelligent Transportation Systems*, 16(3):1199–1209, June 2015.
- [54] C.-C. Lin. *Modelling and Control Strategy Development for Hybrid Vehicles*. PhD. thesis, Department of Mechanical Engineering, University of Michigan, Ann Arbor, 2004.
- [55] X. Lin. *Reinforcement Learning in Hybrid Electric Vehicles (HEVs) / Electric Vehicles (EVs) and Other Cyber Physical Systems*. PhD. thesis, Department of Electrical and Computer Engineering, Northeastern University, Boston, MA, 2016.
- [56] S. Lloyd. Least squares quantization in pcm. *IEEE Transactions on Information Theory*, 28(2):129–137, Mar 1982.
- [57] S. M. Lukic and A. Emadi. Charging ahead. *IEEE Industrial Electronics Magazine*, 2(4):22–31, December 2008.
- [58] G. A. Magallan, C. H. D. Angelo, and G. O. Garcia. Maximization of the traction forces in a 2wd electric vehicle. *IEEE Transactions on Vehicular Technology*, 60(2):369–380, Feb 2011.
- [59] A. Mandow, J. L. Martinez, J. Morales, J. L. Blanco, A. Garcia-Cerezo, and J. Gonzalez. Experimental kinematics for wheeled skid-steer mobile robots. In *2007 IEEE/RSJ International Conference on Intelligent Robots and Systems*, pages 1222–1227, Oct 2007.
- [60] T. Markel, A. Brooker, J. Gonder, M. O’Keefe, A. Simpson, and M. Thornton. Plug-in hybrid vehicle analysis. *National Renewable Energy Laboratory, Report No. NREL/MP-540-40609*, 2006.
- [61] J. L. Martínez, A. Mandow, J. Morales, S. Pedraza, and A. García-Cerezo. Approximating kinematics for tracked mobile robots. *The International Journal of Robotics Research*, 24(10):867–878, 2005.

- [62] K. Moriwaki. Autonomous steering control for electric vehicles using nonlinear state feedback h-infinity control. *Nonlinear Analysis: Theory, Methods & Applications*, 63(6):2257 – 2268, 2005.
- [63] A. Mozaffari, M. Vajedi, and N. L. Azad. A robust safety-oriented autonomous cruise control scheme for electric vehicles based on model predictive control and online sequential extreme learning machine with a hyper-level fault tolerance-based supervisor. *Neurocomputing*, 151, Part 2:845 – 856, 2015.
- [64] J. A. Nelder and R. Mead. A simplex method for function minimization. *The Computer Journal*, 7(4):308–313, 1965.
- [65] H. B. Pacejka. *Tyre and Vehicle Dynamics*. Butterworth-Heinemann, Oxford, second edition, 2006.
- [66] A. Pennycott, L. De Novellis, P. Gruber, and A. Sorniotti. Optimal braking force allocation for a four-wheel drive fully electric vehicle. *Proceedings of the Institution of Mechanical Engineers, Part I: Journal of Systems and Control Engineering*, 228(8):621–628, 2014.
- [67] P. Petrov, J. de Lafontaine, P. Bigras, and M. Tetreault. Lateral control of a skid-steering mining vehicle. In *Intelligent Robots and Systems, 2000. (IROS 2000). Proceedings. 2000 IEEE/RSJ International Conference on*, volume 3, pages 1804–1809, 2000.
- [68] K. Popp and W. Schiehlen. *Ground Vehicle Dynamics*. Springer Berlin Heidelberg, Berlin, Heidelberg, 2010.
- [69] L. E. Ray. Estimation of terrain forces and parameters for rigid-wheeled vehicles. *IEEE Transactions on Robotics*, 25(3):717–726, June 2009.
- [70] I. R. N. Roland Siegwart. *Introduction to Autonomous Mobile Robots*. Intelligent Robotics and Autonomous Agents. The MIT Press, 1st edition, 2004.
- [71] A. Rucco, G. Notarstefano, and J. Hauser. An efficient minimum-time trajectory generation strategy for two-track car vehicles. *IEEE Transactions on Control Systems Technology*, 23(4), July 2015.
- [72] T. Schwickart, H. Voos, J. H. Minaglou, M. Darouach, and A. Rosich. Design and simulation of a real-time implementable energy-efficient model-predictive cruise controller for electric vehicles. *Journal of the Franklin Institute*, 352(2):603 – 625, 2015. Special Issue on Control and Estimation of Electrified vehicles.
- [73] A. Sciarretta, G. D. Nunzio, and L. L. Ojeda. Optimal ecodriving control: Energy-efficient driving of road vehicles as an optimal control problem. *IEEE Control Systems*, 35(5):71–90, Oct 2015.

- [74] S. G. Shadle, L. H. Emery, and H. K. Brewer. Vehicle braking, stability and control. Technical report, SAE Technical Paper, 1983.
- [75] B. Shamah, M. D. Wagner, S. Moorehead, J. Teza, D. Wettergreen, and W. L. Whittaker. Steering and control of a passively articulated robot. In *SPIE, Sensor Fusion and Decentralized Control in Robotic Systems IV*, volume 4571, October 2001.
- [76] R. Sharp, D. Casanova, and P. Symonds. A mathematical model for driver steering control, with design, tuning and performance results. *Vehicle System Dynamics*, 33(5):289–326, 2000.
- [77] R. S. Sharp and H. Peng. Vehicle dynamics applications of optimal control theory. *Vehicle System Dynamics*, 49(7):1073–1111, 2011.
- [78] L. I. Silva, G. A. Magallan, C. H. D. Angelo, and G. O. Garcia. Vehicle dynamics using multi-bond graphs: Four wheel electric vehicle modeling. In *Industrial Electronics, 2008. IECON 2008. 34th Annual Conference of IEEE*, pages 2846–2851, Nov 2008.
- [79] D. Tavernini, M. Massaro, E. Velenis, D. I. Katzourakis, and R. Lot. Minimum time cornering: the effect of road surface and car transmission layout. *Vehicle System Dynamics*, 51(10):1533–1547, 2013.
- [80] M. Thommyppillai, S. Evangelou, and R. S. Sharp. Car driving at the limit by adaptive linear optimal preview control. *Vehicle System Dynamics*, 47(12):1535–1550, 2009.
- [81] J. P. Timings and D. J. Cole. Minimum maneuver time calculation using convex optimization. *Journal of Dynamic Systems, Measurement, and Control*, 135(3):31015–31023, March 2013.
- [82] R. van der Steen. Tyre road friction modelling : Literature survey. Technical report, Eindhoven : Technische Universiteit Eindhoven, 2007.
- [83] E. Velenis and P. Tsiotras. Optimal velocity profile generation for given acceleration limits; the half-car model case. In *Proceedings of the IEEE International Symposium on Industrial Electronics, 2005. ISIE 2005.*, volume 1, pages 361–366, June 2005.
- [84] E. Velenis and P. Tsiotras. Optimal velocity profile generation for given acceleration limits: theoretical analysis. In *Proceedings of the 2005, American Control Conference, 2005.*, volume 2, pages 1478–1483, June 2005.
- [85] R. Wang, C. Hu, Z. Wang, F. Yan, and N. Chen. Integrated optimal dynamics control of 4wd4ws electric ground vehicle with tire-road frictional coefficient estimation. *Mechanical Systems and Signal Processing*, 60-61:727 – 741, 2015.

- [86] T. Wang, C. G. Cassandras, and S. Pourazarm. Optimal motion control for energy-aware electric vehicles. *Control Engineering Practice*, 38:37 – 45, 2015.
- [87] Y. Wang, J. Jiang, and T. Mu. Context-aware and energy-driven route optimization for fully electric vehicles via crowdsourcing. *IEEE Transactions on Intelligent Transportation Systems*, 14(3):1331–1345, Sept 2013.
- [88] J. Y. Wong. *Theory of Ground Vehicles*. John Wiley & Sons, 2001.
- [89] J. Yi, D. Song, J. Zhang, and Z. Goodwin. Adaptive trajectory tracking control of skid-steered mobile robots. In *Proceedings 2007 IEEE International Conference on Robotics and Automation*, pages 2605–2610, April 2007.
- [90] W. Yu, O. Y. C. Jr., E. G. C. Jr., and P. Hollis. Analysis and experimental verification for dynamic modeling of a skid-steered wheeled vehicle. *IEEE Transactions on Robotics*, 26(2):340–353, April 2010.
- [91] Y. Zhang, D. Hong, J. H. Chung, and S. A. Velinsky. Dynamic model based robust tracking control of a differentially steered wheeled mobile robot. In *American Control Conference, 1998. Proceedings of the 1998*, volume 2, pages 850–855, Jun 1998.

# CURRICULUM VITAE

## PERSONAL INFORMATION

**Surname, Name:** Ahıska, Kenan  
**Nationality:** Turkish (TC)  
**Date and Place of Birth:** 21/07/1987, Akstafa-Azerbaijan  
**Marital Status:** Single  
**Phone:** 05056869553  
**Fax:** -

## EDUCATION

<b>Degree</b>	<b>Institution</b>	<b>Year of Graduation</b>
M.S.	Electrical and Electronics Eng. Dept., METU	2012
B.S.	Electrical and Electronics Eng. Dept., METU	2010
High School	Ankara Çağrıbey Anatolian High School	2005

## PROFESSIONAL EXPERIENCE

<b>Year</b>	<b>Place</b>	<b>Enrollment</b>
Jan. 2010 - April 2010	ASELSAN Inc.	electronics design eng.
April 2010 - Jan. 2011	TES Thermoelectric Systems Inc.	founder, design eng.
Jan. 2011 - Present	ASELSAN Inc.	systems eng.

## PUBLICATIONS

### Dissertations

K. Ahıska, *Control and Guidance of an Unmanned Sea Surface Vehicle*, M.Sc. Thesis Dissertation, Department of Electrical and Electronics Engineering, Middle East Technical University, Ankara, 2012.

## National Conference Publications

K. Ahiska and M. K. Leblebicioglu, *Autopilot Design for an Unmanned Surface Vehicle*, Conference on Defence Technologies, SAVTEK'12, Ankara, Turkey, July, 2012, *in Turkish*.

U. D. Gul and K. Ahiska, *Modelling, Control, Guidance and Navigation of Unmanned Sea Vehicles*, Conference on Defence Systems Technologies, SSTKON'12, Ankara, Turkey, November, 2012, *in Turkish*.

K. Ahiska and M. K. Leblebicioglu, *Linear Quadratic Autopilot Design for an Unmanned Surface Vehicle*, Turkish National Conference on Automatic Control, TOK'12, Nigde, Turkey, September, 2012, *in Turkish*.

K. Ahiska, *Guidance Techniques for Tactical Missiles*, Conference on Defence Systems Technologies, SSTKON'15, November, Ankara, Turkey, 2015, *in Turkish*.

K. Ahiska, M. K. Ozgoren and M. K. Leblebicioglu, *Mathematical Modelling for Electric Vehicles: Simulation Results on Various Road Conditions*, Turkish National Conference on Automatic Control, TOK'15, Denizli, Turkey, September, 2015, *in Turkish*.

K. Ahiska, *How Should Smart Land Vehicles be Design*, Seminars on Land Systems, KSS'16, Ankara, Turkey, November, 2016, *in Turkish*.

K. Ahiska, and N. A. Albayrak *Target Classification in Air and Missile Defence Systems*, Conference on Defence Technologies, SAVTEK'16, Ankara, Turkey, September, 2015, *in Turkish*.

## National Journal Publications

K. Ahiska and M. K. Leblebicioglu, *Design of Autopilot and Guidance Algorithms for an Unmanned Sea Surface Vehicle*, Journal of Electrical Engineering Chamber, vol.5, pp. 1-7, Ankara, Turkey, 2014, *in Turkish*.

## International Conference Publications

K. Ahiska, M. K. Ozgoren and M. K. Leblebicioglu, *Energy Optimal Controller for Electric Vehicles on Partially Icy Roads with Heuristic Skidding Compensation*, 15th International Conference on Control, Automation, and Systems (ICCAS'2015), 13-16 October 2015, Busan, Korea.

M. Kumru, I. K. Erunsal, K. Ahiska, and M. K. Leblebicioglu, *A Survey on Tactical Control Algorithms for Path Tracking Unmanned Surface Vehicles*, 12th International Conference on Control, Automation, Robotics and Vision (ICARCV'2016), 13-15 November 2016, Phuket, Thailand.

## **International Journal Publications**

K. Ahiska, M. K. Ozgoren and M. K. Leblebicioglu, *Energy Optimal Controller for an Electric Vehicle on Variable Slope Road*, submitted to International Journal of Control, *under review*

K. Ahiska, M. K. Ozgoren and M. K. Leblebicioglu, *Multi Objective Optimal Vehicle Cornering Behavior under Constant Ackermann Steering*, submitted to Optimal Control Applications and Methods, *under review*

K. Ahiska, M. K. Ozgoren and M. K. Leblebicioglu, *Autopilot Design for Vehicle Cornering Through Icy Roads*, submitted to IEEE Transactions on Vehicular Technologies, *under review*

M. Kumru, I. K. Erunsal, K. Ahiska, and M. K. Leblebicioglu, *Approaches in Tactical Controller Design for Path Tracking Unmanned Surface Vehicles*, submitted to Control Engineering Practice, *under review*